Advanced Signal Processing of Wayside Condition Monitoring of Railway Wheelsets

By

Eleni Giannouli

A thesis submitted to

The University of Birmingham

For the degree of

DOCTOR OF PHILOSOPHY

School of Metallurgy and Materials

College of Engineering and Physical Sciences

University of Birmingham

June 2021

Dedication

To my husband Dr Nikolaos Angelopoulos whose assistance was a milestone in the completion of this study and to our son Georgios Angelopoulos who was born during this project and give me plenty of happy breaks.

Synopsis

Railway transport is an efficient and environmentally benign method of transport. With global warming effects intensifying it has become more urgent that mobility and economic prosperity are maintained by delivering increased transport efficient. Hence, railway transport has a significant role to play in the forthcoming decades.

Punctuality and safety of railway operations is critical in ensuring unhindered transportation for passengers and freight. Rolling stock are required to operate at higher speeds and carry heavier axle loads than ever before. This puts increased pressure to rolling stock operators and infrastructure managers in trying to avoid disruption and potential accidents which also leads to higher transportation costs.

Remote condition monitoring has increased in significance for railway transport over the last few years. However, there are still a lot to be done before breakthrough remote condition monitoring technologies are delivered at commercial scale in the wider international railway network.

Different remote condition monitoring systems are installed wayside in order to evaluate the structural integrity of rolling stock wheelsets, detect any potential rolling stock fault in time and minimize the likelihood of a serious railway accident. The existing wayside condition monitoring system are based on infrared cameras, acoustic arrays and strain gauges. Despite significant investments by the rail industry in this area, false alarms can still occur and many of condition monitoring systems are able to detect faults once they become critical.

In the present thesis, a novel approach based on integration of acoustic emission and vibration analysis together with advanced signal progressing is detailed. Tests ranging from laboratory tests under controlled conditions, all the way up to trials under actual operational conditions in the UK network have been carried out, yielding promising results. The experimental methodology employed has shown that acoustic emission is particularly efficient in detecting and ranking potential axle bearing defects. When acoustic emission is coupled with vibration analysis, it is possible to detect axle bearing defects whilst avoiding misinterpretation of wheel flats for axle bearing defects. The results obtained suggest that the widespread use of the reported methodology in the railway is feasible.

The novel RCM system can enhance the reliability, availability, maintainability and safety of rolling stock wheelsets. Experimental work have been carried out under actual operational conditions in UK rail network at Cropredy, at Chiltern Railway line. The novel RCM system has been installed adjacent to Hot Box Axle Detector for comparison purposes. No interference on the track circuits is the main advantage of the proposed system. During the signal processing module of the system, freight and passenger train waveforms were identified to contain evidence of potential bearing faults. The results still require follow up validation from Network Rail.

Time, frequency and time-frequency analysis have been applied to the acquired data. High amplitude peaks and signal modulation were visible at raw data. The acquired signals were transferred to frequency domain. Harmonics in frequency distribution were clearly seen. These frequency bands can be used as a reference for the band pass filter at HFRT process.

HFRT algorithm has been effectively applied in the captured data in order to identify the fundamental fault frequency and its harmonics. Sidebands were also visible. TSK analysis was also applied in the raw signals. Frequency bands with high kurtosis values can be used as a reference for further analysis.

In addition, laboratory experiments at University of Birmingham and Long Marston trials under controlled conditions have been carried out in order to evaluate the reliability of the system in early diagnosis of wheel and axle bearing defects. Acoustic emission and vibration signals have been collected. From the results obtained, it has effectively demonstrated that fault detection can be achieved using the frequency distribution of the signal. Defect type evaluation can be carried out by detecting the fundamental fault frequency at the HFRT process and fault quantification can achieved by Normalized Moving RMS analysis.

In summary, the research contribution of this work is presented below:

- Development and assessment of the vibroacoustic condition monitoring system for railway wheelsets. Experimental methodology and results considered in this study are the main contributions in the literature of this field.
- In service passenger and freight trains have been monitored. Detection of potential bearing faults has been achieved.
- Novel methodology applied at the acquired in-service data in order to determine the appropriate frequency range for the band-pass filter during the HFRT process. Frequency bands with high kurtosis values can be used as a reference for the band-pass filter. In addition, harmonics have been presented in frequency distribution of the signal. The frequency bands that harmonics were appeared can also be used for the design of the band-pass filter.

- Comparison between advanced signal processing techniques using laboratory, in-field and in in-service signals. Detection of wheelsets faults, identification of type of the defect and quantification of fault severity can be achieved when combination of algorithm is applied at raw signals.

Acknowledgment

- I wish to express my deepest gratitude to my family and recognize the invaluable assistance that provide me during this study.
- I am extremely grateful to my supervisor Dr Mayorkinos Papaelias, who has supported me throughout this project. He convincingly guided me at every step of this study. He encouraged me with his knowledge and his patience. He taught me to act in a professional manner.
- Special thanks to Prof Clive Roberts, Prof Gerard Fernando and Dr Slim Soua for their supervision and problem solving.
- I am indebted to the University of Birmingham for the provision of facilities. The financial support of School of Metallurgy of Materials and the National Structural Integrity Research Centre based in Grant Park are gratefully acknowledged.
- Last but not least, I wish to express my sincere thanks Dr Arash Amini and Dr Zheng Huang about advice and assistance during this project.

Publications

Journal Paper

E. Giannouli, M. Papaelias, A. Amini, Z. Huang, V. L. Jantara Junior, S. Kerkyras, P.Krusuansombat, F. P. Garcia Marquez and P. Vallely Detection and evaluation of rolling stock wheelset defects using Acoustic Emission, Insight Journal, UK ,2021 (accepted journal)

Conference Paper

- Z. Huang, P. Vallely, E.H. Gunel, S.Shi, E. Giannouli, Arash Amini, Francisco Nieves Bogonez, Fausto Pedro Garcia Marquez, Sakdirat Kaewunruen and Mayorkinos Papaelias Dynamic inspection and maintenance scheduling of critical railway infrastructure components using advanced structural health monitoring techniques, 56th Annual British Conference on Non-Destructive Testing, Telford, UK, September 2017
- E. Giannouli, Zheng Huang, Arash Amini, Patrick Vallely, Slim Soua, Fausto Pedro Garcia Marquez and Mayorkinos Papaelias Remote condition monitoring of railway axle bearings based on data fusion from several sensors, WCCM 2017, London, UK, June 2017

- E. Giannouli, Slim Soua and Mayorkinos Papaelias. Advanced Signal Processing of Wayside Condition Monitoring of Railway Wheelsets, NSIRC Annual Conference 2017, Cambridge, UK, June 2017

- P. Vallely , A. Amini, Z. Huang , E. Giannouli, Shengrun Shi, Nikolaos Angelopoulos, Francisco Nieves Bogonez, Jenna Davis, Dek Owen, Slim Soua, and Mayorkinos Papaelias An Integrated Approach to Remote Condition Monitoring of UK Railway Assets, WCRR 2016, Milan, Italy, June 2016
- P. Vallely, S. Kerkyras, A. Amini, Z. Huang, E. Giannouli, Shengrun Shi, Slim Soua, Fausto Pedro Garcia Marquez, and Mayorkinos Papaelias. Improving Maintenance Efficiency of Railway Assets by Applying Effective Remote Condition Monitoring Techniques, 2nd International Workshop Towards performance-oriented design and maintenance, Edinburgh, UK, December 2015

- E. Giannouli. Advanced Signal Processing for on-board condition monitoring of railway axle-bearings, Next Generation Rail Conference, Coventry, UK, July 2015

- E. Giannouli, Zheng Huang, Arash Amini, Patrick Vallely and Mayorkinos Papaelias Multi-sensor Acoustic Emission and Vibration signals data fusion for identifying axle bearing failures, CM 2015 Conference and Exhibition, Oxford, UK, June 2015

Table of Contents

Table of Figures

List of Tables

LIST OF ABBREVIATONS

AE	Acoustic Emission
ACFM	Alternating Current Field Measurement
Bw	Bandwidth
BPFI	Ball pass frequency inner race
BPFO	Ball pass frequency outer race
BSF	Ball spin frequency
CM	Condition Monitoring
DAQ	Data Acquisition unit
dB	Decibel
ECT	Eddy Current Inspection
EMAT	Electromagnetic Acoustic transducer
EUAR	European Union Agency for Railways
Fc	Centre Frequency
FFT	Fast Fourier Transform
FTF	Fundamental train frequency
HABD	Hot Axle Bearing Detector
HFRT	High Frequency Resonance Technique
HDD	Hit Driven Data
KPI	Key Performance Indicator
MPI	Magnetic Particle
MPH	Miles per hour
NDT	Non-Destructive Testing
PAC	Physical Acoustic Corporation
PK-PK	Peak to peak
RAMS	Reliability, Availability, Maintainability and Safety
RCF	Rolling Contact Fatigue
RCM	Remote Condition Monitoring
Sa/s	Samples per Second
SNR	Signal to Noise Ratio
TAADS	Trackside Acoustic array detectors
TSK	Time Spectral Kurtosis
TDD	Time Driven Data
UT	Ultrasonic Inspection Testing
WILD	Wheel Impact Load detector
WPD	Wheel Profile detector

GLOSSARY

Term	Definition
Defect Identification	Detect the type of the defect such as inner or outer race defect in bearings
Defect Quantification	Sort the defective bearings by the fault severity
Harmonics	Multiples of fundamental faulty frequency
Healthy bearing	Defect-free bearing
In- field experiments	Experiments carried out under controlled conditions using a test- train
In-service experiments	Experiments carried out under actual conditions using in-service trains
On-board measurements	When sensors are installed on the test bearing, the collected signals are on-board measurements
Wayside measurements	When sensors are installed on rail track, the collected signals are wayside measurements

1. Introduction

In recent years, the demand for safer and faster rail transportation has increased rapidly. Rail wheelsets and the components they consist of (i.e. axle bearings, axle and wheels) operate continuously under harsh conditions on a daily basis. Hence, wheelset defects can occur at any time during the operational lifetime of the aforementioned components. Therefore, more rigorous remote condition monitoring measures should be taken.

A reliable online condition monitoring system should be able to identify the presence of any incipient bearing flaw. Early detection of a defect can decrease maintenance costs, prevent machine degradation and catastrophic failures. The findings of a recent survey published by the European Union Agency for Railways (EUAR) confirmed that 1721railway accidents have taken place in the EU-28 countries in 2018. The cost of these accidents has been estimated to be at 5 billion Euros. If the precursors of the railway accidents are detected successfully in time, the likelihood of preventing future train derailments will be increased and associated maintenance and disruption costs could be significantly reduced. The main precursors of the railway accidents are the broken wheels, axles and rails, wrong-side signalling failures, track buckles and signals passed at danger (EUAR 2020). Figure 1.1 shows a schematic of railway accident precursors in EU between 2014 and 2018 (EUAR 2020)..

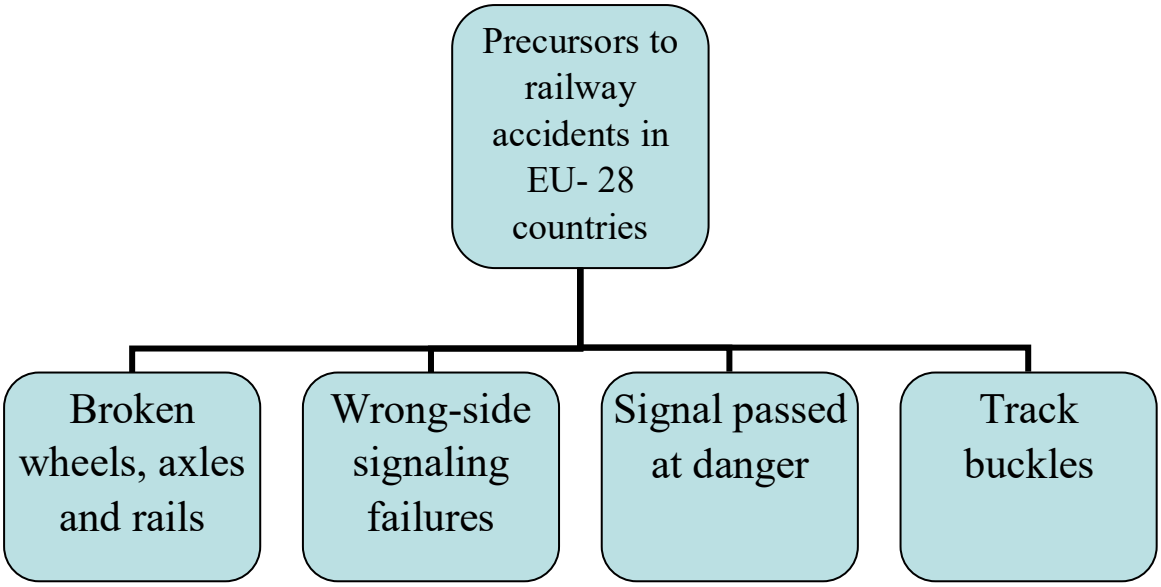

Figure 1-1: Schematic of railway accident precursors in EU-28 Countries between 2014 and 2018 (EUAR 2020)

The rail industry needs to address the following operational challenges in the forthcoming years (F. P. G. M. a. M. Papaelias 2013; Ph Papaelias et al. 2008):

- Reduction of train delays and derailments to an absolute minimum
- Development of new railways to accommodate the continued growth in demand
- Increase railway sustainability in both environmental and financial terms

Rolling stock or infrastructure defects and faults are the main causative factors of train derailments (F. P. G. M. a. M. Papaelias 2013; Ph Papaelias et al. 2008; Ulianov et al. 2014). Various inspection techniques are currently in use or being developed for the evaluation of railway infrastructure defects (Al-Dalabeeh et al. 2012; Edwards et al. 2008; Munoz et al. 2013; Nicholson et al. 2011; M. P. Papaelias et al. 2009a; M. P. Papaelias et al. 2009b, 2010; M. Papaelias et al. 2012; F. P. G. M. a. M. Papaelias 2013; Peng et al. 2014; Peng et al. 2015; Ph Papaelias et al. 2008; Rowshandel et al. 2011; Ulianov et al. 2014; R. Yang et al. 2015).

Wheels containing flats, shelling or metal build-up are sources of repeatable severe impact loads on the rail. Also several cases of severe derailments have been the result of faulty axle bearings. Different types of Remote Condition Monitoring (RCM) systems can be installed wayside in order to identify the presence of rolling stock defects (Amini 2016a; Amini et al. 2016b; Z. Huang et al. 2014a; Zheng Huang 2017; M. Papaelias et al. 2012; M. Papaelias et al. 2014a; M. Papaelias et al. 2016) . RCM of critical rail infrastructure assets is a realistic alternative which should be in place in time in order to accommodate the continuous growing demand for rail transport and avoid capacity bottlenecks in the short to medium term.

Acoustic Emission (AE) and Vibration Analysis (VA) are passive RCM techniques which can be applied for the evaluation of wheels, axle bearings and bogie suspensions. They can also be interfaced with existing RCM state of the art systems.

1.1 Project Aims and Objectives

The main objectives of current work are summarized below.

- A general review of commercial and non-commercial RCM systems for railway wheelsets.Six commercial and three non-commercial systems are described in the current thesis. A comparison between the University of Illinois at Chicago on-board monitoring system and the current study was also carried out.
- A brief review of railway rolling stock wheelsets and faults. Wheel, axle and axle-bearing defects are described. Root causes of fault initiation are also discussed.
- A comprehensive review of Advanced Signal Processing techniques.Comparison between Advanced Signal Processing algorithms is also described
- Evaluation of AE and vibration signal analysis for damage detection of rolling stock wheelsets. On-board and wayside signals have been recorded. Time, frequency and time-frequency analysis have been considered for processing the acquired data.
- Laboratory tests on University of Birmingham, field trials under control operational conditions on Long Marston and in-service measurements under actual operational conditions in the UK network were carried out.
- Development and assessment of the system's signal processing module.Fault detection, defect type evaluation and fault quantification can be achieved using appropriate signal analysis methodology.
- Detect any potential axle bearing fault on in-service trials during the signal processing. A number of potential faults have been detected. The results need to be confirmed with the help of Network Rail.

The main results of the present thesis together with the experimental methodology employed are presented and discussed in the chapter 6 and in chapter 7. Discussion of the results obtained are also presented in Chapter 7. The main conclusions and recommendation for future work are also described in the last chapter of the current thesis.

1.2 Structure of Thesis

The main points of the current work are described at next Chapters.

In Chapter 2, Railway rolling stock wheelsets and faults are reviewed. Wheel, axle and axle bearing defects are presented briefly.

Chapter 3 describes RCM Inspection techniques for railway rolling stock wheelsets. Commercial and Non-Commercial RCM systems for railway wheelsets are described and reviewed.

Chapter 4 presents the fundamental of AE and Vibration Signal analysis. Rolling Stock Integrity can be achieved by the proposed monitoring system.

Chapter 5 presents Signal Processing Techniques that are widely used for wheel and axle bearing fault diagnosis. Step by step algorithm description is presented in order to assist the reader to understand the choice of the proper type of analysis in different case studies.

In Chapter 6, Results and data analysis performed during this work are described. Laboratory and field tests were carried out in order to assess the ability of AE and Vibration Monitoring Techniques in wheel and axle bearing damage detection. Representative results are shown the accuracy and the reliability of the novel system.

2. Railway rolling stock wheelsets and faults

2.1 Introduction

The wheelset is one of the fundamental components of all railway rolling stock. Rolling stock wheelsets consist of wheels, the axle and axle bearings (M. Papaelias et al. 2014b) Various faults can arise in any of these components at any time during their operational cycle but more common are wheel and axle bearing defects (Amini 2016a). Harsh operational conditions such as rolling contact fatigue (RCF), thermal variations and dynamic impact forces are the main reasons for wheelset fault development in service (Amini et al. 2016c). Wheelset defects are also associated with damage to the rails due to impact loads they cause, increasing maintenance costs, environmental noise and vibration, reducing passenger comfort, increasing fuel consumption, resulting in operational delays and even train derailments (Z. Huang et al. 2014a) . Real-time wheel and axle bearing fault detection is of paramount importance for rail infrastructure managers and rolling stock operators. Timely maintenance can thus be planned helping maximise the availability of railway assets.

2.2 Wheel Defects

In-service wheel defects arise due to the adverse operational conditions (e.g. high loads, RCF, etc.) that the wheels are subjected to. The most common wheel defects are flats, shells, cracks, corrugation, cavities and metal build-up. Detrimental effects on track and other vehicle component such as rail, sleepers and bearings may arise by wheel faults, especially

wheel flats (Nielsen and Johansson 2000). Rail structural deterioration and possibly rail failure can occur because of the high dynamic loads caused by wheel thread defects. Therefore, wheel defects should be detected as early as possible and preferably in real-time.

Manual inspection using various NDT techniques (visual, ultrasonic testing, magnetic particle inspection, magnetic flux leakage, eddy current testing or liquid penetrant inspection) are currently employed during scheduled maintenance on out-of-service rolling stock (Anastasopoulos et al. 2010). The main types of wheel defects are discussed next.

2.2.1 Wheel flats

Wheel flats are a common out-of-round wheel defect affecting in-service railway wheelsets. Wheel flats are effectively flat zones on the wheel tread caused by unintentional sliding of the wheel on the rail track when the brakes lock (Vyas and Gupta 2006). When brakes do not function properly or heavy braking is applied, e.g. during an emergency stop, the wheel-rail friction becomes high and the wheel rotation is hindered causing the wheel to slide along the rail, resulting in the development of a flat. Hence, the quality of braking is of paramount importance. Wheel flats cause high impact loads on the railway track, the bearing and other parts of the vehicle (Z. Huang et al. 2014b) resulting in cracked sleepers, damaged rails and act as precursors to bearing defects (Barke and Chiu 2005; Bladon et al. 2004).

According to the standards published by the Rail Safety and Standard Board (RSSB) when a wheel flat is spotted, the length of the flat around the circumference of the wheel should be measured in order to take appropriate maintenance actions. The exact type of action depends on the extent of the wheel flat severity and the type of train affected (RSSB 2010). Generally,

tolerances on wheel flat defects are much smaller for high-speed trains in comparison with freight wagons.

Figure 2.1 shows a railway wheel with multiple wheel defects.

Figure 2-0-1: Photograph showing multiple wheel flats

2.2.2 Cracking

Cracks can be categorized based on the root cause factor, i.e. either rolling contact fatigue (RCF) or thermomechanical fatigue cracks. Figure 2.2 shows RCF cracks on wheel tread surface (Y. Liu et al. 2020). RCF cracks arise because of cyclic stresses in the wheel-rail interface. A crack initiates because of a high contact stresses at the surface of the wheel tread (Ekberg and Kabo 2005). Thermomechanical fatigue cracks are caused by frequent braking resulting in sharp increase in the temperature of the surface of the wheel tread combined by high contact stresses. In order to prevent crack propagation and further damage to rails, cracks should be removed when the wheel is turned during maintenance. However, if turning does not remove completely crack sites then the wheel should be retired.

According to the provisions stated in the relevant RSSB standard (RSSB 2010), when cracks are located in a wheel's tread, rim or flange, the wheelset should be removed from service into repair facilities with a restricted speed of 45 MPH or less. However, where an isolated crack longer than 20 mm is identified, the wheelset is removed from service within 24 hours of the fault being found.

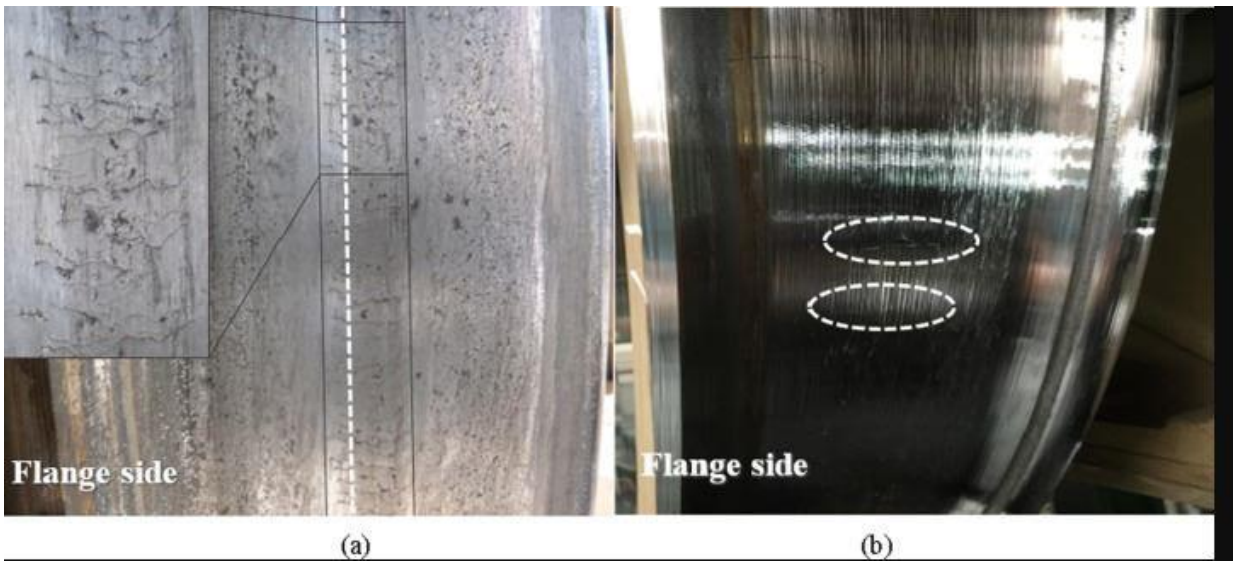

Figure 2-2: Photographs (a) and (b) showing RCF cracks on wheel tread surface(Y. Liu et al. 2020)

2.2.3 Shelling

Shelling is manifested when large pieces of metal along the surface of the wheel break off. Wheel shelling is developed from surface or/and subsurface cracks initiating by localised stress concentration areas within the wheel rail contract zone due to high axle load and creep forces (Saferail). Figure 2.3 shows shelling on wheel tread (M. Papaelias et al. 2014b).

Figure 2-0-3: Photograph showing shelling on wheel tread (M. Papaelias et al. 2014b)

Vermeulen et al. presented the ability of high frequency vibration technique in detecting wheel tread defects. During this case study it was shown that wheel cracks and shelling can be detected based on the response of the accelerometer (Vermeulen et al. 2010).

2.2.4 Wheel metal build –up

This defect is the result of excessive braking force causing the wheel to slide (Cummings and Sammon 2015). As the wheel slides high frictional forces result in an increase in the temperature of the wheel tread whilst material wears out. The material wearing out subsequently melts and adheres onto the wheel surface resulting in metal to build-up on the tread surface. Wheel metal build-up is a common wheel tread defect in cold weather conditions. Figure 2.4 shows wheel with metal build-up defect during experiments at University of Birmingham (Amini et al. 2016a).

Figure 2-0-4 shows wheel with metal build- up defect during AE experiments at University of Birmingham (Amini et al. 2016a).

2.2.5 Corrugation

Corrugation is an undesired and expensive to repair defect that results in decreased rail and wheel lifetime. Appreciable temperature difference between some parts of the wheel tread is a common issue due to wheel blocking during braking. The warmest wheel tread regions are subject to more wear when the temperature decreases. The volume of the material at these regions also decreases resulting in corrugation patterns in the wheel tread (Nielsen and Johansson 2000). Hence, excessive rolling noise and vibration are produced having an adverse effect on the comfort of passengers (Bracciali and Cascini 1997).

2.3 Axle bearing defects

Axle bearings are lubricated rotating components installed between the axle and the wheel. They are critical components in any rotating machinery. Tapered roller bearings are widely used in the rail industry (Z. Huang et al. 2014b) and are the type of the bearing design that has been considered in this study . The schematic diagram in figure 2.5 illustrates a tapered roller bearing assembly(Timken 2015).

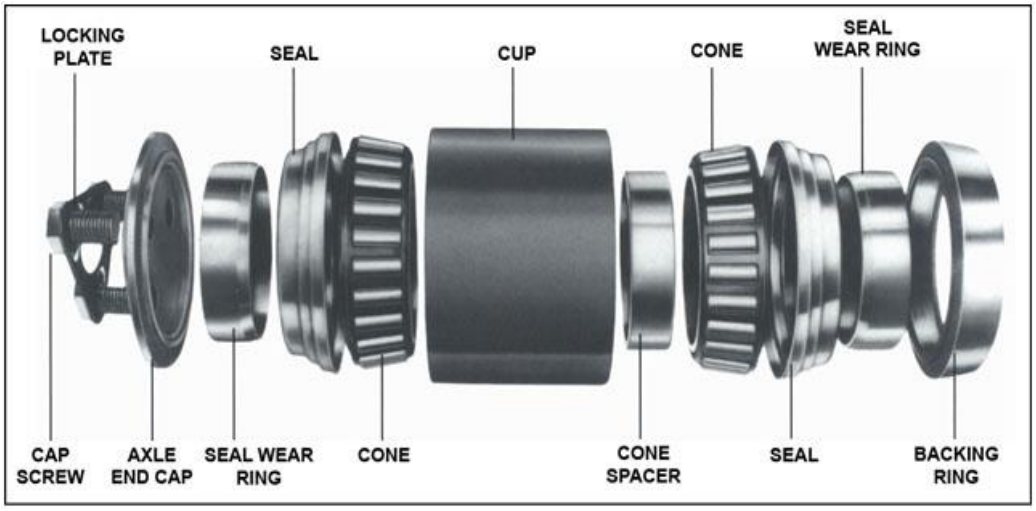

Figure 2-0-5: Schematic of a tapered roller bearing (Timken 2015)

Railway bearings can develop various types of defects in service, including roller skewing, race spalling, loose cone, fretting, lack of sufficient lubrication or contamination, and others. In the UK, rolling contact fatigue of the bearing outer race is the most common bearing defect type encountered (Corni et al. 2015).

Bearing defects can be classified as distributed and localized defects (Patidar and Soni 2013). Table 2.1 summarizes the common types of bearing defect.

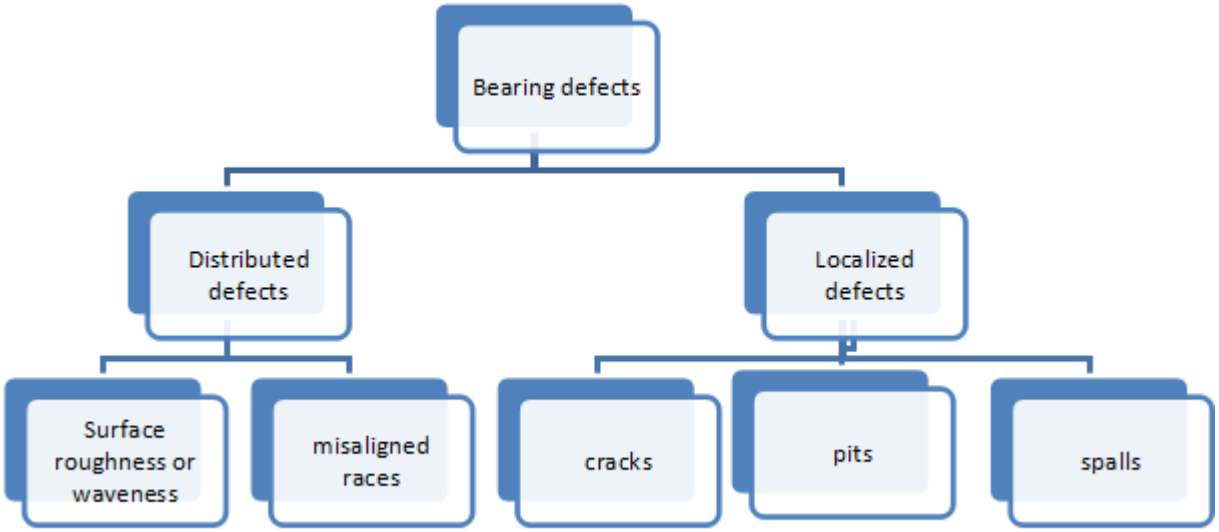

Table 2.1 : Schematic summarizing the common types of bearing defects

Axle bearing fault initiation can result from a variety of root causes. A bearing commonly deteriorates because of external factors such as high impact forces acting through the wheel on the bearing, water ingress and poor assembly (Bladon et al. 2004). Rarely the aforementioned root causes are addressed before the bearing is replaced. Depending on the root cause factor, different bearing failures can occur. According to bearing manufacture SKF, the causes of a bearing damage or failure can be categorized into four main groups (SKF 2017). Figure 2.6 shows bearing damaged or failure causes (SKF 2017).

Generally, a bearing will eventually fail due to the material fatigue. Material fatigue begins from both surface and sub-surface initiated failures (Symonds et al. 2015). When an axle bearing is about to fail, its immediate removal is the only possible option(Snell and Nairne 2008)

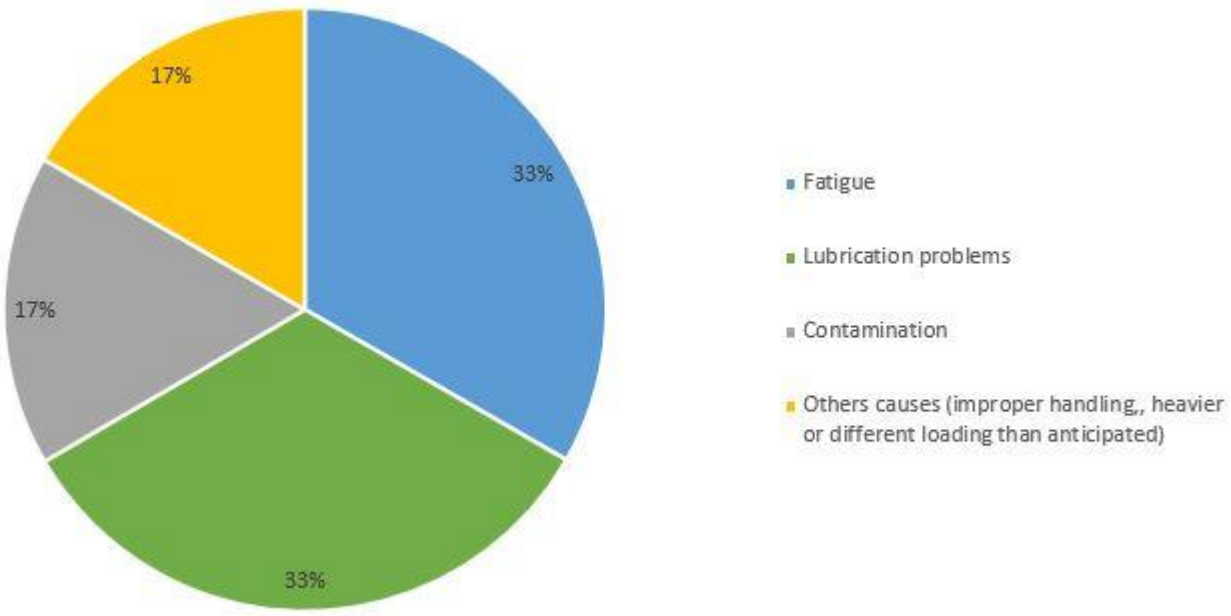

Figure 2-0-6 : Photograph showing bearing failure causes (SKF 2017)

Bearing failures are responsible for train accidents around the world (Z. Huang et al. 2014a). For example, the derailment of Tara Mines freight train at Skerries on 10/01/2008 was caused by a bearing failure (figure 2.7). No temperature alarms were reported by the hot axle box detectors (HABDs) leading to bearing heat up bearing seizure and eventually train derailment (Railway Accident Investigation Unit 2009) .

Figure 2-0-7 : Photograph showing derailment of Tara Mines freight train at Skerries on 10/01/2008

Train derailments caused by faulty axle bearings are associated with axle journal rupture. Once a bearing becomes stuck, one of the wheels is blocked and the other continues to rotate as normal resulting in axle journal rupture after a few kilometres due to the high stresses arising from the abnormal motion of the wheelset (Amini et al. 2016a).

Deterioration of the structural integrity of axle bearings can be detected using AE, vibration or temperature measurement data. Sensors, depending on their type, can be installed either on-board or wayside or both (M. Papaelias 2012). Generally, axle bearing degradation results in an increase in noise and vibration followed by temperature rise (Corni et al. 2015). Noise can commonly detected by acoustic monitors whereas vibration by accelerometers. The temperature of axle bearings is measured by infrared sensors but only a few kilometres before the final bearing failure, the alarm threshold is exceeded.

2.4 Axle defects

Railway axles are components that are subjected to heavy loading conditions during service. The train weight is supported by the axle via the external axle bearings. Vehicle-track interaction (e.g. due to track irregularities) also adds dynamic loads on the axles. Furthermore, asymmetrical axle loading occurs due to the train structure (curving) (Luke et al. 2011).

Axle design can be solid or hollow. In the UK, railway axles are solid with the exception of Eurostar rolling stock which has hollow axles. Railway axles can suffer from different types of faults such as axle rupture, pitting corrosion and fatigue cracks (Vallely 2015). The most common axle integrity issue is corrosion. The current state of the-art corrosion assessment procedure is mainly based on Visual Inspection (VI) (John Rudlin et al. 2014). The extent and the depth of corrosion should be measured in order to take appropriate measures of coping with the resulted corrosion issues. Axle defects rarely occur accounting for less than 2% of the total number of rolling stock defects reported. As a result, the primary concern of railway industry is focused on axle bearing and wheel defects. Figure 2.8 shows of final failures at the railway axle. Cracks have been highlighted by color contract (Rolek et al. 2016).

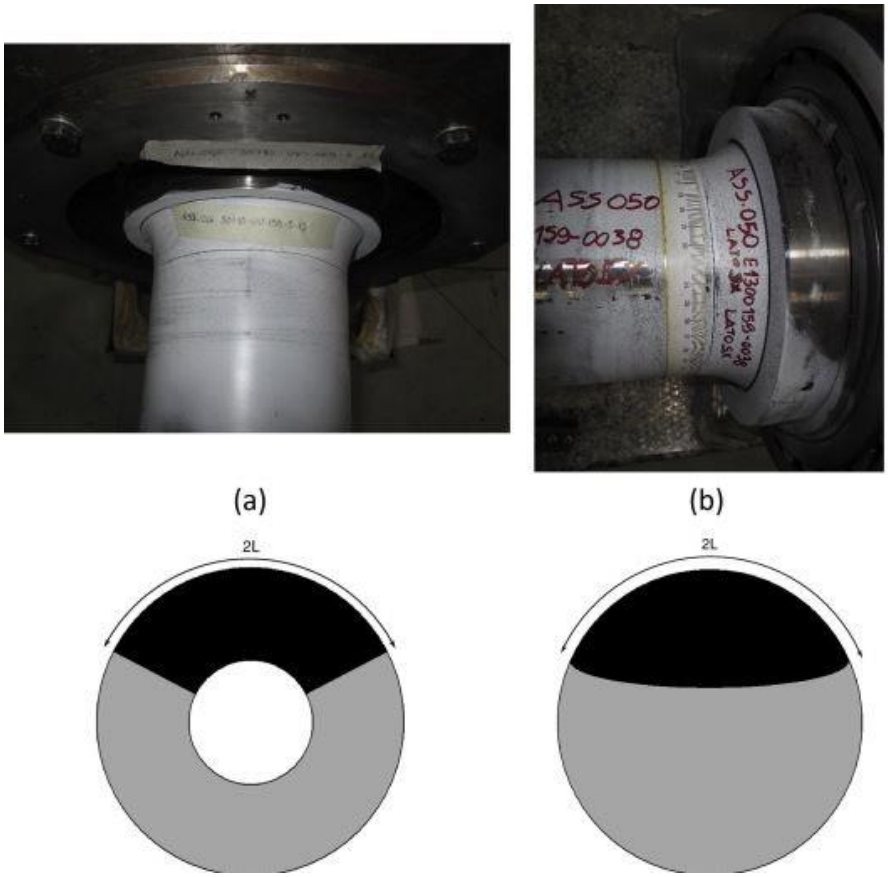

Figure 2-0-8: Examples (a and b) of final failures at railway axle (Rolek et al. 2016).

2.5 Bogie Suspension defects

A typical bogie consists of two wheelsets, primary and secondary suspensions and a brake system (Z. Huang et al. 2014b). The primary suspension is responsible for absorbing shocks between the bogie, the frame and the axle bearing, whereas the secondary suspension is responsible for absorbing shocks between the bogie and the rail vehicle body. Defects either in primary or secondary suspension could lead to the reduction of passengers' comfort due to continuous vibrations, increasing the likelihood of an axle bearing defect or severe wheel damage, and hence possible derailments (Vallely 2015). The photograph in figure 2.9 shows a typical bogie suspension.

Figure 2-0-9: Photograph showing a typical bogie suspension

3 Inspection and RCM techniques

This chapter presents the most common NDT inspection techniques, the RCM systems currently in use by rail infrastructure managers and some examples for non-commercial RCM that are under development for the evaluation of the structural integrity of railway wheelsets.

3.1 NDT for railway rolling stock wheelsets

Rolling stock or infrastructure defects and faults are the main causative factors for train derailment. Various inspection techniques are currently in use or being developed for the evaluation of railway wheelset defects. Among the possible NDT techniques that can be employed for defect inspection at railway wheelsets are Visual Inspection, Magnetic Particle Inspection, Magnetic Flux leakage, Ultrasonic Testing, Eddy Current Testing, Alternating Current Field Measurement, liquid penetrant inspection and lubricant analysis. These key methods are discussed next.

3.1.1 Visual Inspection (VI)

Visual inspection (VI) is inexpensive, simple and does not require any sophisticated equipment in order to be carried out. The condition of the wheel is checked offline. VI is performed using gauges in order to evaluate the contour, flange condition and rim thickness. The development of automated visual inspection systems allows conventional VI methods to be replaced. However, automated VI is practically never used for wheelset inspection due to its cost.

Depth of the defect and beneath the surface defects cannot be detected with visual inspection alone. Due to its limitation, VI must be combined with other NDT methods in order to detect and quantify damage in the inspected component.

3.1.2 Magnetic Particle Inspection

Magnetic Particle Inspection (MPI) is a NDT method for surface and very near-surface flaw detection. A magnetic field is induced in the ferrous material. The principle of this inspection technique is that the magnetic flux distortion caused by a defect will result in some magnetic flux to leak at the surface rendering a crack-type defect detectable (Štarman and Matz 2010). Wheel or axle defects can be revealed by spraying the component with a ferrous particle ink (JR Rudlin and Shipp 2003). In cases where no defect is present, the flux will remain contained below the surface of the ferrous material. Figure 3.1 shows the MPI principle.

MPI for railway axles requires axle removal from service. This can cause inconvenience to rolling stock availability and increase maintenance costs. In addition, as a manual method, the operator's interpretation can influence the inspection results. Therefore, MPI is usually integrated with UT.

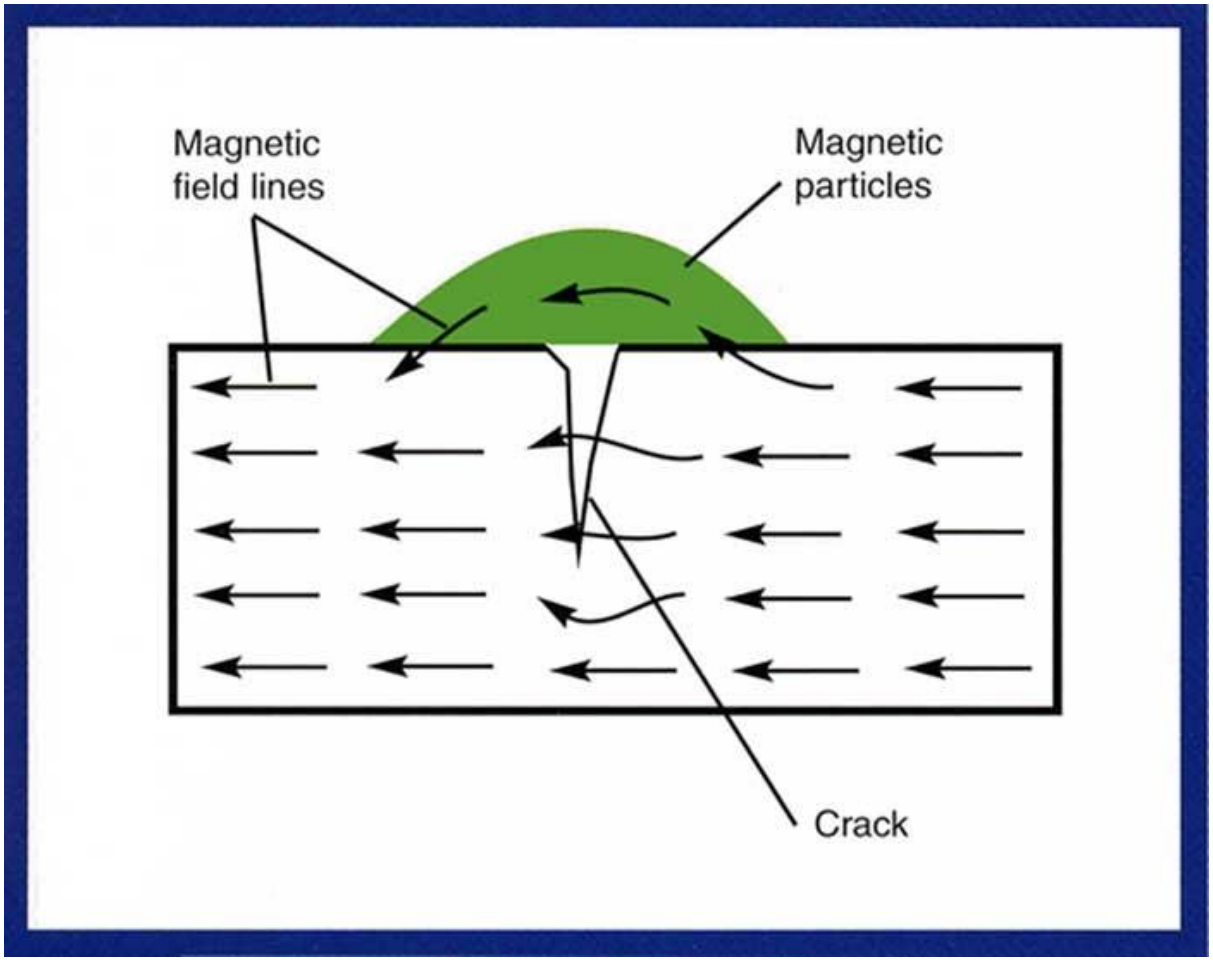

Figure 3-0-1 : Magnetic Practicle Inspection method

3.1.3 Magnetic Flux Leakage

Magnetic Flux leakage (MFL) is a magnetic based NDT technique that has been applied in structural health monitoring of wheel tread. The principle of this method is similar to that of MPI since the magnetic field will leak at areas where a defect exists. Magnetic sensors detect the leakage field. With the help of appropriate signal processing of the MFL data obtained, the damaged areas and the amount of metal loss can identified and evaluated (Xu et al. 2012).

MFL is able to detect large surface and relatively deep near-surface defects. Eddy current testing although more sensitive than MFL, can only inspect the top 3mm of the material.

MFL performance deteriorates at higher inspection speeds but in the case of axle inspection this is not a factor of concern. MFL can be integrated with UT in order to improve quantification accuracy for any defects detected whilst deeper defects can be detected and quantified (Ph Papaelias et al. 2008). Figure 3.2 shows the principle of MFL testing. Figure 3. 2 (a) shows the magnetic field response for a component with no damage present whereas Figure 3.2 (b) shows the change in magnetic flux pattern due to metal loss at the surface of the component. The flux leakage is clearly visible.

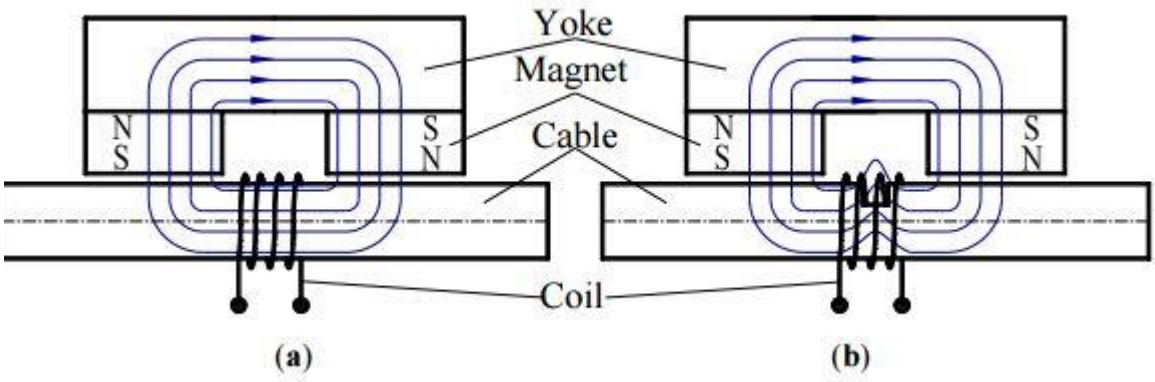

Figure 3-0-2 : a) Undamaged cable ; (b) Cable with metal loss (Xu et al. 2012)

3.1.4 Ultrasonic Testing

Ultrasonic Testing (UT) is one of the most widely used NDT methods with various applications in railways, welding, marine, and aerospace. This inspection technique uses high frequency sound waves (ultrasound) emitted and received using piezoelectric transducers. Typical UT frequency range is from 400 kHz to 25 MHz (Singh 2020) . Various wave modes can be generated but most commonly transverse and longitudinal are employed in the majority of inspections. Typically an UT inspection system consists of two main components, the transducer and a measurement unit. The transducer generates and receives high frequency sound waves. The received waves produce electric pulses which are subsequently digitised

and visualised on the screen of the measurement unit. An example of UT inspection system is shown in Figure 3.3.

A water or water-based gel can be used as a couplant between the inspected material and the transducer in order to enhance the signal to noise ratio (SNR) and minimise acoustic impedance mismatch between the transducer and test piece. However, a couplant is not required when an Electromagnetic Acoustic Transducer (EMAT) is used in ultrasonic testing.

The UT inspection method is sensitive to both surface and sub-surface defect. Ultrasonic techniques enable a fast and non-destructive evaluation of stress states in the rim of railroad wheels (Kappes et al. 2000).

In order to improve the quality of the inspection, ultrasonic phased arrays can be used for both wheel and axle inspection. This advanced method of ultrasonic testing can also contribute in improving its detection ability of smaller defects. However, it can still miss surface defects resulting in combination with other NDT techniques such as MPI and Eddy Current testing (John Rudlin et al. 2006).

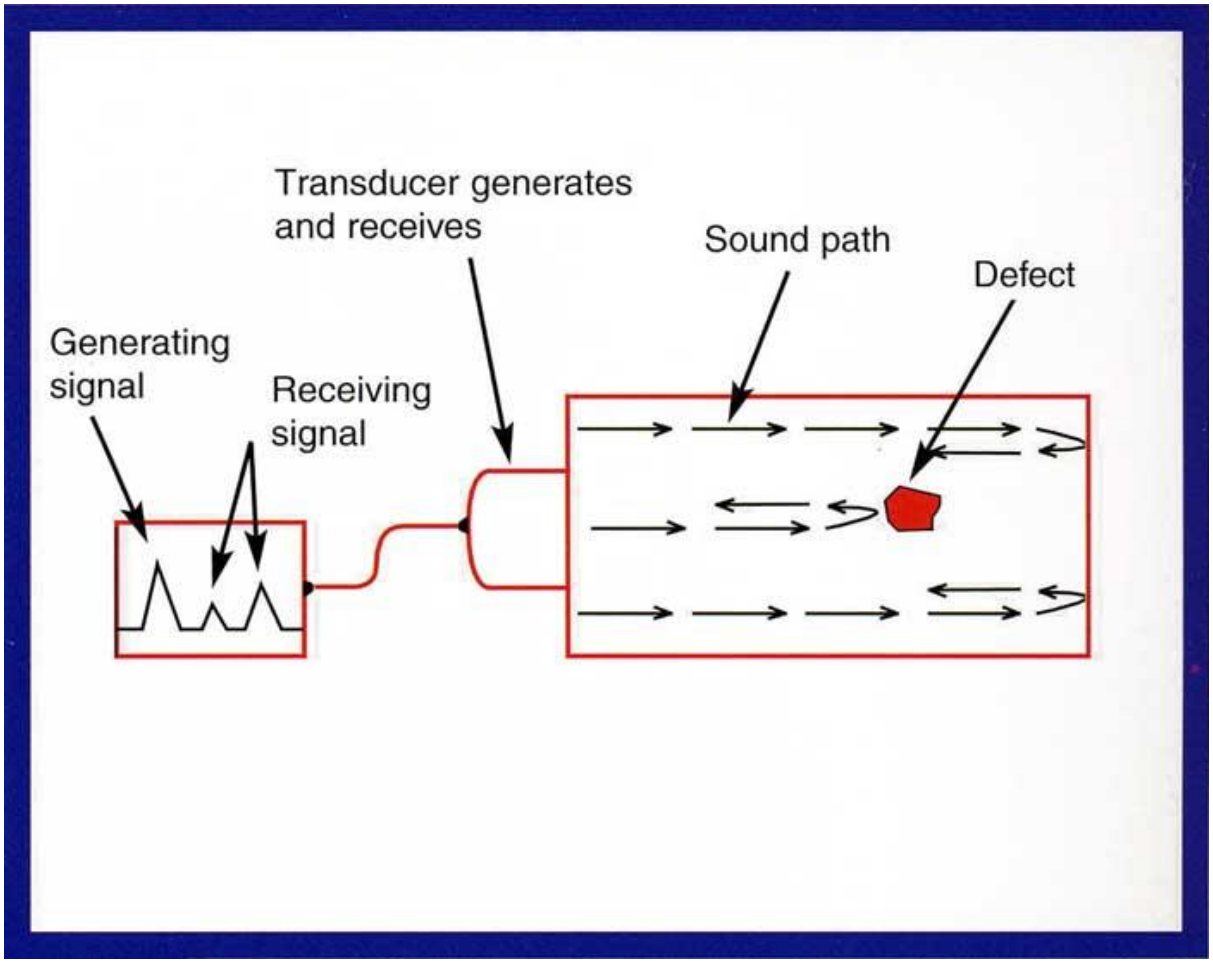

Figure 3-0-3 : Ultrasonic inspection system (NDT)

3.1.5 Eddy Current Testing

Eddy Current Testing is a surface inspection technique that has been used for detecting defects in railway wheelsets. Conventional eddy current sensors typically contain one exciting and one sensing coil (Ph Papaelias et al. 2008). When an exciting coil is fed with alternating current (AC), a varying magnetic field is developed in and around it. If the coil is brought near the surface of a conductor eddy currents are induced near its skin due to the variations in the alternating magnetic field produced by the coil. The induced eddy currents subsequently give rise to a secondary magnetic field which will also vary with time and will get distorted in the presence of a defect. Hence, when a defect is present, the eddy currents

will fluctuate resulting in variations of the secondary electromagnetic field which give rise to impulse changes. If there is no defect, the impedance of the eddy current sensor remains constant. Deeper defects may not be detected by eddy current testing due to the limited penetration depth at higher inspection frequencies.

The eddy current sensors are sensitive to small surface or near-surface defects whereas the conventional ultrasonic transducers have limited ability of detecting these types of defects (Ph Papaelias et al. 2008; Pohl et al. 2004). Eddy current testing can be used not only for defect detection but also for defect quantification.

The principle of eddy current testing is shown in Figure 3.4. When a defect is present, the circumferential eddy current distribution on the material and the defect interact resulting in changes of electrical impedance from Z1 to Z2 as shown in the Figure 3.4. (Pohl et al. 2004).

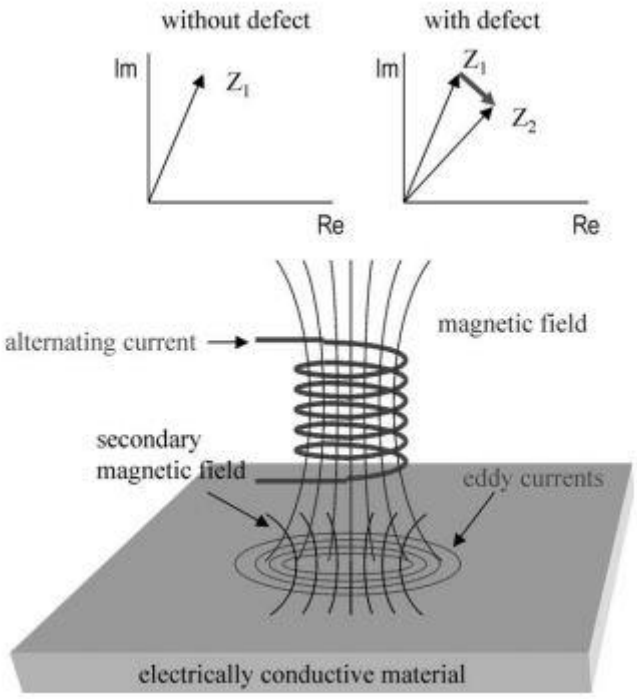

Figure 3-0-4 :Eddy current testing principle (Pohl et al. 2004)

3.1.6 Alternating Current Field Measurement Inspection Technique

The ACFM is an inspection technique capable of both detecting and sizing (length and depth) surface breaking cracks in metals. An alternating current (AC) is placed on or near the test sample. When no defects are present, the electrical current field will be undisturbed. However, if a defect is present, the uniform current field lines are disturbed resulting in current lines flowing around the ends and down the faces of the flaw (Topp and Smith 2005). Figure 3.5 shows alternating current lines flowing when a defect present (M. P. Papaelias et al. 2009a).

ACFM is currently gaining ground into the research NDT community due to its ability for high-speed inspection and quantification of fatigue defects, better tolerance to lift-off variations and for detecting defect with the presence of coatings and grease (Ph Papaelias et al. 2008; Topp and Smith 2005). However, ACFM is not sensitive to detecting sub-surface defects (Ph Papaelias et al. 2008).

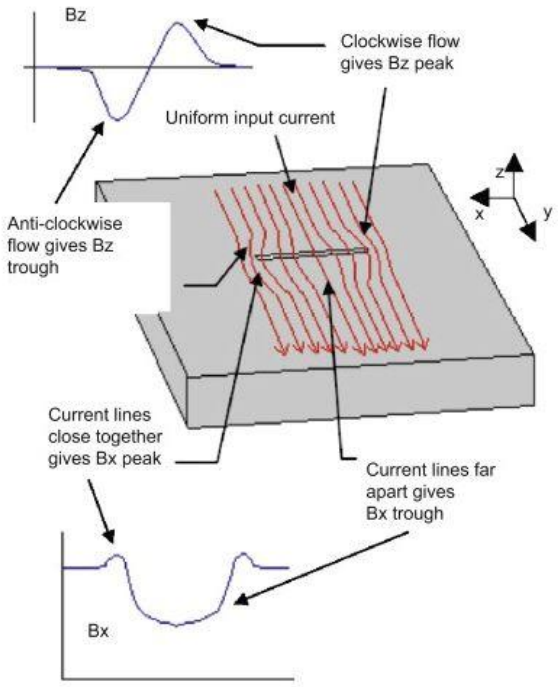

Figure 3-0-5 : ACFM currents flowing around a defect (M. P. Papaelias et al. 2009a)

3.1.7 Lubricant Analysis

One of the main causative factor for axle bearing defect initiation and propagation is lubricant quality degradation. Bearing lubrication can reduce the friction, promoting heat evacuation and increase bearing remaining life (C.Vale 2014). Lubricant analysis can effectively detect bearing defect at its initial stages under laboratory conditions. However, lubricant analysis cannot be performed on-line resulting in undetectable bearing defects that have become critical in service. During the inspection, rolling stock is removed from service and the axle-box is opened for VI and for lubricant sample collection.

3.2 Commercial RCM systems for railway wheelsets

Different types of RCM systems can be installed wayside in order to identify the presence of rolling stock defects, enabling proactively scheduled inspections and initiation of corrective actions without any human intervention (Dornfeld 1990). In order to do this, RCM systems should be inert to any environmental changes and any rolling stock defects should be reliably detectable in time before failure occurs. Moreover, understanding the nature of wheelset flaws can enhance proper maintenance and minimize false trains stops for defects inspection (Bladon et al. 2004). Wayside RCM systems consist of various types of sensors (Barke and Chiu 2005) , which are installed on or next to the track in order to identify the presence of potential wheelset and bogie faults (Z. Huang et al. 2014b). Such systems measure several parameters such as axle bearing temperature and impact loads that are applied on the rail. Wayside sensors should be able to remain unaffected by changes in weather conditions, vibration from passing train and track circuits. The main advantage of wayside over on-board RCM systems is that they can monitor thousands of bearings and wheels on a daily basis (Cline et al. 1998). In addition, on-board RCM systems should be capable of adjustment in different type of train. However, the transmission path between sensor and rolling stock fault

is less in on-board rather than in wayside systems. The cost of the systems should be also taken into account in deciding which types will be employed and where should be installed. The only case that on-board temperature sensors are installed by law is on high-speed (>250km/h) passenger rolling stock to continuously monitor axle bearings for abnormal heat build-up.

Each type of RCM system has its own benefits and limitations. Therefore, a combination of on-board and wayside RCM systems could be a solution in order to maximise reliability. Wayside monitoring technologies can be categorised in two groups; reactive and predictive (Lagnebäck 2007). The existing wayside condition monitoring systems are based on infrared cameras, acoustic arrays and strain gauges (M. Papaelias et al. 2014b). Despite significant investments by the rail industry in this area, these systems do not provide the appropriate information about the condition of the wheelsets and the bogie.

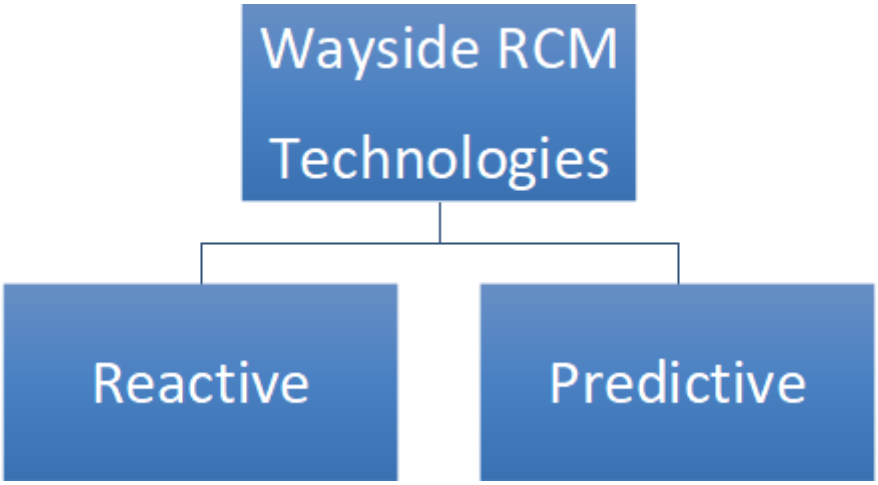

Table 3.1 : Schematic of wayside RCM technologies (Lagnebäck 2007)

Ideally, the key attributes of the wayside detectors are (Bladon et al. 2004):

- Detection of as many rolling stock defects as possible
- Minimizing the number of false alarms

In addition, predictive wayside RCM systems should meet a more rigorous set of additional operating requirements (Bladon et al. 2004):

- A universally applied system in monitoring any train in the rail network.
- Significant number of installations throughout the rail network
- High detection sensitivity in wheelsets defects at initial stage
- Data correlation to evaluate interrelated defects

Therefore, a reliable and cost-effective wayside RCM system should prevent rather than detecting an imminent wheelset failure .

3.2.1 Hot Axle Box Detector (HABD)

Hot Axle Box Detectors (HABDs) are currently among the most commonly used detection technologies in Network Rail (Z. Huang et al. 2014a). A HABD is a reactive RCM technology which applies infrared sensors installed on the wayside of the rail track in order to identify the presence of overheating bearings and stuck brakes indicating the presence of a serious fault (M. Papaelias et al. 2014b). The infrared detectors usually work independent from each other as individual check-points. The operational principle of the HABD is based on the detection of an exceeded temperature threshold of the axle bearing, triggering an alarm which indicates imminent failure (Barke and Chiu 2005). However, HABDs can only detect problems once they have become critical whilst they are also prone to measurement errors. False alarms can occur by other nearby wheelset components such as the brake pad that may be become hot and trigger the alarm. Up to 80% of hot box alarms are false resulting in unnecessary costs and in disruption of the operational network (M. 2012) .The cost of train stop can reach in thousands of Euro. HABDs are expensive systems. As a consequence of their high cost, they are installed in regular intervals every 15-100km throughout the network.

Each site instrumented costs 70-100k Euros. The figure 3.6 presents the Pegasus hotbox detector that is capable of monitoring both in-board and out-board bearings.

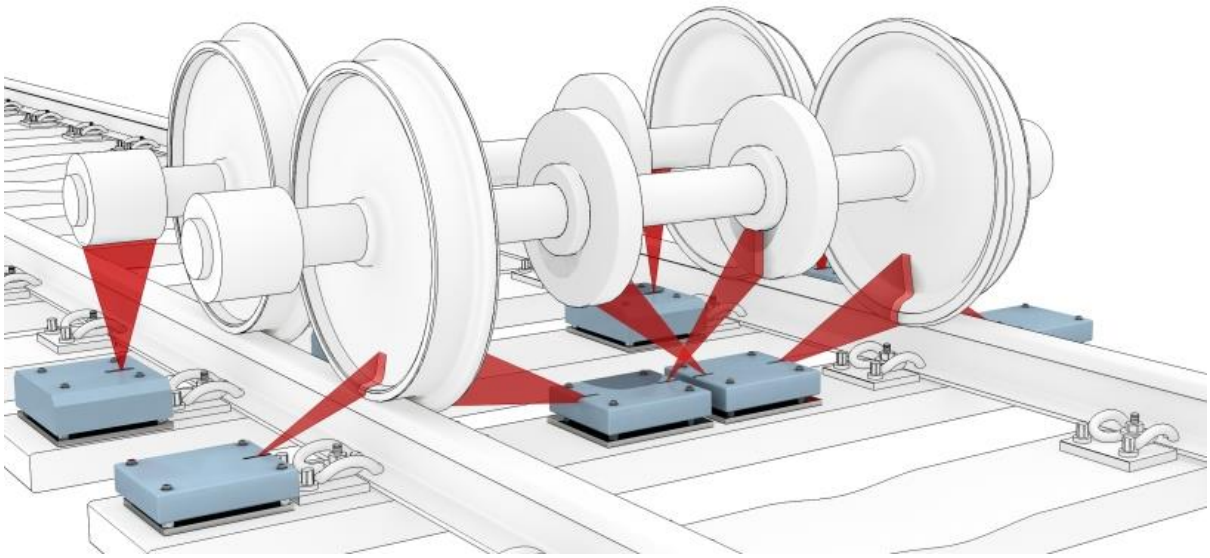

Figure 3-0-6 : Schematic of the Pegasus hotbox detector by MER MEC. The schematic is courtesy of MER MEC Group.

3.2.2 Acoustic Array Detector (AAD)

An Acoustic Array Detector is a predictive monitoring technology which uses arrays of microphones to record the sounds produced by the axle bearings and isolate them from the environmental noise of the surroundings (M. Papaelias et al. 2014b). It uses track-side mounted equipment that is positioned a few metres away from the rail track. The RailBAM (Railway Bearing Acoustic Monitor) and TADs (Track-side Acoustic Detector) systems are commercially available at the moment. The systems are able to recognize a bearing's condition. Then, the analysed data are categorized by the type and the severity of the defect is classified as early, moderate or severe defect. The acoustic signature is transmitted from the bearing, through the structure of the wheelset/bearing housing/bogie and propagated over the

air outwards the sensor arrays. The operational frequency of the microphones is between 22 kHz and 44 kHz. The recorded raw signal consists of the faulty bearing's sound and of the surrounding train noise. In order to isolate and further analyse the faulty bearing signal, data trending is required (Z. Huang et al. 2014b). According to the manufacturers of the system, AADs can potentially identify the presence of bearing faults except defects in the inward rollers and cones (Y.-J. Zhang 2011). In addition, it is claimed that AADs have been considered to be reliable due to their ability to prevent bearing failure and maximize the bearing life at the same time (Snell and Nairne 2008). Acoustic detectors have been predominately used in Australia and United States. In the UK, AADs trials have been carried out to evaluate the technology. After several trials it was suggested that AADs could detect bearing defects considerably earlier than train riders (Snell and Nairne 2008). However, the author of the present study has been unable to find case studies that support the statement for early bearing fault detection. The operational frequency is very low resulting in unwanted noise contamination of the signal. Unwanted noise can be recorded either from the train itself or from the environment and can cause false alarms. In the case of TADs, a wheel flat can cause a bearing alarm. In addition, in-board bearing faults cannot be detected by the arrays due to system's design. The train speed is also a limitation of this technology due to the system requirement for speed between 30 km/h and 130 km/h resulting in no monitoring of high-speed trains by AADs.

Since 2012, AAD systems have been installed in 3 locations in the UK's rail network and are currently undergoing evaluation (Vallely 2015). The cost per instrumented site (around 0.5M Euro) is also a major consideration for its installation. In figure 3.7 the installation site of one of the RailBAM systems on the UK railway network is shown.

Figure 3-0-7: AADs trial in the UK network near London. The photography is courtesy of SIEMENS (M. Papaelias et al. 2014a)

3.2.3 Wheel impact force load detector (WILD)

The Wheel Impact Load Detectors (WILDs) are reactive RCM systems for assessing the wheel tread condition. They use an array of strain gauges or accelerometers on the surface of the rail line to measure the loads sustained by the rail as a train passes over. WILD is a real-time system that also records the train speed and the time of the measurement, the name of the WILD site, the direction of the train and the weight of the wagon (C. Yang and Létourneau 2005).

As a reactive system, it raises an alarm only when the pre-set threshold has been exceeded but it does record the loads for each of the axles measured. In case that a wheel's impact reaches 140kpsi or more, the driver is informed , the train is stopped immediately and the wheel is replaced (C. Yang and Létourneau 2005).

WILDs are used to identify wheel tread defects such as wheel flats, metal build-up and shelling (M. Papaelias et al. 2014b). Timely detection of a wheel thread defects can prevent structural damage in other rolling stock elements, on rails and crossing. In particular, since axle bearing faults are precursors of the wheel thread defects, WILDs may assist to reduce

bearing fault development. The strain gauges of a WILD attached on the rail is shown in figure 3.8.

Figure 3-0-8: WILD based on strain gauges (photography courtesy of Markus Wong)

3.2.4 Wheel Profile Detector (WPD)

Wheel Profile Detectors (WPDs) are real-time predictive RCM systems. They use non-contact sensors such as high speed cameras and lasers to monitor the wheel tread and flange profile (M. Papaelias et al. 2014b). It measures and estimates several wheel parameters such as wheel diameter, wheel flange angle and flange thickness (Bladon et al. 2004). A typical WPD output is illustrated in figure 3.9.

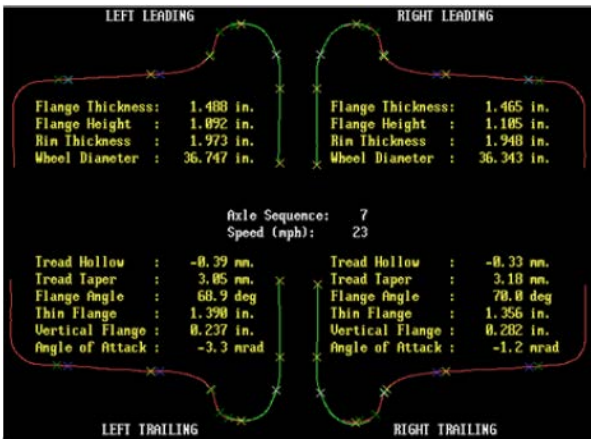

Figure 3-0-9: Typically output of wheel profile detector (Bladon et al. 2004)

The operation of a typical wheel profile system is based on the fundamental principles of predictive systems. It compares the processed wheel profile against the standard profile (Barke and Chiu 2005). A predicted maintenance schedule can then be carried out, if the measured output does not meet the reference requirements.

The main advantages of WPDs are (Lagnebäck 2007) (Barke and Chiu 2005):

- High accuracy of wheel profile generation
- Data trending resulting in the estimation of wheel remaining life
- Correlation with other condition monitoring systems
- Elimination of manual profile inspection

However, the common limitation of WILDs and WPDs is that cannot detect axle bearing faults.

3.2.5 SKF Axletronic

SKF is one of the most popular axle bearing manufacturer, has developed the Axletronic system for on-board condition monitoring of in-service axle bearings. The SKF Axletronic system makes use of temperature sensors and accelerometers. The data acquired from the system include, bearing temperature, rotational speed, direction of movement, vertical and/or lateral acceleration. It can be installed in axle box bearing units or front covers in order to monitor structural integrity of the bearing. The system is also able to monitor other components such as wheel and bogie (SKF).

3.2.6 Perpetuum on-board CM system

Perpetuum is a commercially available on-board system using vibration and temperature sensors in order to detect rail axle-bearing degradation and wheel damage. It was created as a

spin off from the University of Southampton (UK) in 2004. It is a real-time and self-powered monitoring system using wireless sensor nodes (WSNs) developed by Perpetuum Ltd. The sensor node consists of a vibration and a temperature sensor, the vibration energy harvester, electronics and wireless radio communications. The system is mounted onto the wheel bearing cover. The Bearing and the Wheel Health Index (BHI & WHI) are calculated by the captured data. Once a system detects the vibration levels above the pre-determined thresholds an automatic email alerts for a potential fault development being sent to the train operators. The faulty component will be removed or maintained at the depot at the next maintenance cycle. The data acquired from Perpetuum also include, train number, wheel position, date and time, speed of the train, GPS location, direction of travel and temperature. The Perpetuum system apart from monitoring rail axle bearings and wheels, is also able to monitor the health of other assets such as gearboxes, traction motors and tracks. According to the system's manufactures, the installation of the sensors is simple and fast.

The Southeastern Electrostar fleet (148 trains and 4,944 wheels) have been fitted with bearing sensors in order to monitor the integrity of rail axle bearing (Corni et al. 2015).

The current work is focused on correlation between the vibration history of the faulty bearings and the physical damage. Damage severity and characterization have been investigated using in-service rail-axle bearings. The tests samples have been reported as potential faults and removed from the service (Corni et al. 2017).

3.3 Non-commercial RCM systems for railway wheelsets

3.3.1 Acoustic array wayside monitoring system

Acoustic condition monitoring system makes a use of a microphone array which is installed on the track in order to detect bearing defects is under development at the University of Birmingham. A G.R.A.S type 46AE microphone and an array of AKG C417 microphones were used in the lab and field trials respectively. The operational frequency of the first microphone is between 3.15-20 kHz whereas of the second one is 20 Hz-20 kHz. This means that environmental noise (e.g. from the contact of wheel track) can also be recorded. Different methods to reduce the unwanted noise have been considered such as HFRT method and Spectral kurtosis based analysis. However, improvement signal to noise ratio (SNR) is still an ongoing objective of this research (Entezami et al. 2014).

Infrared light gates have been used to trigger the acquisition system automatically. The vehicle speed and the axle position can be calculated. From the results obtained, the developed system was proven capable of tracking the moving train and the sound emitted from the axle box. The performance of different microphone array configurations has been evaluated by a set of trial field tests at Long Marston, UK. The future trial tests will assess the directionality of the microphone array system. The intension of the research team is also to install the developed system on a high-speed line in order to assess it in more challenging environment (M. Entezami 2016). Figure 3.10 shows the layout of the Acoustic array wayside monitoring system (D. Zhang et al. 2020).

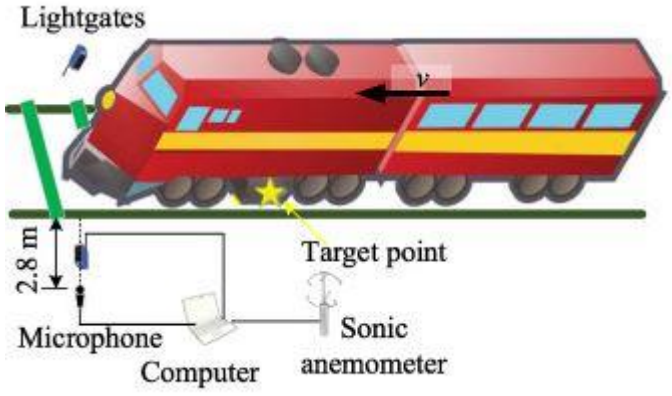

Figure 3-0-10 shows the layout of the Acoustic array wayside monitoring system (D. Zhang et al. 2020)

3.3.2. University of Illinois at Chicago on-board monitoring system

Acoustic emission and vibration on-board monitoring system has been developed by the University of Illinois at Chicago in order to enhance bearing fault diagnosis.. A bearing test rig was used to stimulate acoustic emission and vibration data from four different bearing faults. Experiments were carried out using bearings with inner and outer race faults, rolling element fault and cage fault. For comparison purposes, a healthy bearing was also tested. The experiments were conducted at both high and low shaft speed ranges. The shaft speed was ranging between 2 and 60 Hz. In addition, vibration data were captured from a fatigue cracked gear of aircraft UH-60A helicopter. The same methodology has been extended and validated in this case study (Van Hecke 2015) .

A wide band (WD) type AE sensor and an accelerometer, VibraQuest Pro by SpectraQuest, Inc were used during the experimental part of the project. Data acquisition was accomplished via NI LabVIEW SignalExpress. The sampling rate of the acquisition software was set to 100 kHz for the acoustic emission signals and 102.4 kHz for vibration signals.

A novel signal processing methodology based on synchronous re-sampling and spectral averaging was developed (Van Hecke 2015) . The developed methodology has been compared with the envelope analysis technique. Moreover, the effect of speed at RMS and peak value was presented. High shaft speed increases the RMS and peak value regardless of the fault type. Lastly, a comparison between acoustic emission and vibration based approaches was discussed. From the results obtained, it was concluded that acoustic emission signal analysis outperforms the vibration signal analysis in bearing fault detection.

.

A comparison between the novel monitoring system of this thesis and the on-board monitoring system of University of Illinois at Chicago is presented below. Firstly, wayside and on-board experiments were presented in this thesis. Tests ranging from laboratory to in-service were discussed. In contrast, only on-board test rig trials were carried out at University of Illinois at Chicago. In addition, the sampling rate of AE signals was set up to 500 kHz in this thesis contrary to 100 kHz at University of Illinois at Chicago. Data acquisition was accomplished via Matlab in current project instead of NI LabVIEW SignalExpress. A resonant AE sensor (R50a) was used to collect data in this thesis whereas a wideband (WD) AE sensor was used to acquire signals during the experiments. Lastly, during the signal processing development of each monitoring system different algorithms were applied in the collected data. In current work, Moving RMS, frequency distribution, Cepstrum analysis, HFRT technique and TSK analysis have been used for data processing. However, Peak and RMS value, HFRT technique and spectral averaging have been applied in the acquired signals at the University of Illinois at Chicago.

3.3.3. Safety IDEA Project 16

During the Safety IDEA Project 16 at Washington, railway bearing defect detection has been investigated using rail and car -mounted accelerometers. This project is the precursor for development of a prototype system for detecting defective bearings. Laboratory and field on-board and wayside experiments were conducted in order to evaluate the feasibility of detecting defective bearing by accelerometers. Car and rail - mounted accelerometers have been used in this study (Y.-J. Zhang 2011).

From the results obtained, it was concluded that bearing fault diagnosis can be successfully achieved by on-board accelerometers due to short transmission path. However, the signal to

noise ratio (SNR) was low in wayside measurements resulting in weakened defective bearing signals. The noise from the wheel-rail contact interface masked the useful information.

More sophisticated signal analysis for SNR improvement is proposed as future work for this project.

4. Acoustic Emission and Vibration Monitoring in Rolling Stock Integrity

4.1 Acoustic Emission and Vibration Testing

4.1.1 Fundamentals of AE testing

Acoustic Emission (AE) is a passive non-destructive testing method commonly used for detecting and locating faults in mechanically loaded structures and components. As a passive type of inspection, AE does not require excitation of the sensors but directly measure the noise emitted by the interaction of two different components (Ferrando Chacon et al. 2016).

AE can provide comprehensive information about the origin and the development of a defect in a stressed component (Grosse and Ohtsu 2008). AE is SHM technique which can also be used to monitor in-service structural components.

Acoustic Emission Testing (AET) is widely used for structural integrity evaluation of materials. Recently, AET is gaining acceptance as a reliable CM technique within the research community as it offers very promising fault diagnosis results at the initial stage of defect's development.

The energy released from a structure when is loaded can be detected by the piezoelectric sensors. More specifically, high frequency passive piezoelectric transducers operating in the frequency range of 100 kHz to 1MHz (above the audible range) are mounted on material's surface in order to convert the stress waves generated from a possible defect into electrical signals. Electrical signals can be recorded and digitized by an appropriate data acquisition system and then analysed by advanced signal processing techniques. The AE signals are amplified using appropriate pre-amplifiers and amplifiers and filtered out before the digitization. The principle of AE technique is presented in figure 4.1.

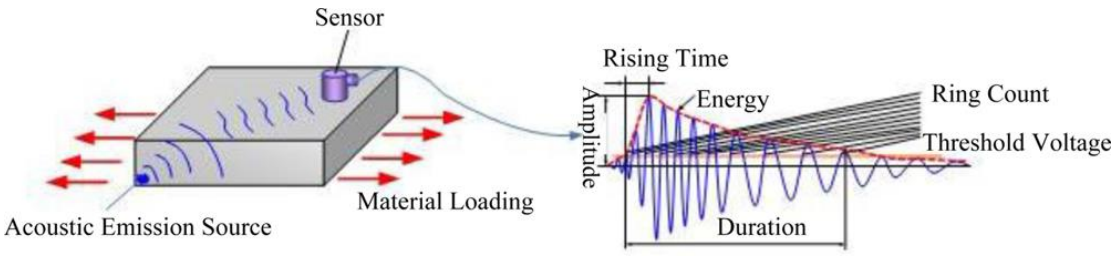

Figure 4-0-1: Principle of Acoustic Emission Testing (Gao et al. 2011)

It is paramount importance to catch the meaningful information. Thus, AE sensor should be mounted as closer as possible to the source of interest. Less high frequency AE signal attenuation is observed as the distance of the testing component decreases (Teti et al. 2010).

4.1.2 AE sensors

Resonant and wideband frequency sensors are the two AE sensor category according to their frequency response. Resonance sensors are particularly sensitive to a narrow frequency range (physicalacoustics). Resonant sensors have been selected for this project. Sensor sensitivity, frequency response, resonance frequency and temperature impact should be taken into account when a traducer is selected. The selection of the appropriate AE sensors is fundamental process for the development of a reliable condition monitoring system. Piezoelectric R50a resonant AE sensors were employed in on-board and wayside measurements in this project. Their operational frequency are between 100 and 700 kHz. Therefore, they are suitable for development of high frequency monitoring system. Since AE transducers operate within a high frequency range, a substantial amount of low mechanical noise is eliminated (Anastasopoulos et al. 2010) . However, unwanted noise is still recorded. Various advanced signal processing techniques are applied in the captured data in order to filter out the noise from the meaningful signal.

The acoustic emission sensors and the material surface are acoustically coupled with an appropriate couplant (i.e. a material in order to improve signal transmission path). In order to achieve consistent coupling, the material's surface should be free from dirt. In this work, Vaseline was used as a couplant in the on-board measurements. It is inexpensive and commercially available on the market and safe to handle. In contrast, AE sensor and rail track were coupled using grease in wayside measurements in order to ensure good transmissibility of the stress waves. Furthermore, the sensors were attached on the track using magnetic hold-downs.

The resistance of the sensors to any environmental condition such as hot or cold weather is also key advantage of the monitoring system.

4.1.3 AE sensor calibration

Before any experimental trial in this study, AE sensor should be calibrated without any reference device. Therefore, pencil lead brake is selected as an appropriate calibration method. Pencil lead breakage is widely used to reproduce a Hsu-Nielsen source (Sause 2011). It is a simple and easy method that used an automatic pencil with 2H lead and 0.5mm or 0.3mm diameter. The pencil lead is broken against the surface of the test material. For instance, in on-board laboratory trial of this study, the pencil lead brake against the faulty bearing. The AE signal that is generated is a strong burst as same as the acoustic excitation produced by a crack (Sause 2011). The time and the frequency response of a generated signal by pencil lead brake is presented in Chapter 7 of present thesis an example. The purpose of this stimulation test is to ascertain the sensor accuracy and at the same time to examine the couplant's consistency between the sensor and the material.

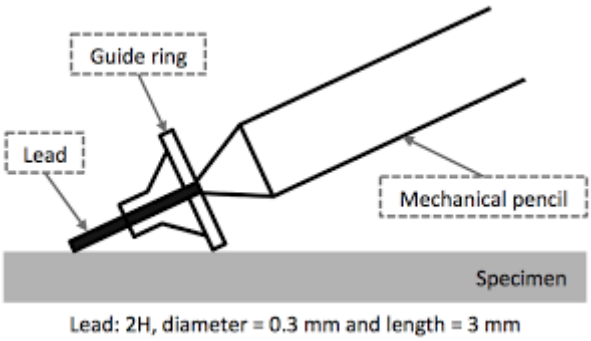

Figure 4-0-2: Pencil lead break testing (Yasuda et al. 2014)

4.1.4 Acoustic Emission Signal

The high frequency noise (or stress waves) that is emitted when a crack propagates comprises the AE signal. The AE signal is recorded using piezoelectric AE sensors at a pre-determined sampling rate. The sampling rate is of paramount importance in order to ensure satisfactory quality of the AE data obtained and avoid aliasing effects. High sampling rates results in a large amount of measurement data that need to be processed using appropriate algorithms in order to remove unwanted noise and detect signal features of interest that are associated with the presence of one or more defects.

Each AE signal is a unique energy wave that comprises two parts of information; the meaningful and the noisy signal. Signal interpretation and evaluation should be applied in the raw captured AE data in order to manage the balance of these parts of information. Signal interpretation is the process of determining whether the collected measurement data are relevant, non-relevant or false according to the purpose of the test (Grosse and Ohtsu 2008). Non-relevant or false signals are noisy signals that should be filtered out before any further data analysis. The relevant signals should also be filtered in order to extract the useful information from the background noise. Different techniques of advanced signal analysis can be used for this purpose. Signal evaluation is the process of signal source assessment in accordance with several acceptance criteria.

AE signals can be categorized into two groups, Hit Driven Data (HDD) and Time Driven Data (TDD) according to the recording method. According to Green (Green 1980), the amplitude of HDD is greater than the amplitude of TDD signals due to different signal generation.

Hit Driven Data are recorded when the signal voltage exceeded a pre-determined threshold. The threshold is set up by the user. Depending on type of the AE signal, different useful parameters can be extracted resulting in evaluation of AE source. The signal waveform that is presented as an output in the measurement system depends on some key parameters such as the characteristics of the AE source, the AE signal transmission path, the characteristics of AE sensors and definitely the properties of the measurement system.

The most useful extracted parameters for HDD data are (Miettinen and Pataniitty 1999):

- Threshold-crossing counts;
- Amplitude;
- Duration;
- Rise-time;
- Energy-envelope

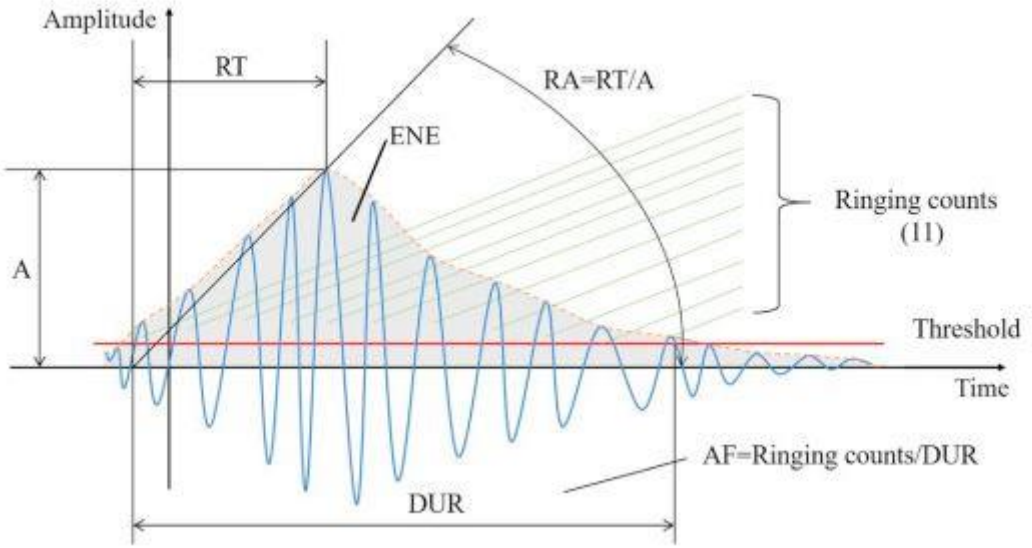

Figure 4-0-0-3 Characteristic parameters of AE burst signal (Du et al. 2020)

On the other hand, TDD are continuously recorded and the signal never ends. In the literature, they are also referred as continuous waveforms. In this work, the useful signals are Time Driven Data. Amplitude and frequency response are the key features of a typical continuous AE signal. AE activity is captured for a specific time duration and is presented by the time waveform. The frequency response of a signal can be calculated using the Fourier transform.

According to the operational principles of AE testing, signals were detected by the sensors during loading. In contrast to other NDT techniques, the materials is loaded before or after the data acquisition.

The effect of environmental noise on the AE measurement is an important issue that needs to be dealt with. In this work, band-pass filters are applied in the captured data in order to remove any unwanted noise before the digitization. In the processing module, the acquired

signals are analysed using advanced signal processing techniques in order to eliminate further the effect of the noise.

AE signal attenuation is one of the main limitations of this powerful technique. Signal attenuation is dependent on sensor's frequency. In order to cope with this issue in the current project, the position of the AE sensors is considered. It is widely accepted that the smallest transition path between AE sensor and AE source, the less signal attenuation that will occur (Teti et al. 2010). Within this study AE sensors were mounted on the surface of the bearing in the on-board measurements and on the rail in the wayside trials.

AE signal can be acquired without requiring physical opening of the component monitored. Hence, the structural integrity of the component in question can be monitored under real-time operational conditions.

The bearing's AE signature can be affected by several parameters such as bearing geometry, location and severity of bearing defect, operational speed and loads of the shafts (Qiao Sun et al. 2004). During tests in Long Marston using rolling stock with artificially induced axle bearing faults, it has been proven that high-frequency acoustic emission is capable of detecting such faults regardless of their severity (Z. Huang et al. 2014a). Moreover, AE is sensitive to minor bearing damage due to the high sensitivity of the high-frequency sensors employed (Bladon et al. 2004).

The main advantages of AE method are:

- Early detection of a bearing defect;
- Real time monitoring in-service structures;
- Minimized possibility of false alarms;
- Low cost equipment;
- Simple installation;
- Ability of working in high speed;
- Co-operation with other destructive and non-destructive techniques

Therefore, AE testing is well-suited for monitoring the damage initiation and degradation in railway wheelsets.

However, AET has a few limitation that are presented below:

- Rapid Signal attenuation;
- Unwanted Noise;
- Loading history of the structure is required;
- No repeatable patterns;
- Temperature limit of sensor;
- No evaluation standard for accessible data are available

4.1.5 State-of –the –art in Acoustic Emission Signal Analysis

Acoustic Emission Technique is now widely used for assessment of structural health integrity in various engineering structures. Acoustic emission monitoring system has been employed for railway wheelsets. In principle, when a wheel or axle bearing is defective, a burst of energy is released. AE sensors can detect this energy enabling the health monitoring of railway wheelsets. Identification of any potential faults in time can enhance maintenance scheduling helping promote long-term train availability.

Elforjani and Mba (M. Elforjani and Mba 2010) investigated the ability of AE to detect natural race bearing defects in low speeds. Time and frequency domain analysis have been employed for analysing the measured AE data. Spectral analysis and information entropy were used to detect the presence of cracking and its propagation. Elforjani and Mba also stated that AE signal analysis is able to determine the size of the defect. The duration of AE bursts and the angular velocity were used to calculate it.

Amini et al. (Amini et al. 2017) evaluated the effect of speed and defect size on high frequency AE and vibration signals from defective bearings. Laboratory and filed experiments were carried out under different speeds. Roller and outer race faulty bearings were used during this work. Peak to peak, RMS, Kurtosis and Crest Factor values were calculated and compared in each case study. From the results obtained, it can be concluded that signal‘s amplitude increased as the rotational speed also increased in both acoustic emission and vibration signals. In addition, Peak to peak and RMS values raised proportional to size of the defect. However, kurtosis and Crest Factor values were not able to distinguish the size of the bearing fault.

Elasha et al. (Elasha et al. 2017) employed AE and vibration analysis to diagnose bearing fault in a planetary gearbox. Bearing in three different conditions were used during the experimental part of this study. A heavily damaged bearing, a slightly damaged bearing and a defect-free bearing were utilized for comparison purposes. Combination of adaptive filter, spectral kurtosis and envelope analysis were applied to the captured signals. Elasha et al reported that AE signal analysis is capable of detecting earlier than vibration signal analysis. In addition, small defect can only be detected by AE analysis.

Cockerill et al. (Cockerill et al. 2016) discussed the effect of speed and load in AE signal. Outer race and inner race faults have been tested. From the results obtained, it was shown that speed was more sensitive than load resulting in increasing the amplitude of RMS when a rise of speed or load was appeared.

Elforjani (Mohamed Elforjani 2018) demonstrated the applicability of AE in diagnosis bearing cracks. Comparison between AE and vibration signal analysis in fault detection was presented. AE is more sensitive to early detection of bearing defects than vibration analysis. Estimation of remaining useful life for bearing was discussed. In addition, investigation of the influence of grease starvation condition of detecting bearing faults was reported. Correlation between AE features and bearing wear have been achieved resulting in promising conclusions.

Liu et al. (D. Liu et al. 2018) proposed a new method based on Kurtogram in order to enhance the early bearing fault diagnosis. The novel method combines autocorrelation function, Shannon entropy and Kurtogram. Simulated and measured acoustic emission

bearing signals were processed in order to demonstrate the effectiveness of the proposed method. Outer race bearing faults have been considered as test bearings to evaluate the effectiveness and the reliability of the new processing technique.

Hawman (Hawman and Galinaitis 1988) has shown that AE can provide a significant improvement in bearing health monitoring over vibration when a small size defect appears. Detection and classification of bearing defects were achieved earlier by AE signal analysis.

Anastasopoulos et al. (Anastasopoulos et al. 2010) demonstrated the ability of AE wayside monitoring to detect wheel faults. Trains and trams wheelsets have been measured. Time signal analysis and Pattern Recognition NOESIS software were used to analyse the acquired AE data. Reference signals from a defect-free wheelsets have been compared with the measured AE data.

Liu et al. (C. Liu et al. 2017) successfully processed AE signals using signal feature extraction to enhance bearing health monitoring. Signal Reconstruction has been achieved using sensing. The new data contains sufficient information as the original signals with lower sampling frequency and less computational cost.

Mba (Mba 2003) reported that the increase in AE counts are irrespective of outer race defect size. However, inner race defect size gave reverse results. It also stated that increase in speed and load can lead to increase in AE counts.

Miettinen er al. (Miettinen and Andersson 2000) noted that AE time signal analysis is the most reliable method to indicate the hardness of contaminated particles. AE rolling bearing measurements were captured during laboratory tests. Grease mixtures used for the lubrication of the bearings. Structural health monitoring was based on measuring AE pulse count levels.

Sandoral et al. (Usgame Sandoval et al. 2013) demonstrated the ability of AE time signal analysis to indicate the presence of a fault. Different severity levels of outer and inner race faults were studied. He concluded that ring down count and kurtosis values can be a good indicators for bearing fault diagnosis. However, RMS and peak values have low sensivity in the early stage of faults. In addition, time domain analysis cannot discriminate between inner and outer race defects.

Siroishi et al. (Shiroishi et al. 1997) investigated the effect of vibration and AE analysis to detect and diagnose outer and inner race bearing defects. High Frequency Resonance Technique and Adaptive line enhancer have been applied in the captured signals. Bearing Fault Frequency and its harmonics have been identified to the spectrum. AE signal analysis is also less sensitive to inner race defects.

Dukas et al. (Dykas et al. 2017) reported that RMS and count rates can distinguish a dry bearing from newly greased bearing. AE sensor, accelerometer and high frequency microphone were used in the experiments. The accelerometer and the microphone also showed a rise in RMS signal power as the lubricant quality degraded.

Niknam et al. (Niknam et al. 2013) also evaluated AE time signal processing to distinguish between lubricated and dry bearings. Eight levels of rotational speed and four levels of radial load were applied. Four statistical parameters such as standard deviation, max, variance and mean were sensitive to lubrication mode. Lack of lubrication increased these signal parameters.

Al-Ghamd et al. (Al-Ghamd and Mba 2006) investigated the capability of AE to detect bearing defects earlier than vibration. Outer race bearing fault has been seeded in varying defect size. Three different AE parameters (maximum amplitude, RMS and Kurtosis value) are sensitive to fault identification and size estimation. The results also demonstrated that the monitoring of bearing fault degradation in unachievable with vibration testing.

Mornain and Mba (Morhain and Mba 2003) utilised the Acoustic Emission Testing to monitor outer and inner race bearing defects. AE parameters such as RMS and Count Values have been validated as effective monitor techniques to detect bearing damage. However, RMS and Count Analysis cannot distinguish between small and large inner race defects.

4.1.6 State-of –the –art in Vibration Signal Analysis

Vibration is the oscillation or repetitive motion of an object around an equilibrium position. A vibration signature of a faulty component can provide useful information about its operation in a non-destructive matter. In order to obtain the vibration signal of rotating machinery, piezoeletronic accelerometers are used. These are low cost and reliable sensors due to their high frequency response compared to displacement and velocity sensors

(McFadden and Smith 1984). In addition, accelerometers are usually light weight (0.4-50 gram). A typical frequency operation range of an accelerometer lies between 5 kHz and 25 kHz. Operating characteristics should be taken into account when the accelerometers are selected as sensing method. In addition, proper mounting of the sensors should also be considered in order to avoid missing useful information. In a typical fault analysis, the recorded vibration signal compared with a reference signal both in time and in frequency domain. An acceptable level is considered as a healthy threshold. For more accurate results, vibration data trending is required (Z. Huang et al. 2014a).

The vibration signal of a rolling bearing close to failure is often non-linear and non-stationary. In wayside measurements, the vibration signal analysis is not powerful unless severe defect is considered (Amini 2016b).

It is also evident that wheel defects such as flats, cracks and shelling can be identified by the vibration's signature using high frequency spectral analysis (Vermeulen et al. 2010).

Symonds N et al. (Symonds et al. 2015)used vibration signal analysis to monitor on-board bearings to Electrostar fleet. Outer race damage has been identified at early stage. The ultimate goals of this case study are to link in bearing vibration signature with damage level and to detect causing fault factors.

Cao et al. (Cao et al. 2016) developed a novel condition monitoring technique to detect wheel-bearing faults. Empirical Wavelet Transform has been applied to the acquired

vibration data. Outer race fault, roller fault and compound of fault of roller and outer race was investigated. Both stimulated and real-time data were collected. From the results obtained, it is obvious that this method can enhance wheel-bearing fault diagnosis.

Ho and Randall (Ho and Randall 2000) has shown that in self-adaptive noise cancellation (SANC) conjunction with envelope analysis enable identification of bearing defects in both stimulated and real conditions. Vibration signals have been collected. Roller Bearing Frequency has been successfully revealed into signal's spectrum.

Zhang et al. (Z. Zhang et al. 2017) used vibration monitoring analysis to enhance early stage bearing fault diagnosis. Roller and outer race defects have been investigated during laboratory trials at the University of Birmingham. The measured data were acquired at a variety of speeds and noise environment. Empirical mode decomposition (EMD) and minimum entropy deconvolution (MED) have been applied in the acquired data. The results have been shown that the proposed method enhance bearing fault detection at the early stage.

Mauricio et al. (Mauricio et al. 2020) investigated the effectiveness of a novel bearing diagnostic tool in order to minimize the influence of the strong Electromagnetic Interference at raw vibration signals. Cyclic Spectral Coherence have been applied on the captured data improving the envelope analysis results. Automated detection of the optimal frequency band for the band pass filter design was achieved. The proposed methodology validated and evaluated using a planetary gearbox test rig. Inner and outer race faults were used during the experimental part of this project. From the results obtained, the fundamental bearing frequencies have been successfully presented in the envelope spectrum.

Klausen and Robbersmyr (Klausen and Robbersmyr 2019) reported the capability of the cross correlation spectrum to enhance an accurate bearing fault detection at low speed conditions (20rpm). A bearing test rig with three different faulty bearings (damaged rollers, outer race and inner race faults) was used in order to stimulate vibration signals. Cross correlation between whitened vibration signal and its envelope was calculated. The whitening vibration signal was computed using synchronous averaging and an autoregressive model. The resulting signal contains amplified frequency components related to bearing faults. The new signal was analysed using the High Frequency Resonance Technique. Prominent harmonics and sidebands were revealed at the envelope spectrum.

He and He (He and He 2020) demonstrated the ability of vibration analysis technique to achieve bearing fault detection using a new hybrid deep signal processing approach. The proposed method combines vibration analysis technique with time synchronous resampling mechanism. Bearing test rig was used in order to validate the effectiveness of the proposed method. Bearings in five different conditions (healthy, inner and outer race faults, rolling element fault and cage fault) were considered at the experimental part of this work. The RMS and the peak values were calculated from the reconstructed vibration signals indicating better performance in bearing fault diagnosis than the raw signals.

4.2 Current state of work using AE and Vibration signal analysis

RCM system for railway wheelsets has been developed by University of Birmingham during the MaxBe project. In this work, AE and Vibration signal analysis have been performed in order to detect faults prior to failures, assess the severity of fault and identity the type of the

faults. State-of-the-art signal analysis has been employed in the acquired data. If no defect is detected, the KPIs results are stored for future trending. In case of wheelset defect is detected, further analysis using intelligent algorithms is performed in order to confirm the presence of a defect and to assess the severity.

During the project, on-board and wayside experiments have been employed. The ultimate goal is to integrate the on-board and wayside systems in order to improve results accuracy. In this approach, if a fault is detected by the wayside system then the train will be stopped and monitored by the on-board system. In case of the two systems have the same response then the train will be driven to the maintenance de-pot.

The proposed customised system can also be integrated with commercial system which monitor the wheel condition such as WILDs and WPDs. The aforementioned wheel systems are not capable of monitoring railway axle bearings.

From the results obtained, AE signal analysis have higher SNR compared to vibration. Thus, wheelset faults can be detected noticeably earlier. However, AE analysis is more expensive than Vibration analysis. Therefore both type of analysis techniques are employed in current work.

A customised AE and vibration monitoring system has been developed by the University of Birmingham. The R50a resonant sensor is connected to the preamplifier and to amplifier. The amplifier is connected to data acquisition board. A computer is used to storage the results. An accelerometer was also used for the vibration data.

Acoustic emission and vibration signals were acquired during experimental work carried out at laboratory in field and in-service. Two test rigs were used for signal acquisition. Defect free bearings and faulty bearings have been tested during experimental part of this project. The effect of speed and load in signal amplitude and in RMS amplitude were also discussed.

Different signal processing techniques were discussed such as Normalized Moving RMS, Cepstral analysis for multiple defects, Frequency distribution and HFRT algorithm. Trolley test were also carried out using wheel flat defect. Vibration signal analysis is more effective than AE when wheel flat defect is appeared. Different bearing roller defects were tested at Long Marston, UK. Frequency distribution has been proved as the optimum option for data analysis in order to detect the type of the defect. High Frequency Resonance Technique has been applied in the captured signals and the bearing faulty frequency has been revealed. Therefore, the origin of the fault was identified. In addition, the customised system has been installed on the UK rail network at Cropredy at Chiltern Railway line, adjacent to Hot Box Axle Detector for comparison purposes. The integrated system consists of 6 channels (4 AE and 2 vibration). The gain used for Cropredy trials has been set up to 29dB in order to minimize the environmental noise and enhance SNR. The Sampling rate was set up at 500 kHz for AE signals and at 25 kHz for vibration measurements.

Freight and passenger trains signal have been acquired. Trains with potential faults defective wheelsets have been detected. Several signal processing techniques have been applied at the raw signals. Comparison between frequency responses was presented. Sharp peaks in specific frequencies were visible. These frequencies can be used as a reference for further processing. The HFRT algorithm was also applied at the captured data. Freight and passenger trains with potential faults have been identified. Fundamental frequency and its harmonics can been clearly seen at HFRT plot. Sidebands were also visible. These patterns can indicate the type of the defect.

Spectrogram and TSK plots were also presented in the results of this work. High kurtosis value at specific frequency band indicated the presence of a defect. In addition, strong signal modulation was demonstrated in raw signals indicating the presence of a fault. Harmonics in

frequency distribution and in Spectrogram were presented enhancing the presence of a potential wheelset fault.

5. Signal processing Algorithms

In this chapter, an overview of advanced signal processing techniques for diagnosis of wheel and axle bearing condition is being presented. Three approaches of signal analysis are discussed, the time, the frequency and time-frequency domain. According to this study, a combination of them can enhance the wheel and axle bearing fault detection and diagnosis.

5.1 Time domain analysis

Time domain signal analysis can be used to detect the present of a defect based on evaluation statistical parameters such as moving kurtosis and moving RMS.

5.1.1 Moving RMS

RMS is a non-dimensional statistical indicator of the energy of a signal. The RMS value for a signal with length n is described by the equation below (Lebold et al. 2000) :

$$RMS = \sqrt{\frac{\sum_{i=1}^{n} Xi^2}{n}} \quad (5.1)$$

The main limitation of RMS analysis is that the time information is lost. Moving RMS is an approach of analysis that reverses the time information. In this type of process, the RMS value is calculated in terms of moving window analysis.

In a moving RMS analysis, high amplitude peaks are most likely related to bearing defect. In this study, the severity of a bearing defect can be evaluated using moving RMS signal processing.

5.1.2 Moving Kurtosis

Kurtosis is a non-dimensional statistical descriptor of the sharpness of peaks in a raw signal. The kurtosis value for a signal with length n is provided by the equation

$$K = n\frac{\sum_{i=1}^{n}(Xi-\bar{X})^4}{\left(\sum_{i=1}^{n}(Xi-\bar{X})^2\right)^2} \qquad (5.2)$$

Where $Xi - \overline{X}$ is the difference between each value and the mean of the signal .

A healthy threshold can be applied in order to evaluate the structural integrity of a component. For a healthy bearing with normal distribution, the kurtosis value is close to 3. Any value greater than that indicates damage development (Tandon and Choudhury 1999).

Moving kurtosis is calculated as moving RMS.

The main limitation of kurtosis is that it may not be suitable analysis method in noisy environments. When SNR is high, measure kurtosis in specific frequency bands might be more effective (Amini et al. 2016c).

5.1.3 Moving Crest Factor

Crest Factor is a time-waveform analysis which provides a value for the impact caused by the strikes in a fault bearing. The Crest Factor value for a signal is provide by the equation

$$CF = \frac{\max peak\ value}{RMS\ value} \qquad (5.3)$$

CF is a unit-less ratio that depends on the severity of fault. CF usually exceeds value of 5 early in the wear cycle. In contrast, a value of 2.5 is presented late in the wear cycle (Graney and Starry 2012).

Moving CF s is calculated as moving RMS with the advantage of more accurate results compared with CF value due to high number of points at the waveform.

5.1.4 Peak to Peak analysis

Peak to peak analysis (PK to PK) is used in bearing defect detection since it gives more accurate results than peak value. It is a statistical parameter that used for bearing condition assessment at Vibration and AE signals analysis. In this study, Maximum peak value and Normalized Moving RMS peak value are used to evaluate the effect of speed and load at AE testing. The results are presented in Chapter 7.

5.2 Frequency domain

Railway wheelset health assessment can be also evaluated using several frequency analysis techniques. The presence and the type of fault can be established using AE or vibration frequency processing (Amini et al. 2016a). Fast Fourier Transform, High Frequency Resonance Technique and Cepstrum analysis are discussed in this work.

5.2.1 Fast Fourier Transform (FFT)

One of the most common AE signal analysis technique is the power spectral analysis that is based on Fast Fourier Transform (FFT) algorithm. The Fourier Transform is a reversible transformation of signal from time domain to frequency domain. The Fourier Transform for a continuous time signal $x(t)$is defined as (Phillips et al. 1995):

$$X(\omega) = \int_{-\infty}^{\infty} x(t) e^{-i\omega t}\, dt \qquad (5.4)$$

and the Inverse Fourier Transform (IFT) is defined as

$$x(t) = \frac{1}{2\pi}\int_{-\infty}^{\infty} X(\omega)e^{i\omega t}\,d\omega \quad (5.5)$$

The FFT algorithm performs the same function as the Discrete Fourier Transform (DFT) but in less computational time.

The FFT algorithm can be described as follows (Transform):

The frequency distribution of an AE or vibration signal can be used to enhance the bearing fault diagnosis. A benchmark frequency distribution for a healthy case can be cross-correlated with any frequency distribution in order to evaluate the health component. Harmonics in power spectrum of an axle bearing might also be an indicator for a defect initiation.

In the current study, high amplitude peaks in frequency distribution have been used also as a reference for further processing. The signal can be band-pass filtered based on these peaks and further processed using the envelope analysis technique. Envelope analysis is discussed later to this thesis.

High amplitude peaks can be related to resonance frequencies of the sensor or of the component. The resonance frequencies of the R50a sensor are 170 kHz and 350 kHz. Calibration curve of R50a sensor based on ASTM E976 is shown in Figure 5.1 (physicalacoustics). Pencil break tests can be used to confirm the sensor calibration accuracy by confirming the resonance frequencies whereas the resonance frequencies of an axle bearing can be detected using an impact test.

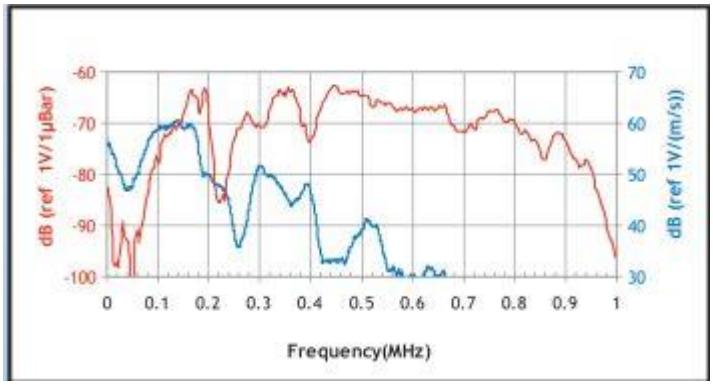

Figure 5-0-1:Calibration curve of R50a sensor based on ASTM E976 (physicalacoustics)

5.2.2 HFRT (high frequency resonance technique)

Rolling element bearings consist from four main components: outer and inner race, cage and rolling element. Balls, rollers and tapered rollers are the most common rolling elements nowadays.

Bearing defect can be presented in any of these four components. A series of vibration impacts generated periodically when the rolling element passes over the defect. These impacts recur at Bearing Fundamental Frequencies (BFF) (Tyagi 2003).

According to rolling bearing kinematics the four BFF can be calculated with the following mathematical equations below (Table 5.1) while the bearing geometry and the shaft speed are known in advance (Graney and Starry 2012) :

Bearing Fundamental Frequencies	**Acronym**	**Mathematical Equations**
Ball Pass Frequency Inner race	BPFI	$\frac{N}{2}\times F\times\left(1+\frac{B}{P}\times\cos\Theta\right)$
Ball Pass Frequency Outer race	BPFO	$\frac{N}{2}\times F\times\left(1-\frac{B}{P}\times\cos\Theta\right)$

Fundamental Train Frequency	FTF	$\frac{F}{2}\times\left(1-\frac{B}{P}\times\cos\Theta\right)$
Ball Spin Frequency	BSF	$\frac{P}{2B}\times F\times\#\left[1-\left(\frac{B}{P}\times\cos\Theta\right)^2\right]$

Table 5.1 : Bearing Characteristic Frequencies and their acronym(Graney and Starry 2012)

Where:

N = number of ball bearings

F = shaft frequency in Hz

B =ball bearing diameter in mm

P =pitch diameter in mm

Θ = contact angle.

The manufacture of the bearing generally provides the BFF.

The schematic in Figure 5.2 (left) is shown a ball rolling bearing defects illustration and in Figure 5.2 (right) a diagram of the BFF inputs explanation (Segla et al. 2012) :

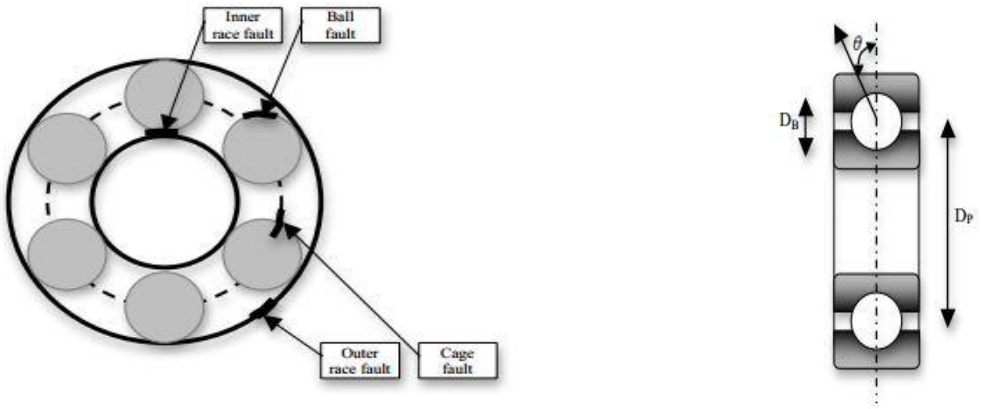

Figure 5-0-2: Bearing defects illustration (left) and diagram of inputs explanation (right) (Segla et al. 2012)

Early stage bearing damage may not be detectable using conventional spectrum analysis due to wide energy distribution (Robert B. Randall and Antoni 2011; Tyagi 2003). The HFRT (also known as envelope demodulation processing) provides superior sensitivity to bearing fundamental frequencies in AE and vibration applications (Amini et al. 2016b; Tandon and Choudhury 1999) . The main idea of the HFRT is to separate the signal generated by the defective part with in the envelope spectrum, from the signal generated by the other machine elements using the band pas filter around the resonance frequency (McFadden and Smith 1984). This approach of analysis shifts the frequency analysis from high frequency range to lower frequency allowing better resolution (Robert B. Randall and Antoni 2011).

Before the presentation of the HFRT algorithm, the Hilbert Transform is described.

For a signal $g(t)$, the HT is defined by the equation below (Kschischang 2006):

$$H[g(t)] = g(t) * \frac{1}{\pi t} = \frac{1}{\pi}\int_{-\infty}^{\infty} \frac{g(\tau)}{t-\tau} \quad (5.6)$$

The Hilbert Transform of $g(t)$is the convolution of $g(t)$with the signal $\frac{1}{\pi \cdot t}$.

The HFRT process employed in AE and vibration signals of this study and is shown in figure 5.3

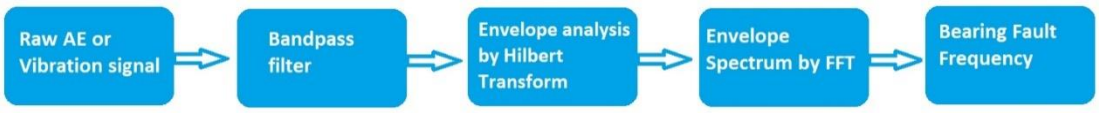

Figure 5-0-3: Schematic showing the high frequency resonance technique process

The HFRT algorithm consists of 3 main steps in order to locate the faulty characteristic frequency in the envelope spectrum (Segla et al. 2012):

Band-pass filter is applied to the raw data. The bandwidth of the filter is crucial to guarantee the results. The bandwidth is suggested to be at least four times the highest fundamental faulty frequency (McFadden and Smith 1984). The band passed signal is then subjected to envelope analysis. In this work, Hilbert Transform (HT) has been used to calculate the envelope signal. HT extracts the amplitude modulating signal from the amplitude modulated signal (Mjit et al. 2011). The repetition rate of the impact has been revealed in this step. In third step, the envelope spectrum is estimated using the FFT algorithm.

5.2.3 Cepstrum analysis

Multiple faults in rolling element bearings or gearboxes may not be detectable using power spectrum or envelope analysis. Vibration cepstrum analysis has been considered as most appropriate method for detecting and distinguishing the families of harmonics in power cepstrum (Robert B Randall ; Spectra Quest 2006). The power cepstrum of a signal $x(t)$ is defined by the equation below (R. Randall 1982) :

$$C(\tau) = IFT\langle log\{FFT\{x(t)\}\}^2\rangle^2 \quad (5.7)$$

Power cepstrum is described as the Inverse Fourier Transform of the natural logarithm of the power spectrum of the original signal. The horizontal axis is the Quefrency that is reciprocal of Frequency and it is measured in seconds. Table 5.2 shows the Cepstrum terminology.

Spectrum analysis	Cepstrum anlysis
Frequency(Hz)	Quefrency (sec)
Harmonic	Rahmonic
Filter	Lifter
Magnitude	Gamnitude
Phase	Saphe

Table 5.2: Cepstrum Terminology

Figure 5.4 shows an example of Cepstrum analysis. The raw data is a vibration signal from a defective bearing from the test rig in 500RPM rotational speed. Damage in both races and in roller has been artificially induced. The fundamental frequencies of the bearing are BPFO= 76.9Hz, BPFI= 98.1Hz, BSF=65.85Hz. The peaks at $0.01288=\frac{1}{77.64}, 0.01008=\frac{1}{99.2}, 0.01588=\frac{1}{62.97}$ confirms the presence of the faults. There is a slight offset between the theoretical and the observed fundamental frequencies due to the slight variation in the rotational speed during the test.

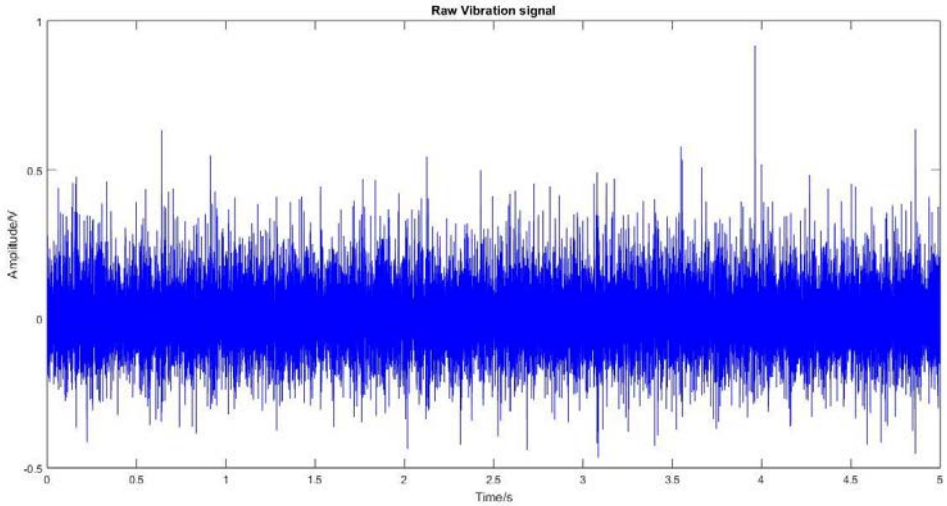

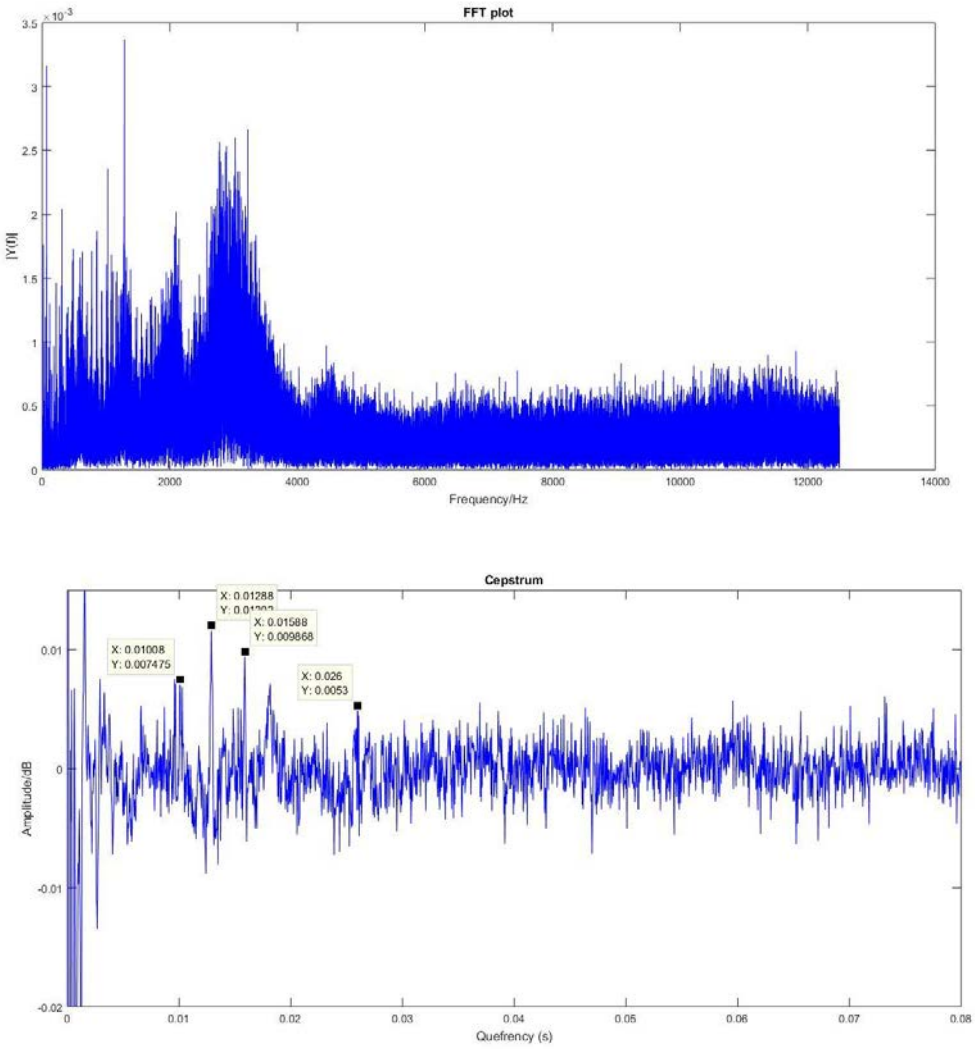

Figure 5-0-4: Defective bearing F7 test rig: Raw signal- power spectral analysis-power cepstrum analysis (from top to bottom)

5.2.4 Cross correlation technique

Cross correlation technique is a useful tool to determine the similarity of two signals as function of the time-lag shift τ. A reference signal from a defective bearing is created and an input signal is compared with the reference signal using the cross correlation function.

The cross-correlation function of two continuous signals $f_1(t)$ and $f_2(t)$ can be calculate by the following function (Kaphle et al. 2012) :

$$R_{12}(\tau) = \int_{-\infty}^{+\infty} f_1(t) f_2^*(t-\tau) dt \quad (5.8)$$

In this study, frequency spectrum similarity between two signals from same source or from different source is also presented in Chapter 7. When two signals acquired by the same bearing fault, their frequency spectrum have the same pattern. Spectral coherence function can also be used for the same reason.

5.3 Time-frequency domain techniques

5.3.1 Time-Spectral Kurtosis (TSK)

Spectral Kurtosis (SK) is a useful signal processing technique of decomposing the kurtosis value of a signal as a function of frequency (J. J. M. s. Antoni and processing 2006; J. Antoni and Randall 2006). However, time information is lost. SK has been extended to time domain by developing Time-Spectral Kurtosis (TSK) (Chen et al. 2014). TSK is a three-axis representation of the signal: time, frequency and kurtosis value. Bearing fault diagnosis can be enhanced using TSK technique (Amini et al. 2016c) by detecting the series of transients in frequency domain and their location in time domain. Kurtosis value of 3 is considered as normal distributed signal that is corresponds to healthy machine. Any values greater than 3 could be related to mechanical faults. However, false alarms may be caused in real world environment when wheel-bearing signals are analysed by SK due to spare interference impulses (Chen et al. 2014).

The ability of the TSK algorithm to distinguish the axle bearing defects and random noise has been shown by Amini et al. Wayside AE signals have been collected by artificially damaged axle bearings. TSK has been applied for the analysis of the experimental data. High amplitude kurtosis values in specific frequency bands have been related to bearing defects. Therefore, TSK analysis can enhance the bearing fault diagnosis in this case study (Amini et al. 2016c).

The kurtogram (fourth-order spectral analysis tool) has been recently introduced as an efficient analysis technique for non-stationary signals. The detection of abnormal transients in a signal and their corresponding frequency band (s) by identifying the maximum kurtosis value can be achieved using the kurtogram technique (J. Antoni 2007). The optimum frequency band for the design of a band pass filter is the main purposes of this type of analysis. The centre frequency and the window size (bandwidth) can be calculated without requirement of historical data. Hence, automated envelope spectrum analysis can be applied in the signals.

Fast kurtogram is another approach of Kurtogram that has the same quality of results in less computational time. Therefore, it is more appropriate in on-line industrial applications (J. Antoni 2007).

Eftekharnejad et al. investigated the ability of kurtogram in bearing fault diagnosis. Acoustic emission and vibration measurements performed on naturally degraded roller bearing. The kurtogram has been applied for the analysis of experimental data. From the results, obtained, SK-based filtering has been considered as an effective method of signal-to-noise ratio improvement (Eftekharnejad et al. 2011).

Spectral kurtosis has also been applied in fault detection of WT gearboxes by Barszcz and Randall (Barszcz and Randall 2009). A band-pass filtered has been design based on the frequency of the highest spectral kurtosis band. Periodicity of the highest amplitude peaks were clearly seen in the filtered signal. The tooth crack in the planetary gear was confirmed by this time period.

Figure 5.5 shows a typical example of fast kurtogram (J. Antoni 2007) illustration from AE signal obtained by this study. A band-pass filter can be designed based on the results below. The centre frequency will be 185546.875 Hz and the Bandwidth 3906.25 Hz.

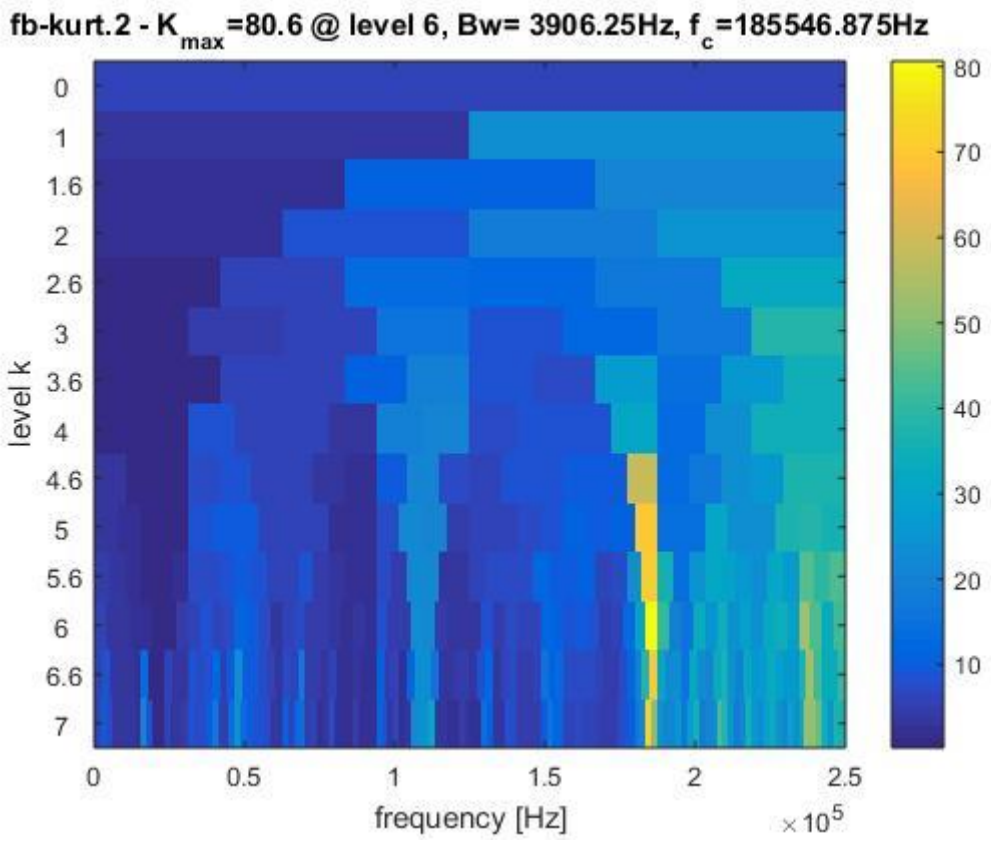

Figure 5-0-5: Kurtogram of a raw AE signal from the Cropredy tests

5.4 Comparison of Advanced Signal Processing techniques

Signal processing techniques	Simple and easy to implement	Detection of faulty characteristic frequency	Improve SNR	Detect faults at early stage	Time information is lost	Detect multiple defects	Distinguish fault severity
Moving RMS	✔						✔
Peak to peak analysis	✔						
FFT			✔	✔	✔		
HFRT		✔	✔	✔	✔		
Cepstrum	✔					✔	
TSK			✔	✔			

Table 5.3: Comparison between each domain analysis

From the results obtain during this thesis, the main conclusions about the comparison of advance signal processing techniques were presented in Table 5.3. The recorded AE and Vibration data were analysed using the advanced signal processing that are presented in this work.

As it can be seen, Moving RMS is simple and easy to implement and is suitable for distinguish the defect severity. In addition, Peak to peak analysis is easy and simple to implement to raw signals. Frequency distribution can improve SNR and enhance fault detection at early stage. HFRT algorithm can identify the faulty characteristic frequency resulting in improvement of SNR. Multiple defects can be revealed using Cepstrum analysis.

In addition, Cepstrum Transform is simple and easy to implement. Time information is lost in frequency domain analysis. Therefore, TSK algorithm is a three axis representation. High Kurtosis value in specific frequency can indicate the presence of a potential fault. The information provided by this technique can be used for further processing. The time is also available resulting in detection of the faulty spacemen.

6. Experimental Method

6.1 Equipment and experimental method

The present chapter discusses the experimental procedure employed in this study. A customised integrated RCM system has been built for the tests (shown in Figure 6-1). This novel system consists of the following components:

- High frequency accelerometers with a sensitivity of 100mV/g manufactured by Wilcoxon (W. S. Technologies 2020b),
- A 2531A Agilent 4-channel data acquisition card with a maximum sampling rate of 2MS/s in single-channel mode (K. Technologies 2020a) ,
- A 4-channel decoupling hub manufactured by Agilent
- AE analogue amplifiers manufactured by Krestos
- Pre-amplifiers manufactured by Physical Acoustics Corporation (PAC) (Acoustics' 2020),
- An accelerometer power supply manufactured by Krestos
- R50α resonant AE sensors manufactured by PAC (Acoustics 2020)
- An industrial computer with a customised data logging and analysis software developed in collaboration with other colleagues written in Matlab.

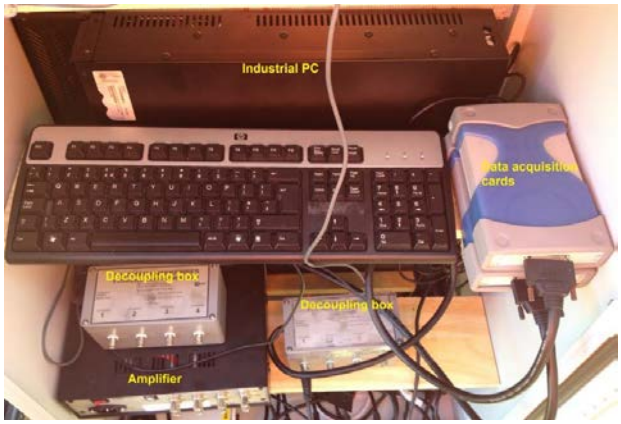

Figure 0-0-0-1: The customized data acquisition equipment used during laboratory and field trials (Amini 2016b)

Figure 6-2 shows the experimental configuration applied at AE data acquisition. An R50α resonant AE sensor is connected to the preamplifier, which in turn is connected to an amplifier. The amplifier is connected to a data acquisition board, which converts the amplified electric signals generated by the AE sensor into digital data that are subsequently fed to the acquisition software. The data acquisition board is connected to a computer via USB connection. The preamplifier's gain was set to 40dB and the amplifiers gain was ranging between 22dB and 40dB according to the test's requirements. The sampling rate of the acquisition software was set to 500 k Samples per Second. The data recording duration was set to 5 seconds for laboratory trials and 5-18 seconds for the Long Marston and Cropredy trials. The acquired AE and vibration data were analyzed using signal processing tools developed using Matlab in collaboration with other researchers.

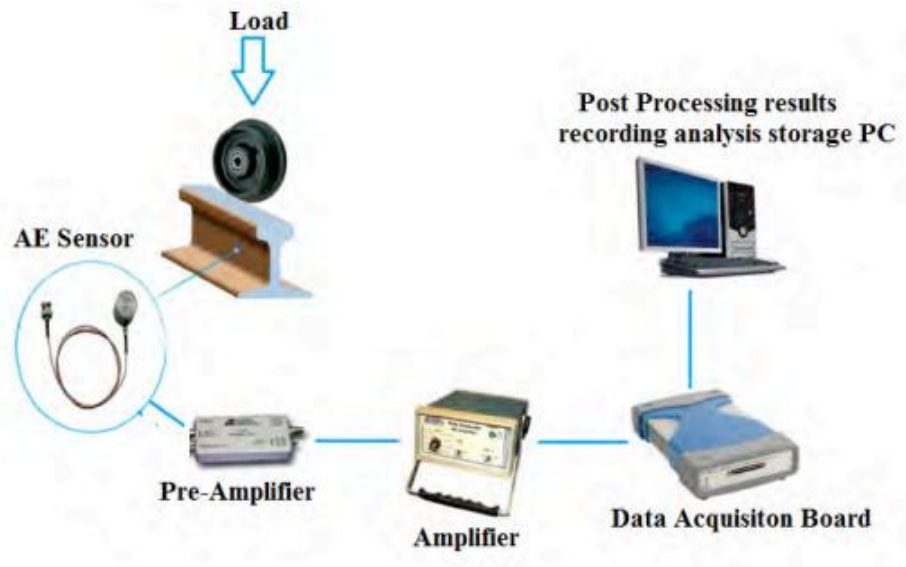

Figure 0-0-0-2: Experimental configuration for AE tests (Yilmazer et al. 2012)

A Wilcoxon 712F piezoelectric accelerometer with has sensitivity of 100mV/g and a 4-channel power supply manufactured both by Krestos were employed for the vibration data acquisition. The operational frequency range of the accelerometer is between 1.5 Hz - 15 kHz. Figure 6-3 a shows the calibration process of the Wilcoxon 712F piezoelectric accelerometer during the experiments of this study. Figure 6-3 b shows the frequency spectrum that confirms the accurate calibration of the piezoelectric accelerometer.

a)

b)

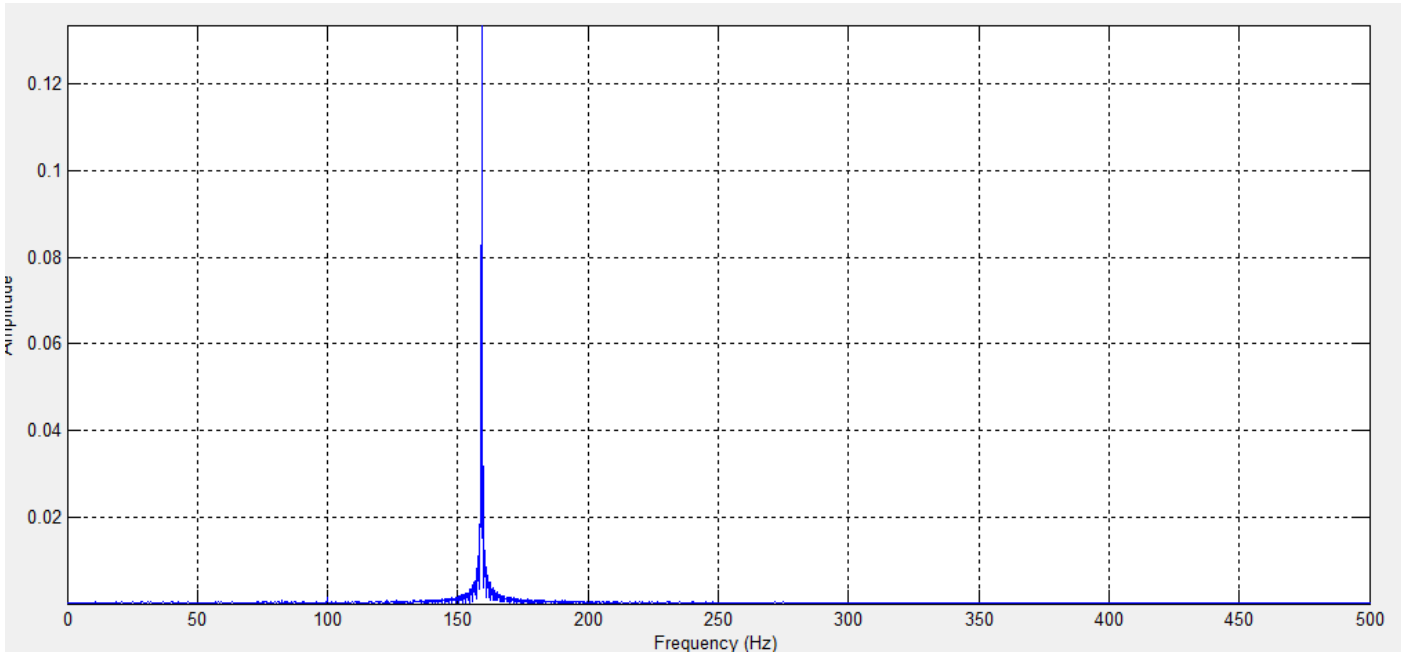

Figure 0-0-0-3: a)Calibration process of the Wilcoxon 712F piezoelectric accelerometer and b) Frequency spectrum shows that calibration process is accurate.

6.2 Laboratory-based testing

6.2.1 Case study 1 – On-board testing on defective bearings

Laboratory experiments have been performed on healthy and defective bearings in order to evaluate the customised monitoring system. The tests have been employed under variable shaft speeds, different loads and with various levels of damage severity.

Customised test rigs were used for the trials. The rotation speed was between 100 - 1000 RPM. The bearing samples were PW29530037CSHD PFI model. Figure 6-4 shows the customised test rig 1. An accelerometer and an AE sensor installed on the bearing's surface. AE sensor was coupled using Vaseline. A dust tape also used in order to keep in place the sensor.

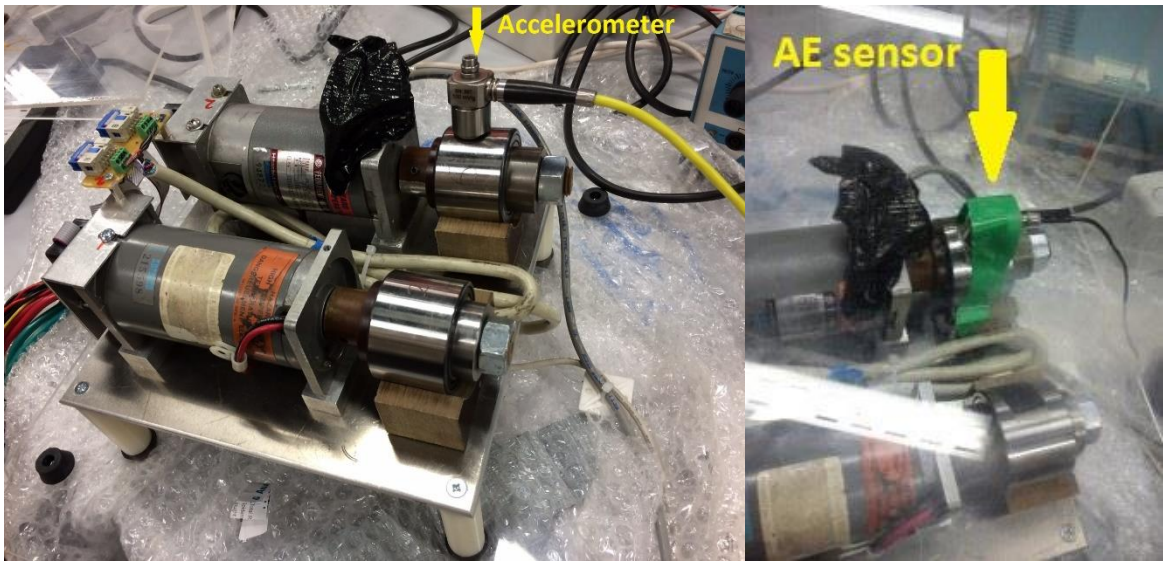

Figure 0-0-0-4 : Customized bearing test rig 1 at the University of Birmingham

Figure 6-5 and Figure 6-6 show the experimental configuration employed at laboratory experiments using the test rig 2. The photographs on Figure 6-5 present the experimental instruments used at the Laboratory trials. A customised Acoustic Emission and Vibration logger developed by Dr Arash Amini was used for data acquisition. AE and vibration measurements were recorded and saved for further processing. The AE sensor and accelerometer installed at the test bearings are shown in Figure 6-6.

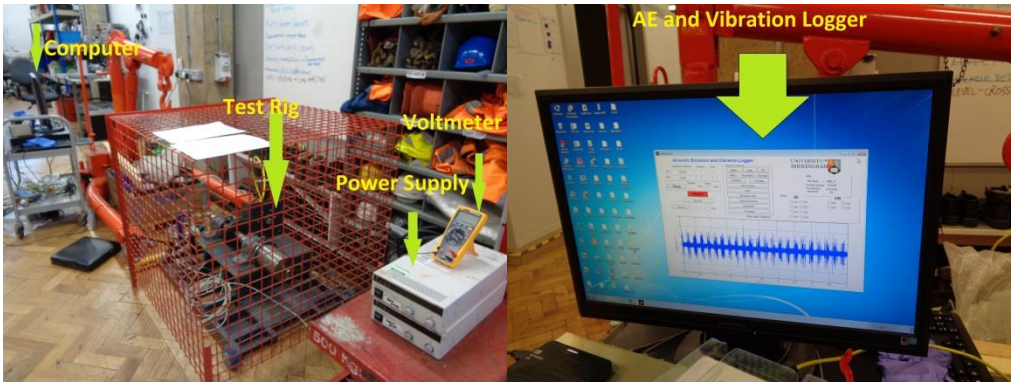

Figure 0-0-0-5: Customized bearing test rig 2 at the University of Birmingham. The photograph on the right shows the AE and Vibration data logger.

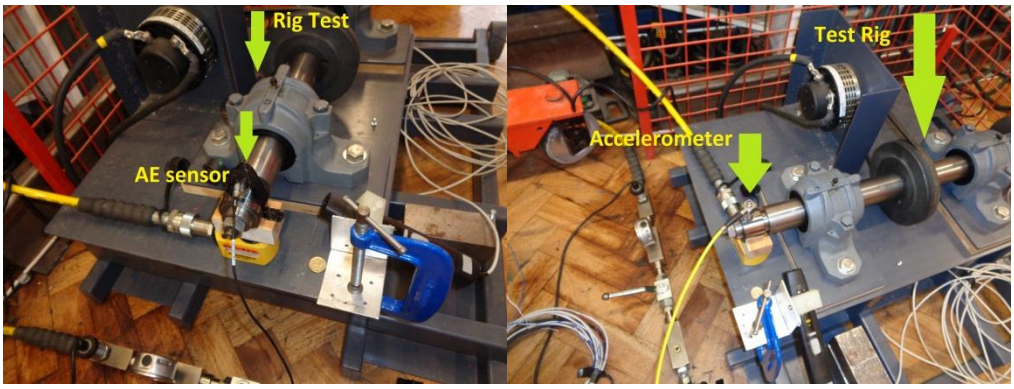

Figure 0-0-0-6: AE sensor (left) and accelerometer (right) installed on the bearing's surface

The on-board set of tests were carried out on free of defects and defective bearings using the two customised test rigs. Various faults such as outer race defects, roller defects and bearings with multiple defects were simulated during the trials. Table 6-1 describes the different induced bearing faults employed on test rig experiments. Photographs showing the aforementioned bearing faults are illustrated on Figure 6-7.

Table 6.1: Description of different induced bearing faults used on on-board test rig experiments (Amini 2016a)

Lab Test ID	Description
F0 (Healthy)	Good Condition, no induced defects
F1	Minor damage to one small area on each outer race, consisting of surface roughening by means of an electrical discharge engraver. Fault length 1.7% of

	circumference.
F2	Minor damage to one small area of one roller in each cage, again consisting of surface roughening by electrical discharge engraver. Fault length 10% of circumference.
F3	Similar to F1 above, but damage is a little larger and deeper, inflicted by means of a small rotary grinder. Fault length 2.9% of circumference.
F4	Similar to F2 above Single faulty roller in each cage. Small rotary grinder. Fault length 50% of circumference.
F5	Single ground and roughened fault, same position on each outer race. Damage inflicted by small cutting wheel and engraver. Fault length 6.6% of circumference.
F6	Significant damage, both races. Damage inflicted by small cutting wheel and engraver. Fault length 35% of circumference.
F7	Significant damage, both races and 6 rollers on each side. Debris from grinding left in bearing. Fault length 35% of race circumference, 12% of roller circumference.

F0

Figure 0-0-0-7: Induced bearing faults used during the test rig experiments

A power tool was used to generate the bearing defects on its surface. Tapered roller bearings have been used as test bearings on laboratory experiments. An example of a rig double raw tapered roller bearing is shown in Figure 6-8.

Figure 0-0-0-8: A rig double raw tapered roller bearing disassembled

6.2.2 Case study 2– Wayside testing on artificial – induced wheel flat

Wayside AE and vibration testing have been carried out using an artificial-induced wheel flat. Motorized trolley trials have been performed using a defect-free and a defective wheel for comparison purposes. The wheel diameter was 0.16m and the trolley speed was approximately 1 m/s. The wheel flat dimensions were 1mm in depth and 1cm in length. The high frequency AE and vibration reliability was assessed at this case study. The results in next chapter have shown that the vibration signal analysis has successfully detected the faulty wheel. The type of fault has also been identified during the signal processing module.

Photographs on Figure 6-9 shows the accelerometer installation wayside and the motorized trolley used at the experimental trials. Wheel flat length illustrated on photograph on Figure 6-10.

Figure 0-0-0-9: Wayside installations (left figure) and motorized trolley (right figure)

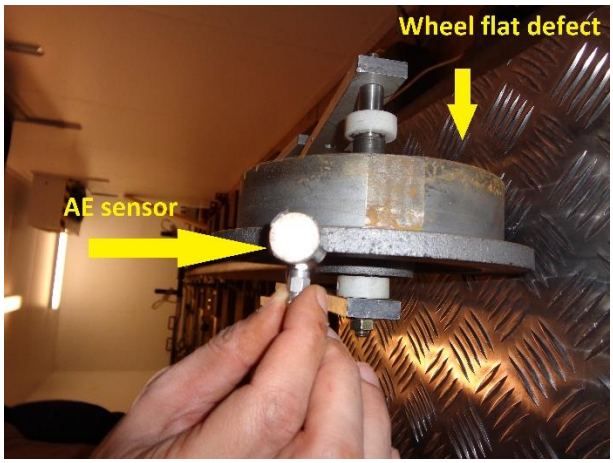

Figure 0-0-0-10: Wheel flat defect

6.3 Long Marston field trial

The customised AE and Vibration RCM system has been installed wayside at Long Marston. Field trials in collaboration with VTG Rail Limited were carried out in order to evaluate the capability of the RCM system to confirm the presence of artificially induced wheel and axle bearing faults. During the experiments, axle bearings with roller defects at different severity (2, 4, 8 mm deep) have been captured. Severity fault quantification was also achieved using the Normalised Moving RMS algorithm at the signal processing module.

Freight tanker wagons with no artificially induced fault have used at experimental trials. A locomotive with no wheelsets faults provided by Motorail Logistics used to pull or push the test train depending on the direction of movement is shown in Figure 6-11. The train was moved forward and backward over the rails with constant speed of 48Km/h and 32Km/h

respectively. Schematic on Figure 6-12 illustrates the test vehicle and the layout of the sensors.

Figure 0-0-0-11: Photograph showing the yellow locomotive and the freight test wagons (Amini 2016b)

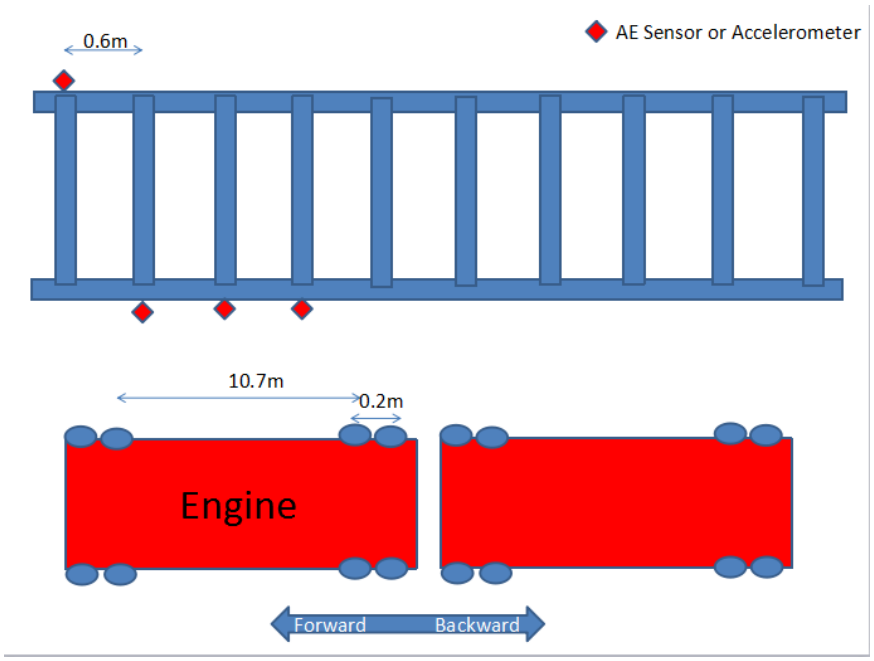

Figure 0-0-0-12: Schematic showing the test vehicle and the sensor layout at Long Marston trials

AE sensors and accelerometers were mounted on track using magnetic hold-downs. Vaseline was also used to couple the AE sensor on the web rails. The sensors were installed above the

sleepers in order to reduce the noise effect on the signal acquired due to rail bending moments. The installation of AE sensors and accelerometers is shown in Figure 6-13. Four R50a AE sensors and two Wilcoxon 712F accelerometers were used during the field trials. The sampling rate was set up to 500 kHz and 25 kHz for AE and vibration acquisition respectively. The time duration of the captured signals was 12 sec.

Figure 0-0-0-13: Photograph showing the AE sensors and accelerometers installed on the web rail at Long Marston, UK (Amini 2016b)

Schematic on Figure 6-14 shows the experimental set-up at Long Marston wayside trials. The bearing faults was at one side of train keeping the other side defect-free for comparison purposes. Photographs on Figure 6-15 show the first wagon of the test vehicle. One of the bogies contains a healthy axle bearing and three different severity axle bearing roller faults.

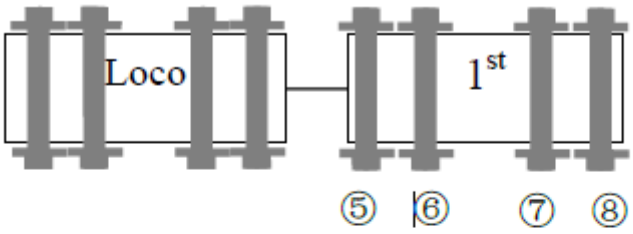

⑤: healthy bearing

⑥: 2mm roller defect

⑦: roller defect (>4mm)

⑧: roller defect (>8mm)

Figure 0-0-0-14: Schematic showing the experimental set-up with all the bearing defects (Zheng Huang 2017)

Figure 0-0-0-15: Photographs showing the first wagon of the test vehicle. The tanker contains a healthy and three fault axle bearings

An optical infrared triggering system was also used in order to trigger automated the data acquisition system when the test vehicle pass over the detection zone. Two pairs of infrared sensors were employed in the form of optical gates. Train speed can be calculated when distance between the sensors is known. When the wheelsets pass through the detection zone, the AE and vibration activity arising from the train is captured. The meaningful signal can be truncated in order to increase data storage and reduce computational time. The advantage of multiple sensors on the experiments is redundancy in case of sensor failure. Signals from multiple sensors can also be fused into a signal with the same information and less data

storage. Figure 6-16 shows the optical trigger system used for activating the data logging system at Long Marston measurements.

Figure 0-0-0-16: Photograph showing the optical trigger system used at Long Marston trials

6.4 Cropredy in-service trial

The novel RCM system has been installed on the UK rail network at Cropredy at Chiltern Railway line, adjacent to Hot Box Axle Detector for comparison purposes in October 2015. The system has been housed in a special cabinet with air ventilation. The integrated system consists of 6 channels (4 AE and 2 vibration). A mechanical treadle was used in order to activate the data logging system. The sensors in Cropredy have been put 18.5 meters away from the triggering system in order to provide enough time for the system to wake up from sleep mode (two seconds). Also the distance between the sensors is such so as to ensure at least one full rotation of the wheel occurs within the space defined by the sensor distance.

Measurement data are recorded and stored automatically. Figure 6-17 shows the schematic of sensors layout at Cropredy trials. The gain used for Cropredy measurements has been set up to 29dB in order to decrease the environmental noise that affects the AE raw signal. The Sampling rates was set up at 500 kHz and 25 kHz for AE and Vibration measurements respectively. The time duration was 6 sec due to high speed of the trains at the certain line.

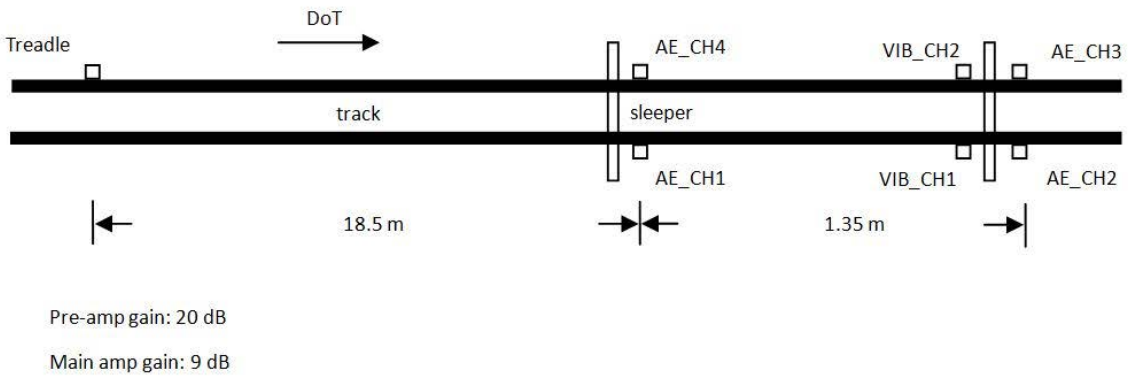

Figure 0-0-0-17: Schematic showing sensor layout at Cropredy trials. A mechanical treadle was used for activating the data logging system (Zheng Huang 2017).

The RCM system has been instrumented at Chiltern Main Line (direction from London to Birmingham). The maximum allowable train speed of line is 100MPH (160 km/h). The speed of trains can also be confirmed by the processed signal. Therefore, system has been installed properly.

Passenger and freight trains signals have been recorded. The processed measurements are discussed in the following chapter. The raw signals have been analysed using different advanced signal processing techniques. Freight and passengers trains with potentially defective wheelsets have been detected. The time and the date of the record signal were also available. Therefore, the faulty trains can be identified for further inspection. Comparison and validation between the existing technology and the purposed RCM can also be achieved using the data of Hotboxes and the signals of the potential faults.

No interference on the track circuits is the main advantage of the proposed monitoring system. The ceramic face of the AE sensors isolates electrically the sensor from the rail track enabling the installation of the system in electrified lines without obstacles. Furthermore, the installation was simple and no time-consuming (less than 1h). Figures 6-18 shows different aspects of the system's installation including the AE resonance sensors and associated pre-amplifiers and amplifiers procured from PAC, two industrial accelerometers procured from Wilcoxon, the computer logging and data storage system (2 U2531A Agilent USB DAQs) and the special cabinet.

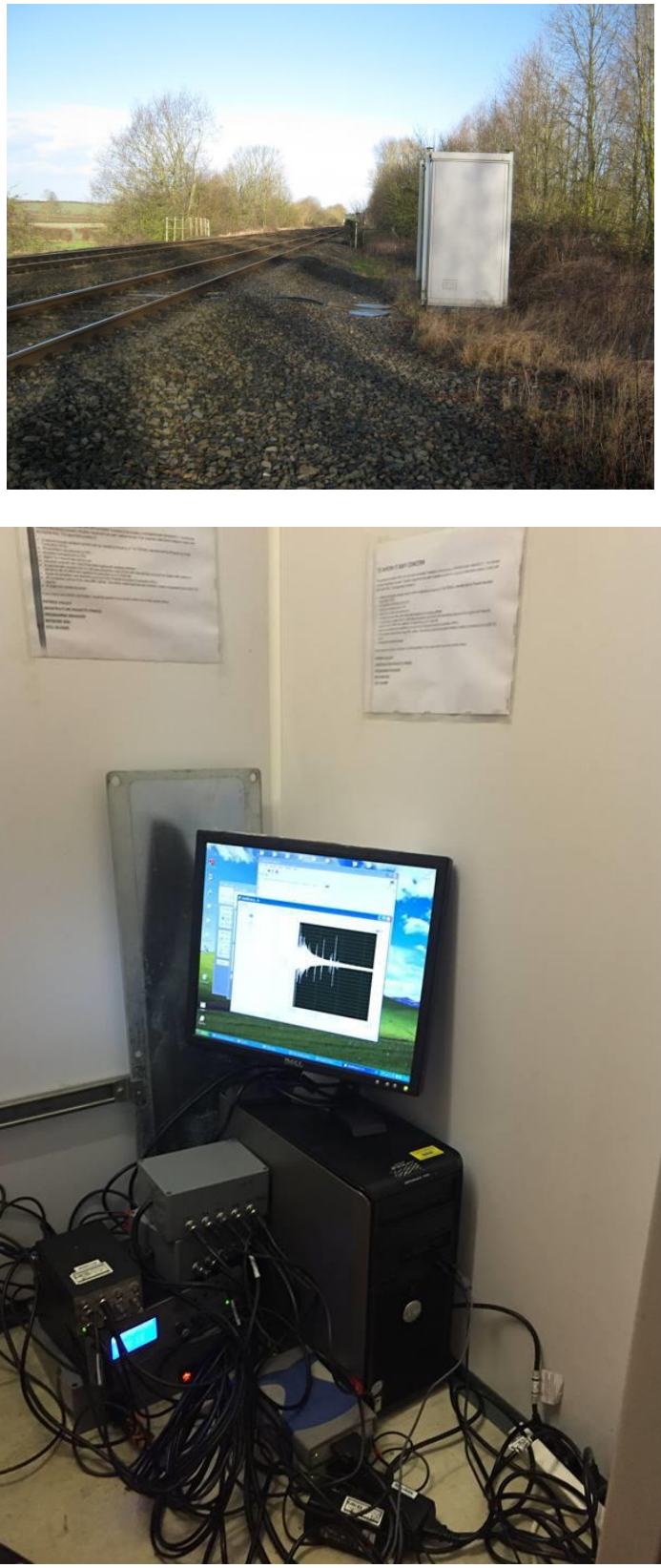

Figure 0-0-0-18: RCM system installation at Cropredy

The 168 DMU Chiltern passenger trains normally consists of 3 or 5 carriages and passed by the inspection zone at Cropredy. The aforementioned passenger trains have a maximum speed of 160 km/h.

The Type 66 freight trains are also passed by the inspection zone at Cropredy. This type of trains reach a maximum speed of about 90 km/h. The Type 66 freight trains consist of more than 25 wagons. The Chiltern Rail Line uses magnetic axle counters and is not electrified.

A safety study with all the details of the customised RCM system was submitted at Network Rail in order to authorise the system's installation at any suitable location on the UK rail network, including Cropredy. A Certificate of Acceptance with reference number PA05/06524 was issued by Network Rail.

7. Results and data analysis

The results presented in this chapter shows the effectiveness of AE and vibration analysis techniques in detecting and evaluating various types of rolling stock faults under laboratory, simulated and in-service conditions. The data analysis methods employed on the recorded signals are also discussed. Time, frequency and time-frequency analysis are applied on the raw signals. In the first part on-board measurements under laboratory conditions were carried out on healthy and faulty bearings. Two different types of test rigs were used to simulate various defects and obtain the associated AE and vibration signals. In addition, wayside AE signatures were acquired from simulated wheel flats using a test trolley. The following sections of the present chapter are concerned with the field experiments at Long Marston. The performance of the integrated customised system was evaluated under a controlled railway environment. Wheel and axle bearing defects were artificially induced on the test rolling stock. The third and last section of the results chapter presents the case of in-service trials at Cropredy site on Chiltern rail line connecting London to Birmingham. These trials served for the evaluation of the integrated technique under actual operational conditions.

7.1 Laboratory experiments on wheel and bearing defect detection

7.1.1 Impact tests

Pencil lead tip breaks (Hsu-Nielsen) tests were carried out in order to evaluate the AE sensors. The response of the accelerometers were evaluated using impulses using hammer strikes. Prior to any stimulation on laboratory or field measurements, simulated signals have been considered to validate the time and frequency response of the transducers. Hsu-Nielsen source tests were performed in order to assess the proper installation of AE sensors. During test rig measurements, an R50a AE sensor was installed on the bearing cage. The simulated signal test involved a pencil lead tip breaks against the testing surface. Figure 7-1 shows an example of multiple simulated AE signals. Each peak was generated by a lead tip break

represented a separate simulated signal. This burst type AE signal has similarities with the waveform produced by a propagating crack. From Figure 7-2 up to Figure 7-5 the zoomed-in plots of the previous signal are presented.

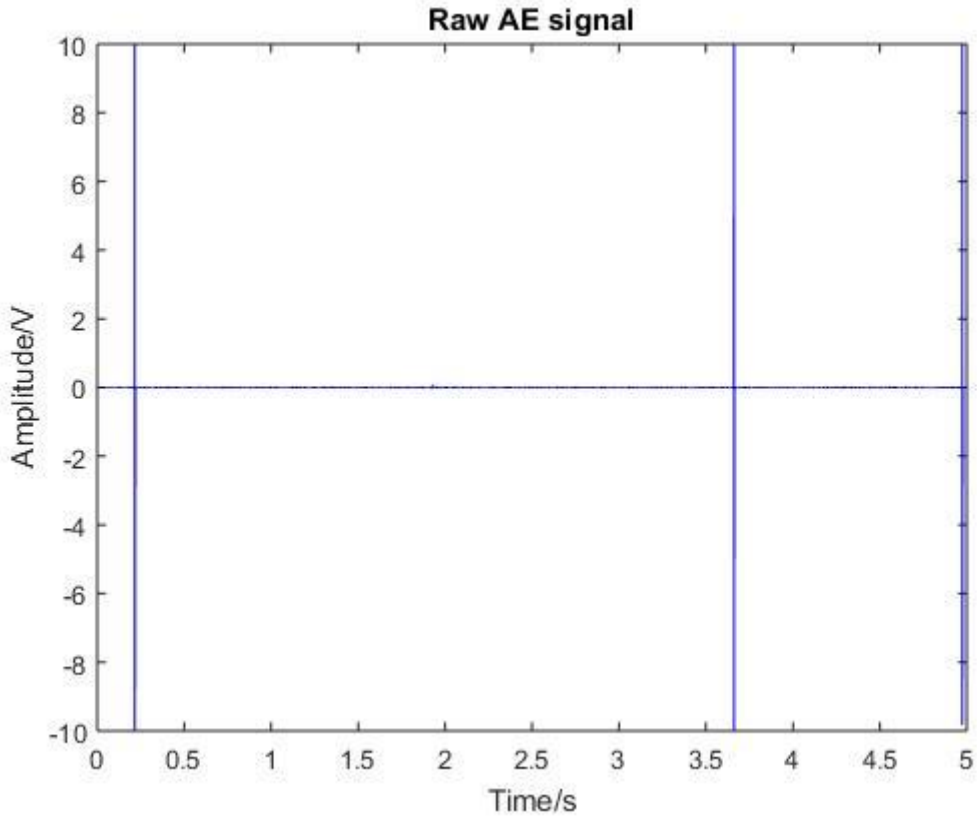

Figure 7-0-1 : Raw AE burst signal generated by pencil brake tests

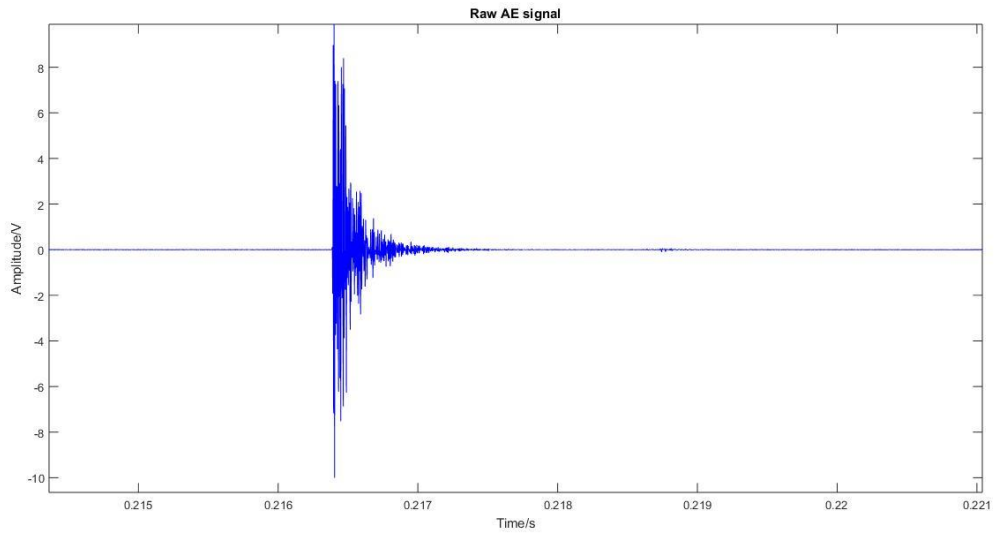

Figure7-0-2: Raw AE burst signal zoomed-in

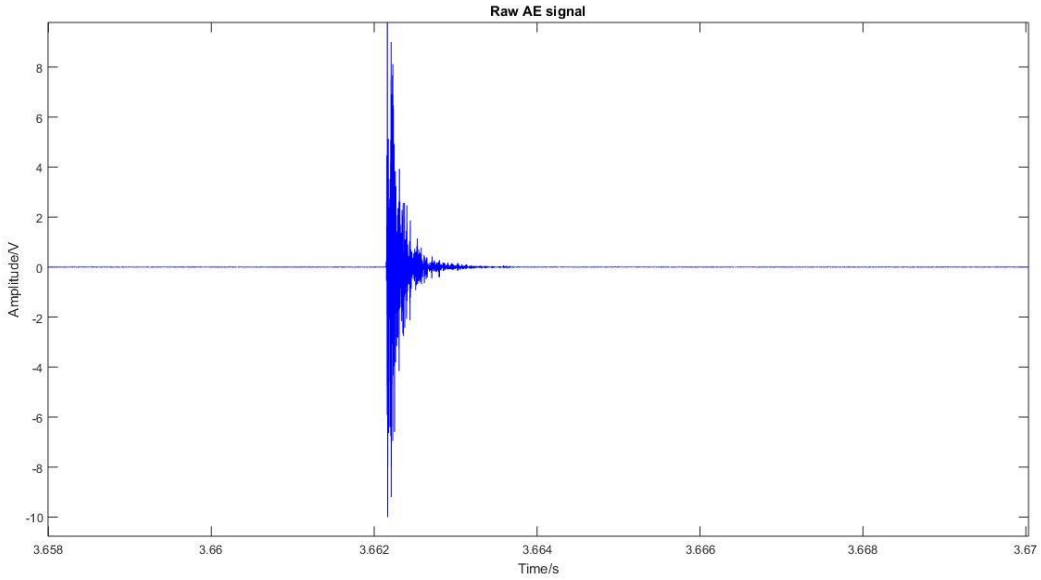

Figure 7-0-3: Raw AE burst signal zoomed-in

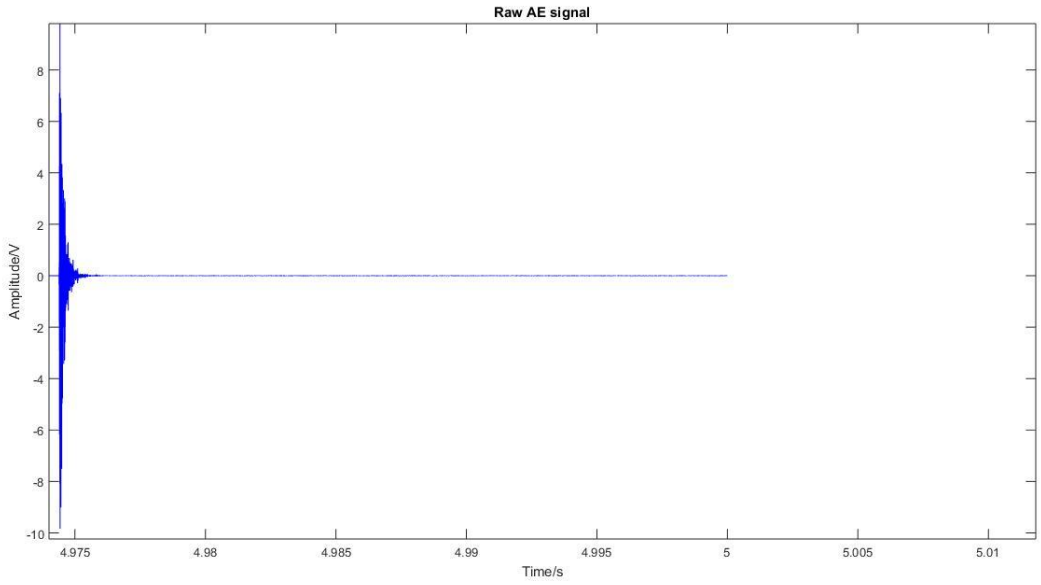

Figure 7-0-4 : Raw AE burst signal zoomed-in

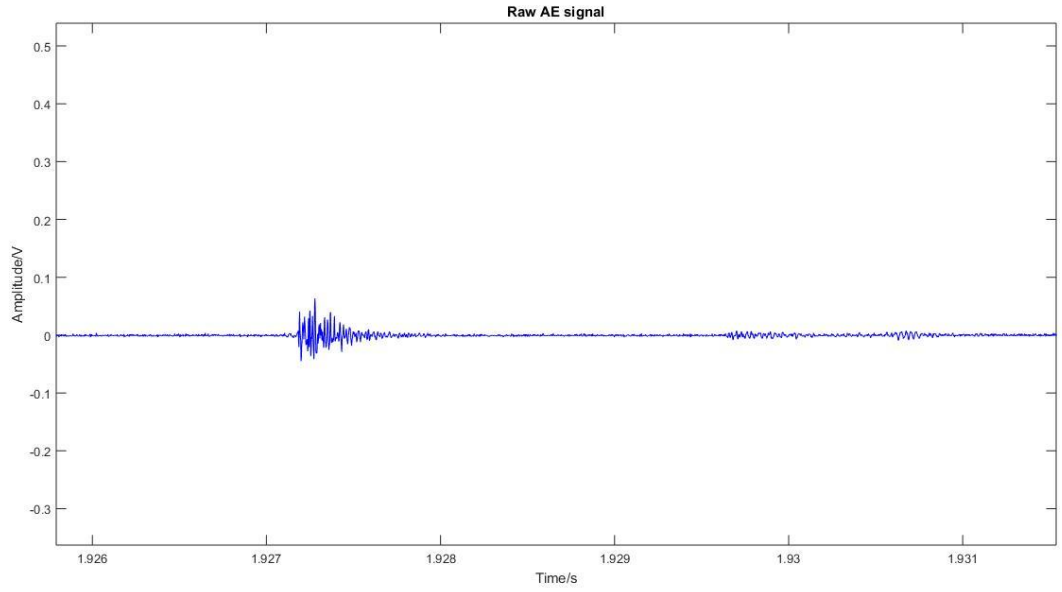

Figure 7-0-5 : Raw AE burst signal zoomed-in

The power Spectrum of the simulated signal is shown in Figure 7-6. As it can be seen, the frequency response of the signal is mostly excited between 165 and 185kHz.This is expected since the resonance frequency of R50a AE sensor is 170 kHz.

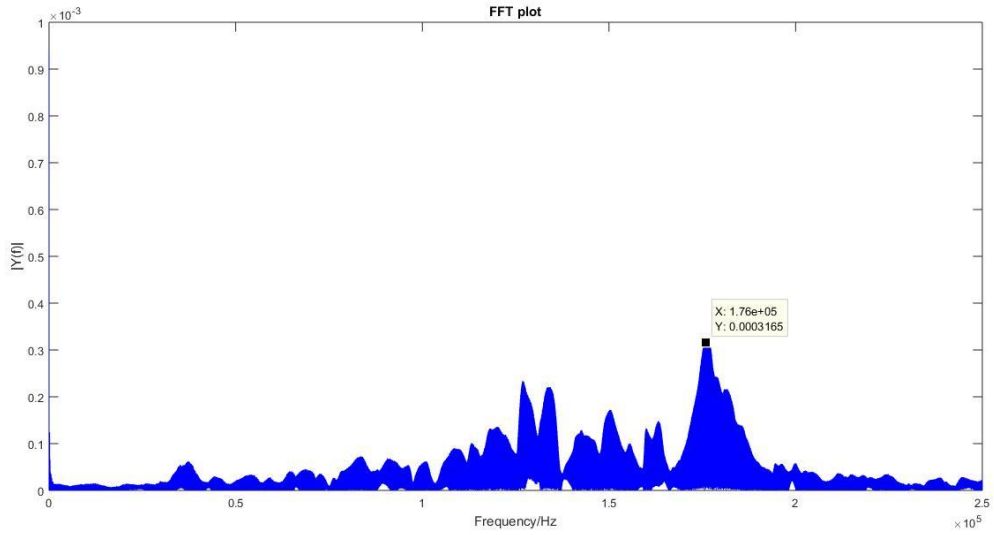

Figure 7-0-6: Power spectrum of the impact test

Figure 7-7 shows a raw vibration signal captured during impact test on the bearing. Figure 7-8 presents the zoomed-in plot of the previous signal. The frequency spectrum is illustrated in Figure 7-9. Looking into frequency response of the captured signal, high multiple peaks between 2 kHz and 4 kHz can be recognized.

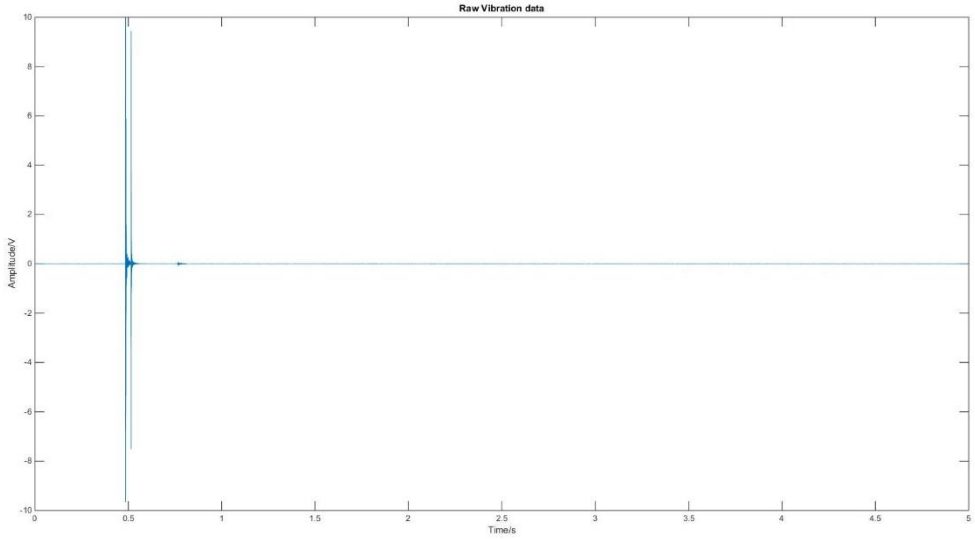

Figure 7-0-7: Impact test on the bearing

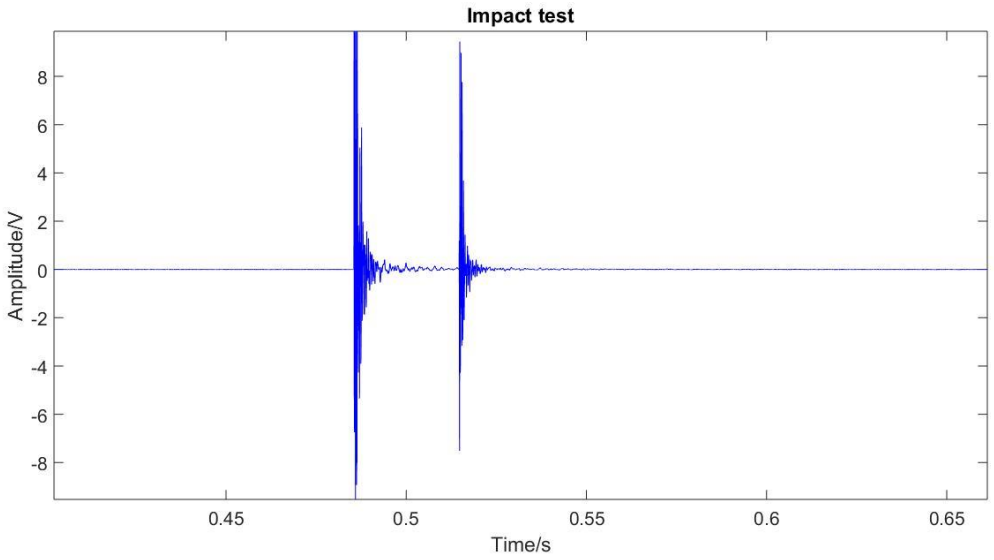

Figure 7-0-8: Zoomed-in raw Impact test signal

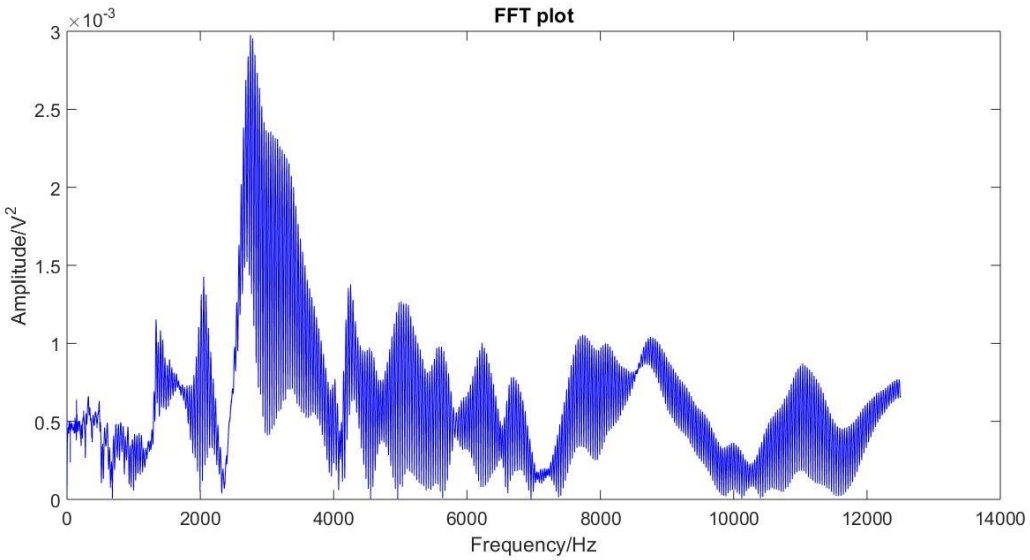

Figure 7-0-9: Power spectrum of the previous signal

7.1.2. Case study 1 - Outer race defective bearings

As part of the test rig experiments, the detection and evaluation of outer race bearing defects were investigated. On-board AE and vibration signals were recorded using the customised test rig 1. Figure 7-10 shows the raw AE signature acquired for a bearing with an outer race defect at a rotational speed of 500 RPM. The peaks seen in raw AE signature are the impacts of the outer race fault each time the bearing rotates. Modulation of the waveform is also clearly visible.

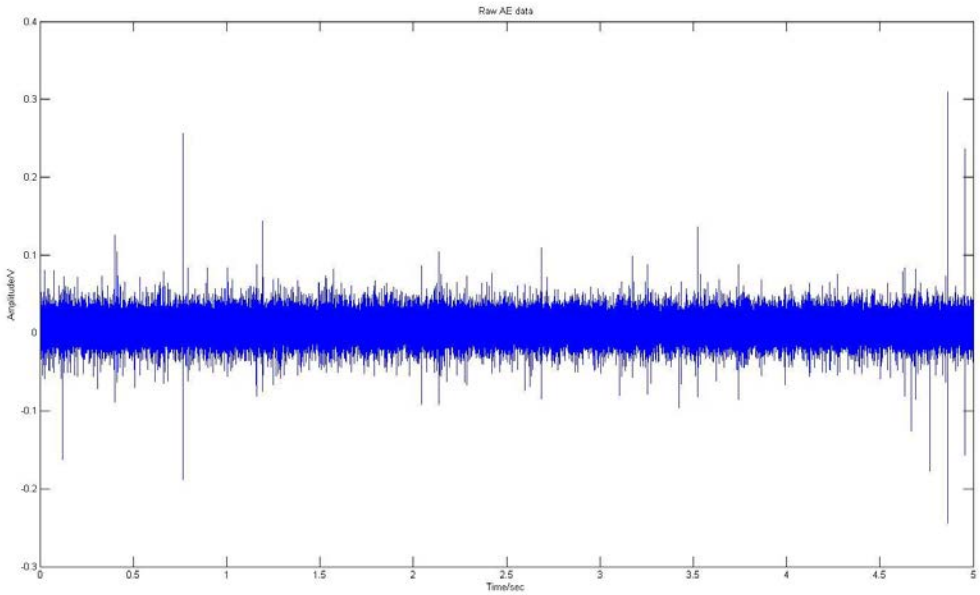

Figure 7-0-10: Raw acoustic emission signal obtained from an outer race defective bearing at 500RPM

The acquired signal processed using frequency domain analysis in order to identify the characteristic frequency and its harmonics at spectrum. HFRT algorithm has been applied on the raw data. As it can be seen in Figure 7-11 a characteristic fault frequency of 74 Hz and its harmonics are clearly seen. This corresponds to a known race faulty frequency for this model of bearing at 500 RPM (see table 7.1). Hence, the outer race defect has been identified successfully on this particular the test bearing. There is a slight offset between the theoretical and observed faulty frequency due to slight variation of the actual rotatio0nal speed during the experiments. In addition, a dominant peak at 8.3 Hz $(8.3Hz = \frac{500\,rpm}{60s})$ is observed at the HFRT plot due first order of turning speed of the test rig.

Table 7.1: Bearing Fundamental Frequencies in the customized test rig- 76.9Hz frequency and its harmonics were expected to appear in the HFRT plot (Amini 2016a)

	Speed (RPM)						
Defect types	150	250	300	400	500	600	1000
FTF	1.1	1.8	2.2	2.9	3.6	4.4	7.3
BPFO	23.1	38.4	46.1	61.5	76.9	92.3	153.8
BPFI	29.4	49.05	58.8	78.5	98.1	117.7	196.2
BSF	19.7	32.9	39.5	52.7	65.85	79	131.7

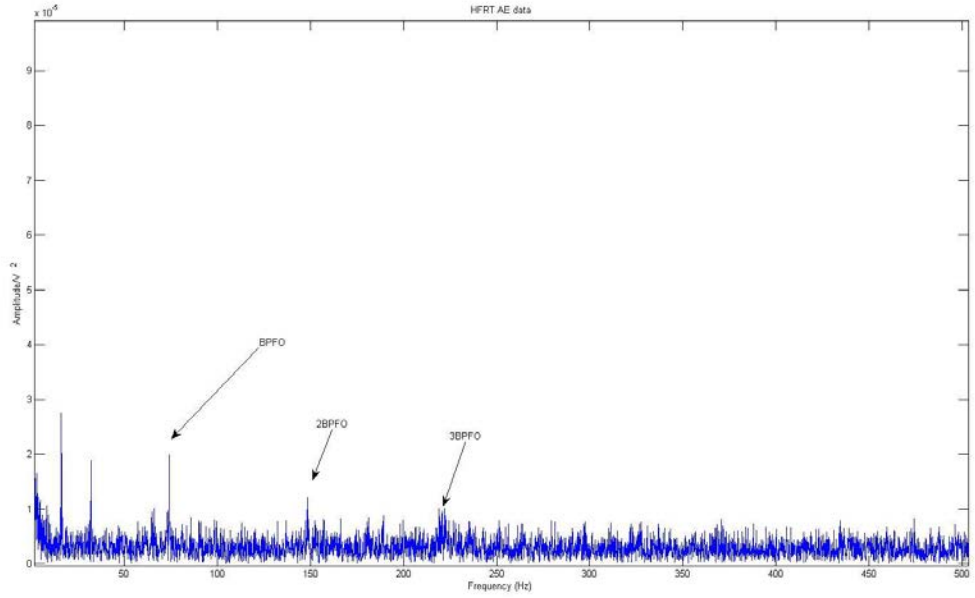

Figure 7-0-11: HFRT plot of the previous raw acoustic emission signal. The BPFO frequency and its harmonics are clearly revealed

In case of vibration analysis, the same pattern is observed. Impacts generated by the outer race defect are visible in the raw vibration signal acquired at 500RPM (Figure 7-12). The HFRT plot of the raw signal is shown in Figure 7-13. This algorithm is employed for detecting the faulty characteristic frequency at the spectrum. Peaks related to BPFO and its harmonics are identified. Therefore, the accuracy of the proposed method is validated.

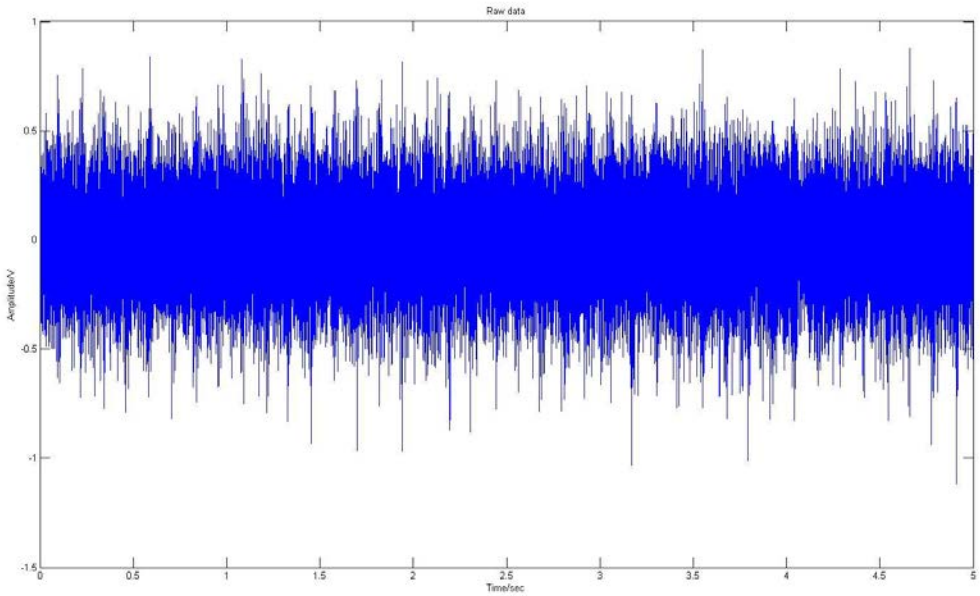

Figure 7-0-12: Raw acoustic vibration signal obtained from an outer race defective bearing at 500RPM

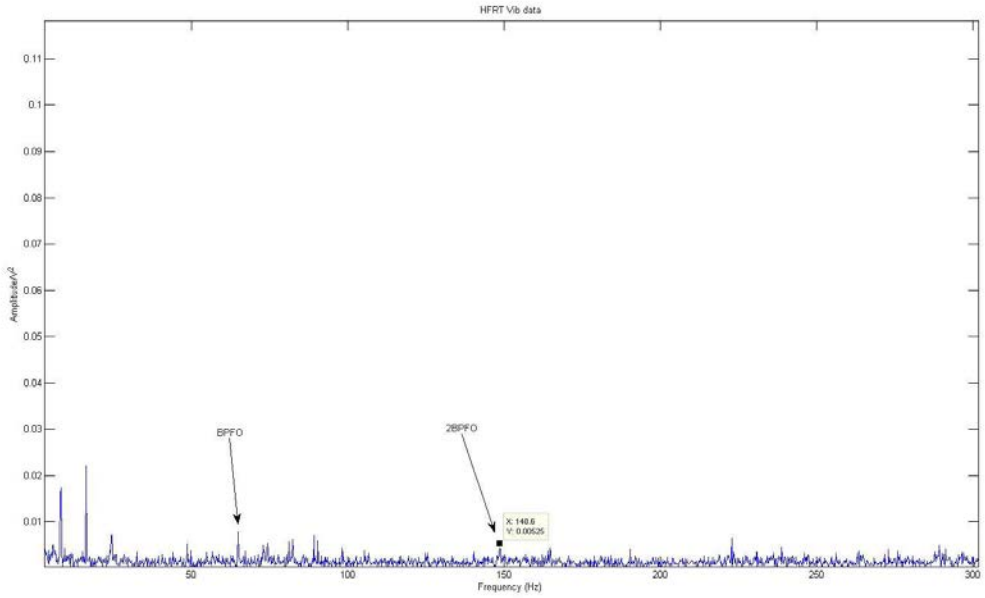

Figure 7-0-13: HFRT plot of the previous raw vibration signal. The BPFO frequency and its harmonics are clearly observed

7.1.3 Case study 2- Roller defective bearings

Bearing defect quantification was also evaluated by performing normalisation of the moving RMS and associated frequency analysis. AE and vibration signals were recorded using two roller defective bearings with different severity (F2 and F4 at Table 6-1). Defect-free signals were also acquired for comparison purposes. Test rig 2 used for this part of experiments.

Figure 7-14 shows three AE signals recoded from two rollers defective bearings with different defect severity and a healthy bearing at 500rpm. The fault length was 10% and 50% of circumference respectively. Figure 7-15 presents the Moving RMS plots of the above signals after they have been normalised. It can be observed that the fault length has an effect on signal's amplitude. Therefore, normalisation of the Moving RMS permits the sorting of the signals with respect to the actual severity of the defect. Establishing the threshold for the healthy condition can also be used for automated signal analysis.

The power spectra of the previous AE signals are shown in Figure 7-16. The results obtained indicate that the high-amplitude peaks generated by the bearing with a roller defect with 10% fault length and the healthy bearing have no clear difference. Hence, it is not feasible to evaluate the defect severity using frequency domain analysis.

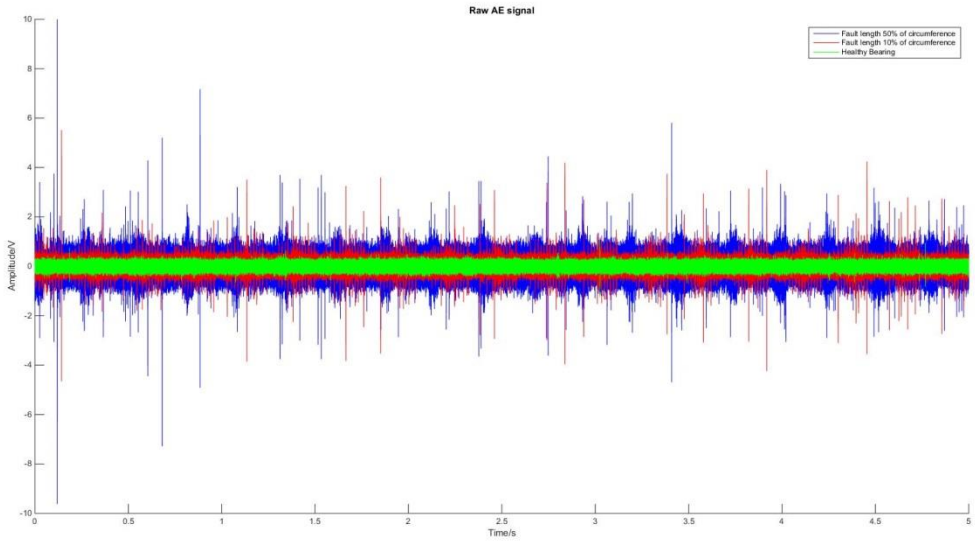

Figure 7-0-14: Results from three raw acoustic emission signals obtained from two roller defective bearings and a defect-free bearing (50% fault length of circumference- blue signal, 10% fault length of circumference- red signal and defect- free bearing - green signal)

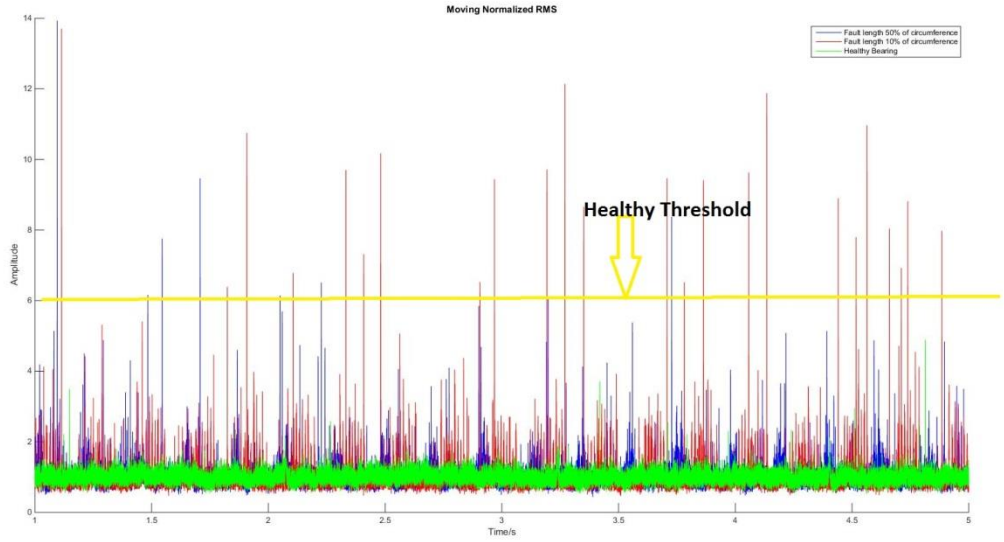

Figure 7-0-15: Normalized Moving RMS plots of the above acoustic emission signals. The difference between the defective bearings and the defect-free bearing is clearly evidence.

(50% fault length of circumference- blue signal, 10% fault length of circumference- red signal and defect- free bearing - green signal)

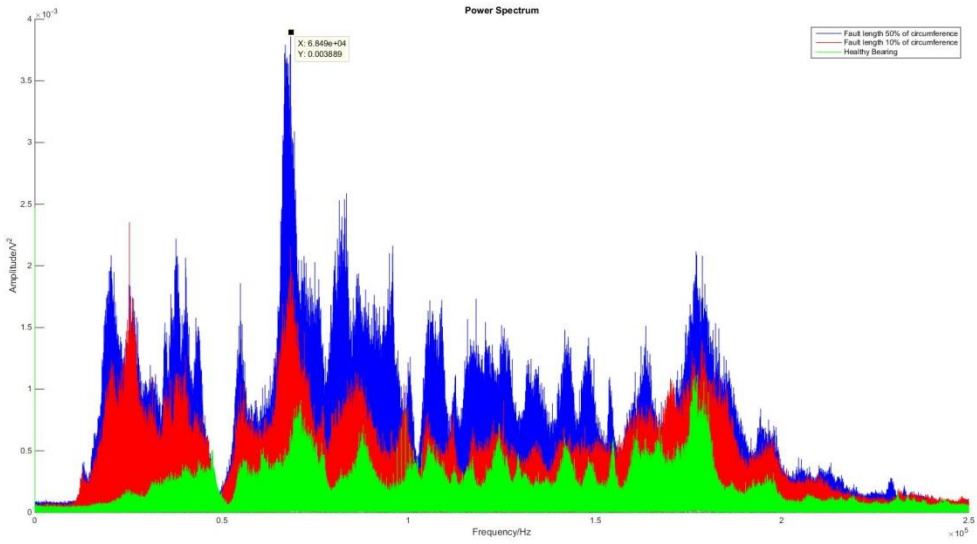

Figure 7-0-16: Power Spectrum results of the previous acoustic emission signals. (50% fault length of circumference- blue signal, 10% fault length of circumference- red signal and defect- free bearing - green signal)

Figure 7-17 shows three raw vibration signal generated by two bearings containing roller defects with different level of severity and a healthy bearing at a rotational speed of 500rpm. As the bearing condition deteriorates, the signal amplitude increases. Figure 7-18 shows the Moving RMS plots after normalisation obtained from the above signals. Based on the results of the analysis presented below, the same conclusions as discussed earlier in the present chapter section can be drawn. Hence, the severity of the bearing defects can be evaluated through normalisation of the Moving RMS results.

The frequency spectra of the above three vibration signals are shown in Figure 7-19. High amplitude peaks between 2 kHz and 4 kHz are clearly seen in the spectra of the two defective bearings. This frequency range can be used as a reference for further processing.

Peaks between 2 kHz and 4 kHz are no longer visible in the spectrum of the defect-free bearing. Therefore, the results suggest that frequency analysis can be used to identify bearing roller defects.

HFRT analysis was carried out to process a dataset where the bearing tested contained a roller defect with 50% fault length of circumference. Looking into the HFRT plot of the recorded signal (shown in Figure 7-20) the bearing characteristic frequency of 62 Hz and its harmonics can be recognized. This frequency corresponds to a known roller fault frequency for this bearing model at 500rpm. In addition, a dominant peak at 3.8 Hz, which corresponds to a fundamental train frequency (FTF), is clearly seen.

Thus, HFRT algorithm can be applied for the identification of the type of the bearing defect.

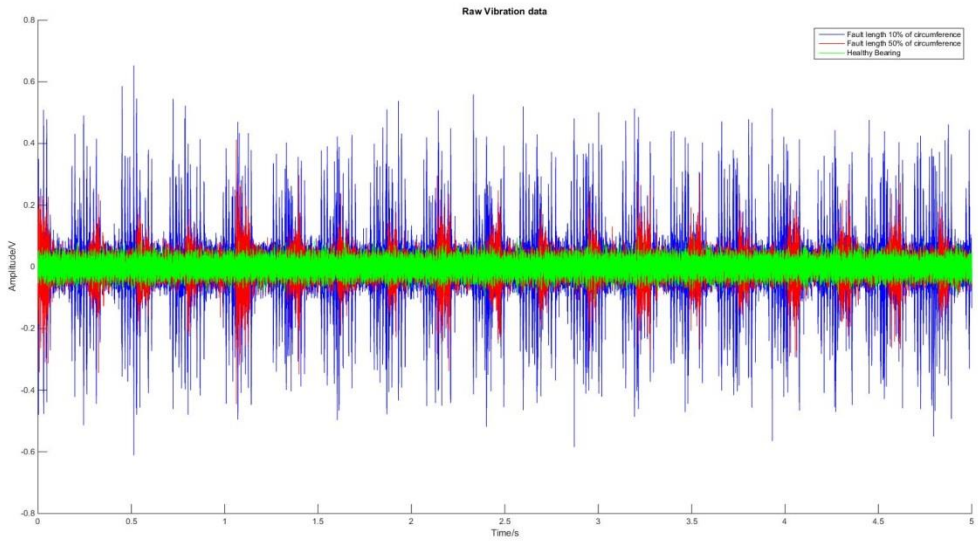

Figure 7-0-17: Three raw vibration signals recorded by two rollers defective bearings with different defect severity and a healthy bearing at 500rpm. (50% fault length of circumference- blue signal, 10% fault length of circumference- red signal and defect- free bearing - green signal)

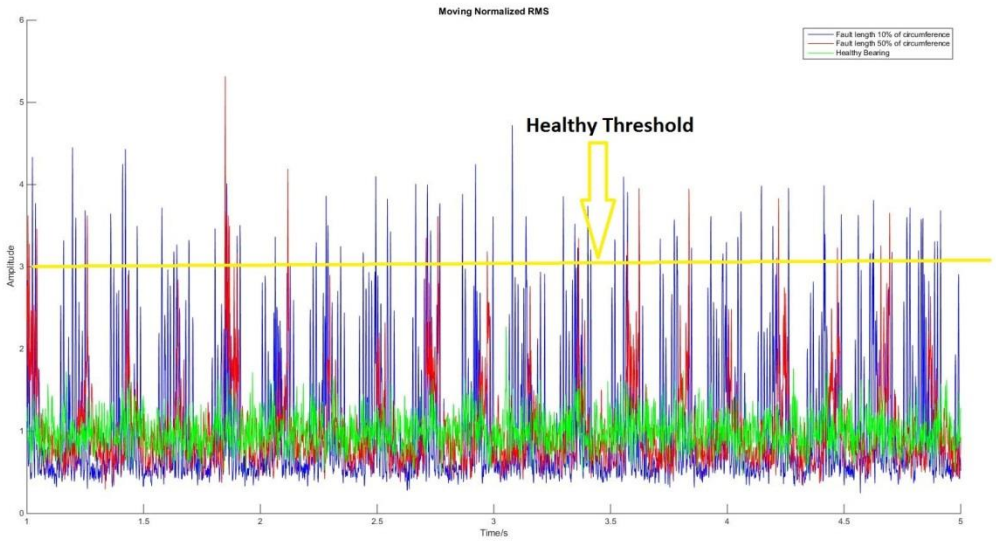

Figure 7-0-18: Normalized Moving RMS plot of the previous vibration signals. The conclusion from the previous Normalized Moving RMS plot of the acoustic emission example still applies. (50% fault length of circumference- blue signal, 10% fault length of circumference- red signal and defect- free bearing - green signal)

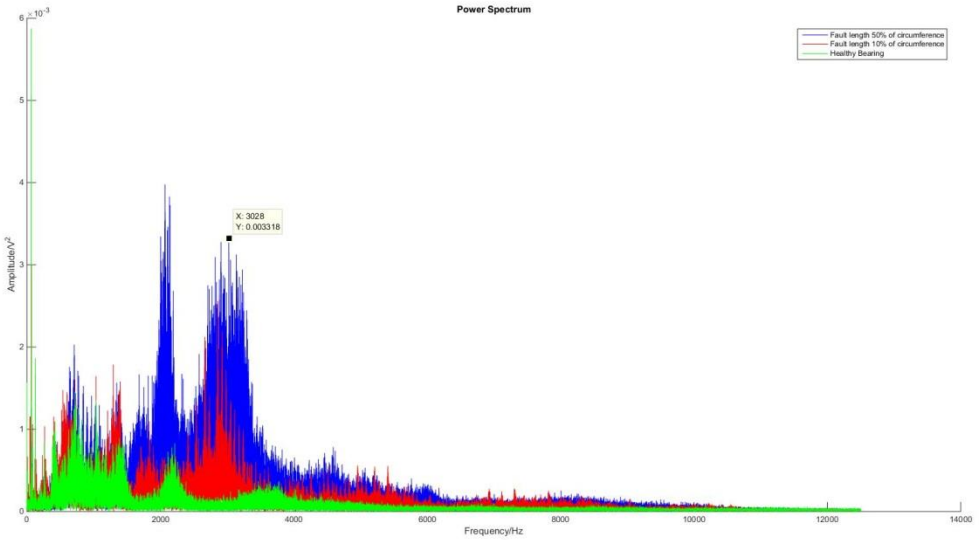

Figure 7-0-19: Power Spectrum of the previous vibration signals. High amplitude peaks between 2 KHz and 4 KHz are clearly visible at the datasets from roller defective bearing. (50% fault length of circumference- blue signal, 10% fault length of circumference- red signal and defect- free bearing - green signal)

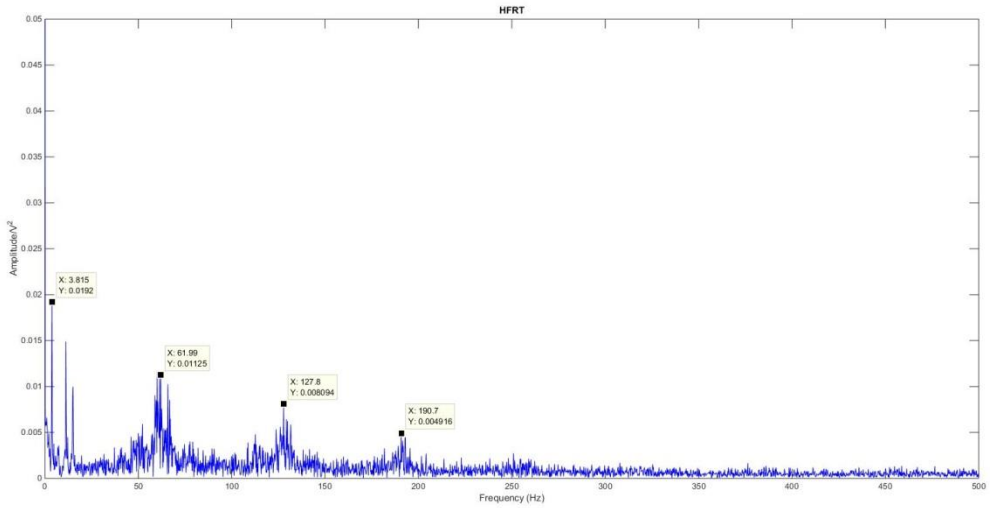

Figure 7-0-20: HFRT plot of the vibration signal generated by the roller defective bearing with 50% fault length of circumference is illustrated. BSF, its harmonics and FTF are clearly visible

7.1.4 Case study 3 - Bearing with multiple defects

As part of the laboratory test plan, the performance of the AE and vibration technique in detecting bearings with multiple defects was evaluated. Two sets of experiments were carried out using a larger test rig. The rotational speed of the tests was between 100 and 700 RPM. The first testing configuration considered, involved a bearing with significant damage in both outer and inner races and six rollers on each side. The second one involved a bearing with damage in both outer and inner races. Results on healthy and defective bearings are presented and discussed.

The plot in Figure 7-21 shows an example of comparison between defective and defect-free bearings. AE signals were recorded at 500RPM. A visible difference in amplitude can be recognised. High amplitude peaks at blue signal generated by the impacts of the defect. The Moving RMS results after normalisation are provided in Figure 7-22. The peaks related to defective bearing can be clearly seen. The power spectra are shown in Figure 7-23, further confirm the presence of the defective bearing.

HFRT algorithm has been performed to analyse the raw AE signals generated by the defective bearing. The HFRT plot is shown in Figure 7-24. The fundamental frequencies of the bearing are BPFO= 76.9Hz, BPFI= 98.1Hz, BSF=65.85Hz. The aforementioned frequencies are observed in the plot. The harmonics of BPFO are also visible. However, harmonics of BPFI and BSF are not observed. There is a slight offset between the theoretical and the observed fundamental frequencies due to the slight variation in the rotational speed during the test.

Cepstral analysis is more suitable for detecting multiple defects. The Cepstrum plot is shown in Figure 7-25. The peaks at $\frac{1}{95.79} = 0.01044$, $\frac{1}{77.04} = 0.01298$ and $\frac{1}{66.75} = 0.01498$ confirm the presence of three different faults and identify the type of the defect by correlating the peaks in the cepstrum plot with the BPFI, BPFO and BSF of the bearing at 500 RPM rotational speed. Therefore, Cepstrum processing provides consistent results.

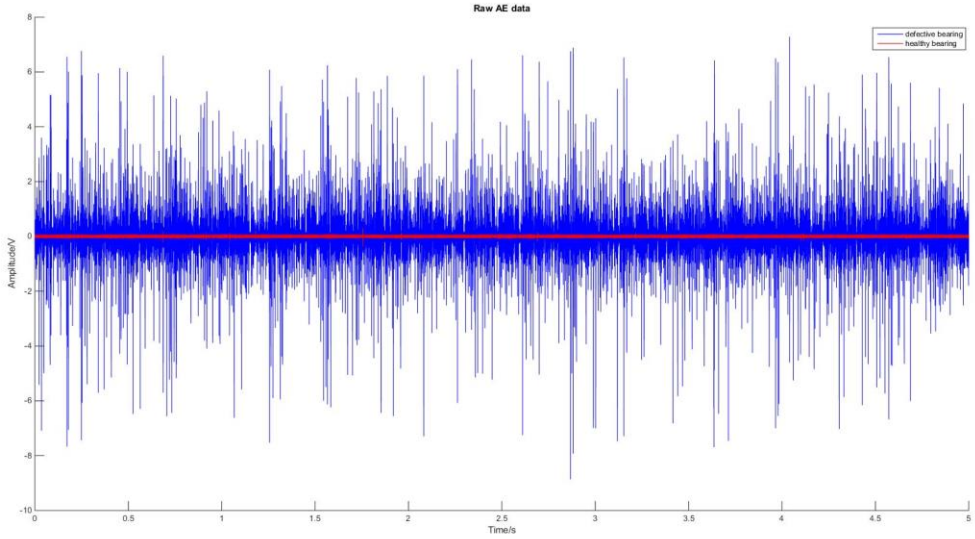

Figure 7-0-21: Acoustic emission signals acquired by a defective bearing with multiple faults (blue signal) and a defect-free bearing (red signal)

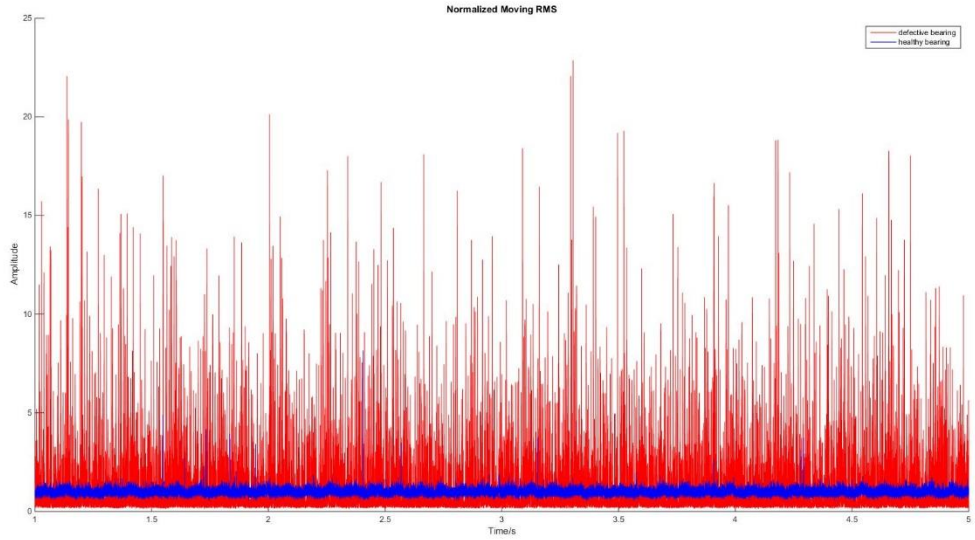

Figure 7-0-22: Normalized Moving RMS plots. High amplitude peaks are visible at signal generated by the defective bearing (red signal). No obvious peaks at signal recorded by the healthy bearing (blue signal)

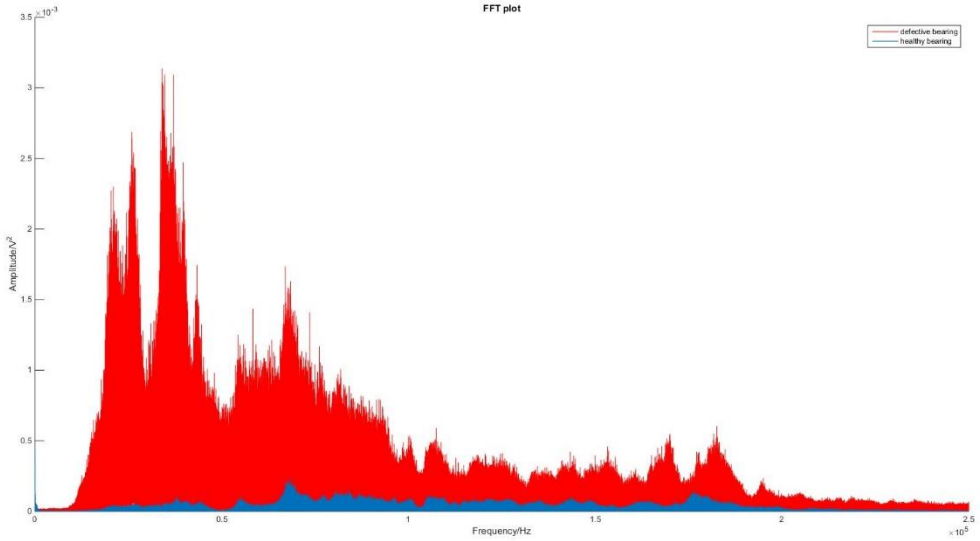

Figure 7-0-23: Power spectrums of the previous acoustic emission signals. Defective bearing is the red signal and healthy bearing is the blue signal

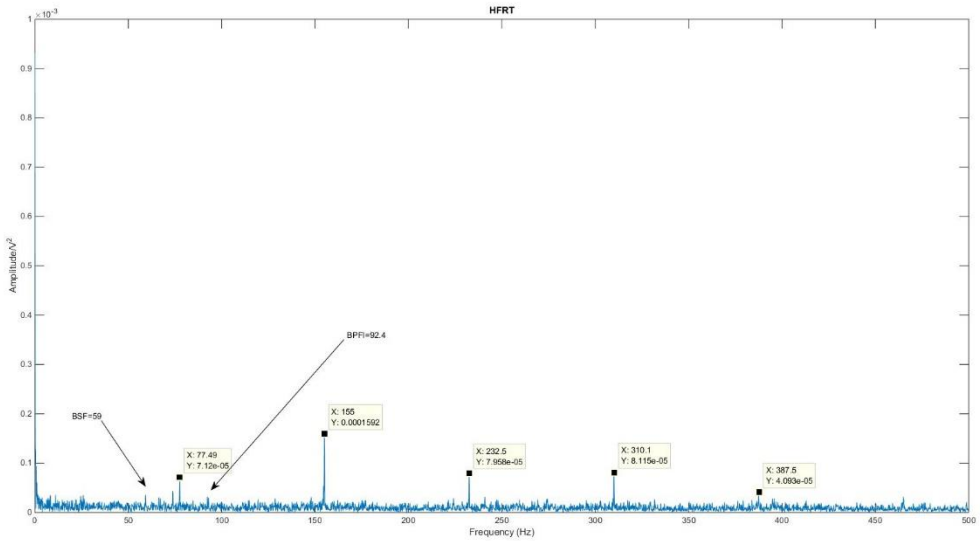

Figure 7-0-24: HFRT plot for the defective bearing showing clear the fundamental frequencies and the harmonics of the BPFO.

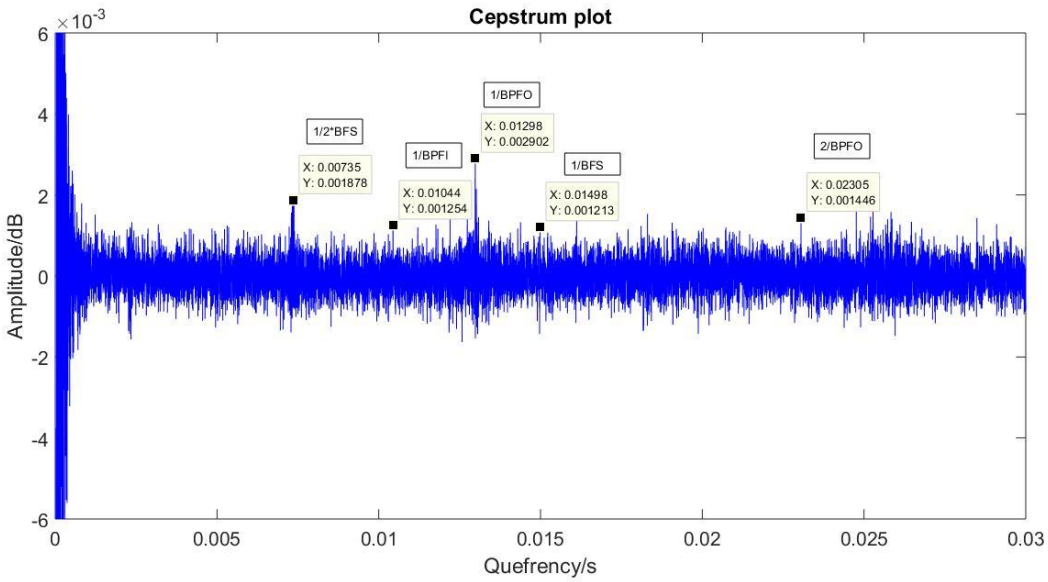

Figure 7-0-25: Cepstrum plot of defective bearing showing clear the three fundamental frequencies of the bearing at 500RPM

The raw vibration signal generated by a defective bearing with damage in both outer and inner races and in six rollers is shown in Figure 7-26. The rotational speed is 500 RPM. Figure 7-27 presents the power spectrum analysis of the previous signal. High amplitude peaks are generated between 2 kHz and 4 kHz indicating the presence of the bearing defects. This frequency range has been used as a reference for the band-pass filter at HFRT analysis.

Cepstrum analysis has been performed at the vibration signal (Figure 7-28). The fundamental frequencies of the bearing at 500RPM are BPFO= 76.9Hz, BPFI= 98.1Hz, BSF=65.85Hz. The peaks at $0.01288 = \frac{1}{77.64}, 0.01008 = \frac{1}{99.2}, 0.01588 = \frac{1}{62.97}$ confirms the presence of the faults. There is a slight offset between the theoretical and the observed fundamental frequencies due to the slight variation in the rotational speed during the test. The plot in Figure in Figure 7-29 is the zoomed-in of the Cepstrum results.

HFRT algorithm has also been applied at the vibration signal. Figure 7-30 shows the HFRT results. The BPFO frequency and its harmonics are visible. The plot in Figure 7-31 is the zoomed-in of the HFRT result. The BSF frequency was revealed. However, the BPFI frequency was not observed. Therefore, Cepstrum analysis of the vibration signal obtained is more suitable for detecting the fundamental frequencies when multiple faults are considered.

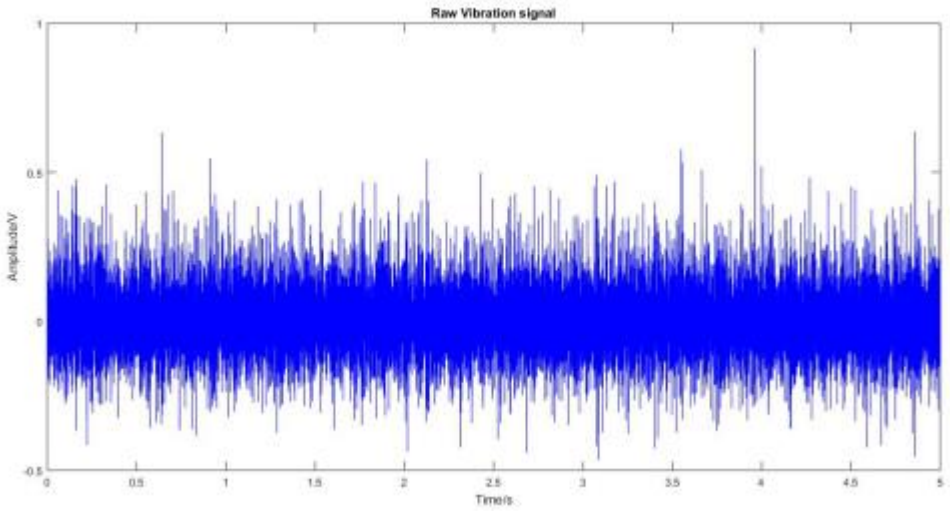

Figure 7-0-26: Raw vibration signal recorded by defective bearing with significant damage at both races and in six rollers at 500 RPM

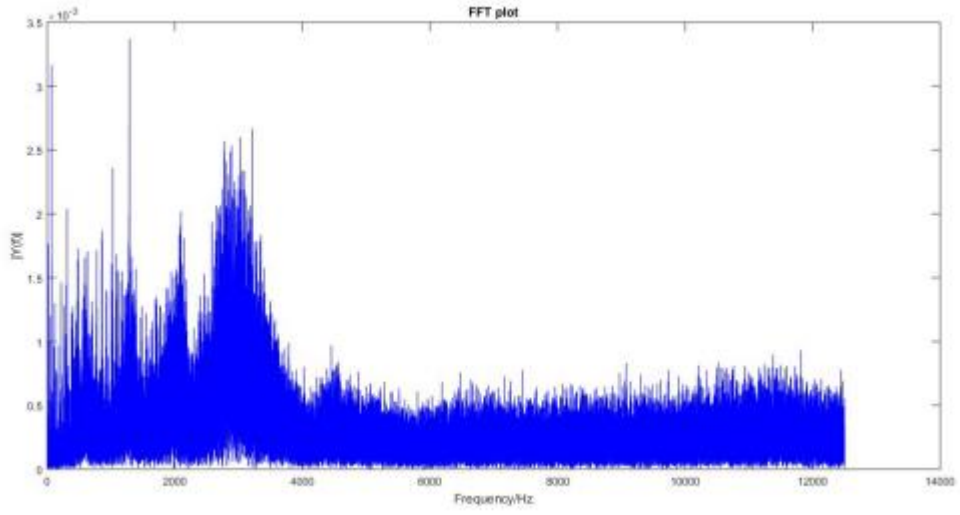

Figure 7: 0-27: Power spectrum of the previous vibration signal. High amplitude peaks are visible between 2 kHz and 4 kHz. These frequency range can be used for further processing

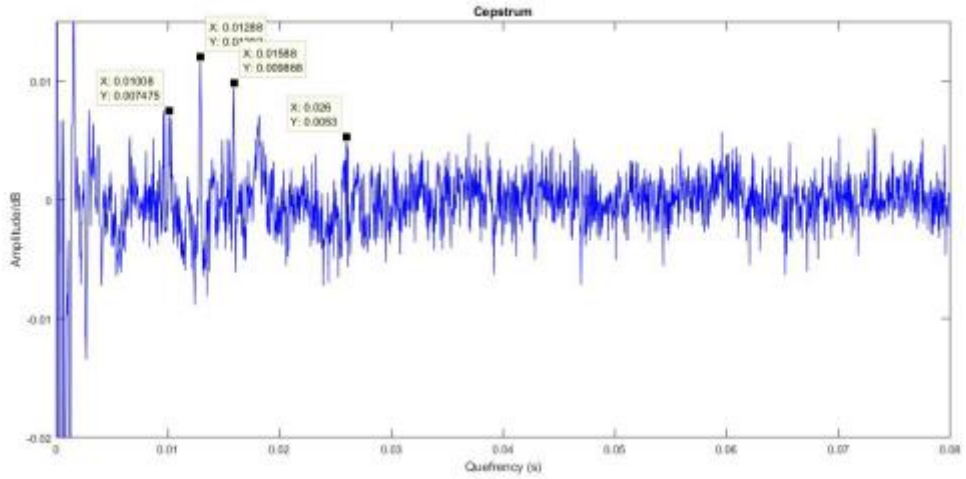

Figure 7-0-28: Cepstrum plot of the previous vibration signal

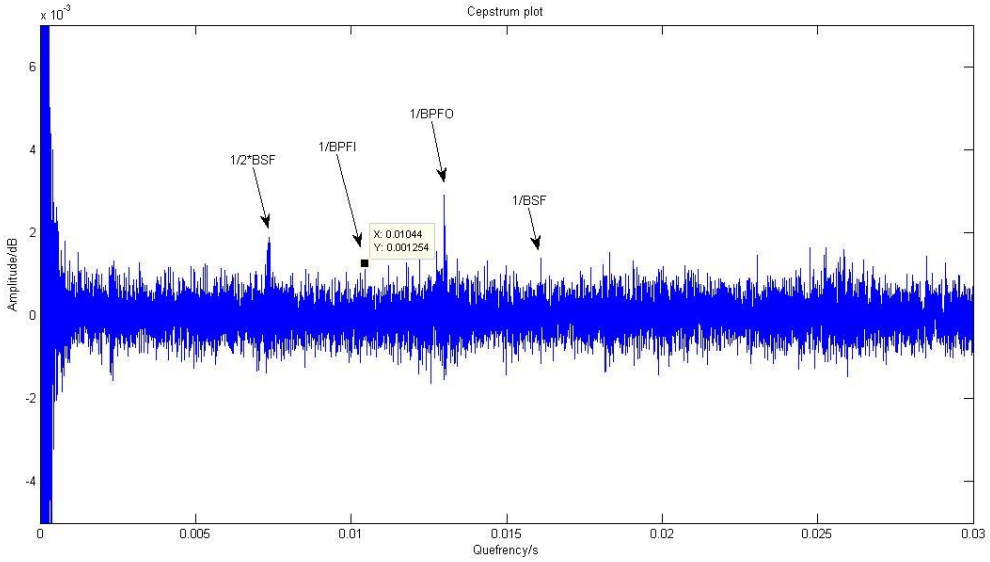

Figure 7-0-29: Zoomed-in of Cepstrum plot. The BPFO, BPFI and BSF frequencies are visible. Cepstrum algorithm is the most suitable type of analysis when multiple defects are considered

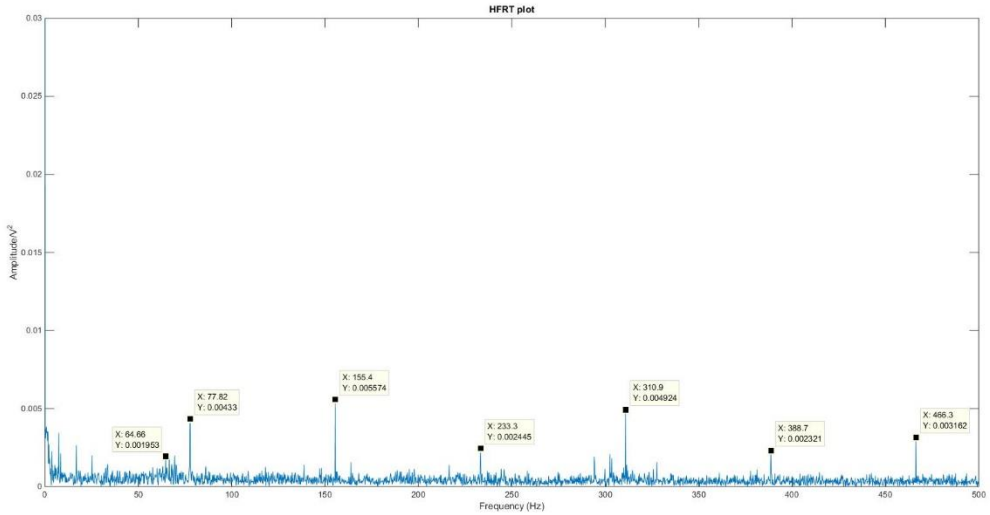

Figure 7-0-30: HFRT results showing the BPFO frequency and its harmonics. BSF frequency is also obvious. In contrast, the BPFI frequency is not presented

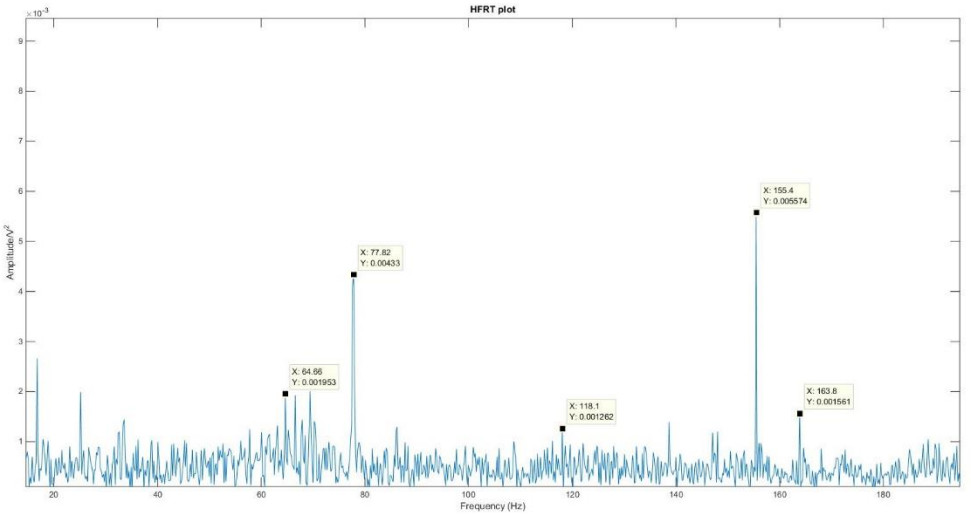

Figure 7-0-31: HFRT results zoomed-in

Laboratory tests were also carried out on a bearing with damage in both outer and inner races to investigate the capability of AE and vibration analysis to detect the defects. Data were recorded for a few seconds and the rotational speed was between 100 and 700 RPM. Two signals were selected to represent the ability of AE and vibration techniques to detect multiple defective bearings. Figure 7-32 shows an example of an AE signal generated by a defective bearing with damage in both inner and outer race. The rotational speed was 500

RPM. The power spectrum plot of the previous signal is provided in Figure 7-33. The results shows high amplitude peaks after 100 kHz are related to the bearing defects. The Cepstrum plot is shown in Figure 7-34. No obvious peaks related to defects are visible to cepstrum results. Therefore, the cepstrum analysis is no longer suitable for this particular dataset. HFRT algorithm has been applied on the AE signal. The result is provided in Figure 7-35. The BPFO frequency and its harmonics are clearly observed. In contrast, BPFI frequency is not visible at the HFRT plot.

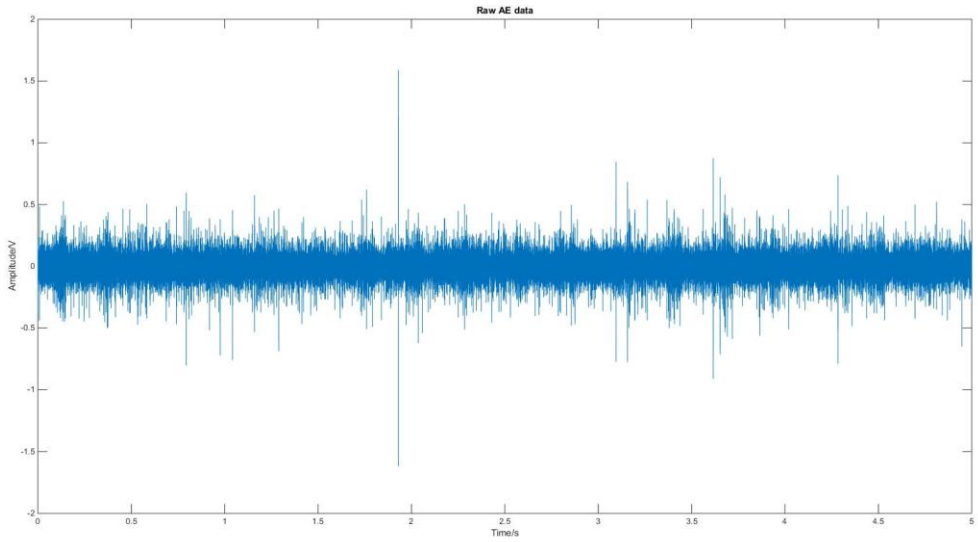

Figure 7-0-32: Raw acoustic emission signal generated by defective bearing with damage in both races at 500 RPM

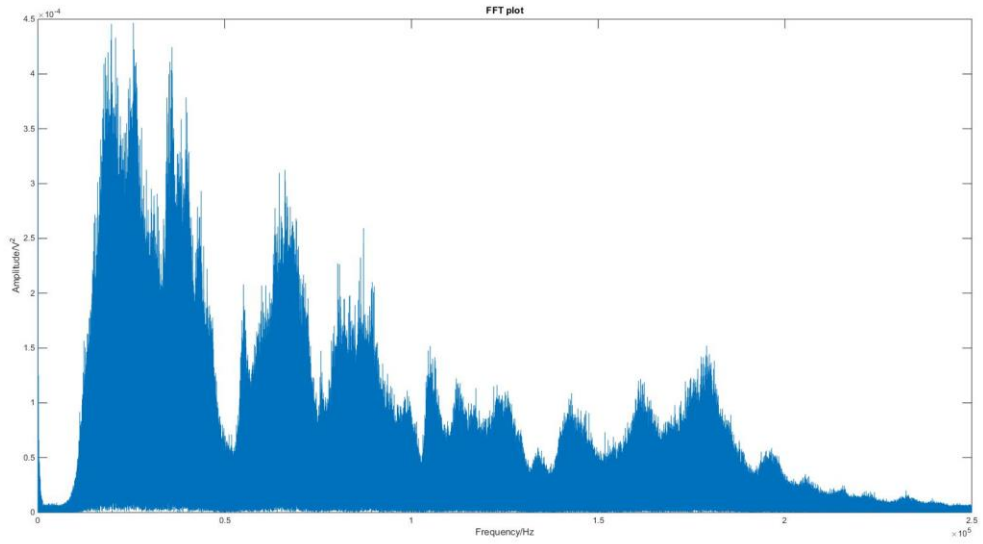

Figure 7-0-33: Power spectrum of the previous acoustic emission signal

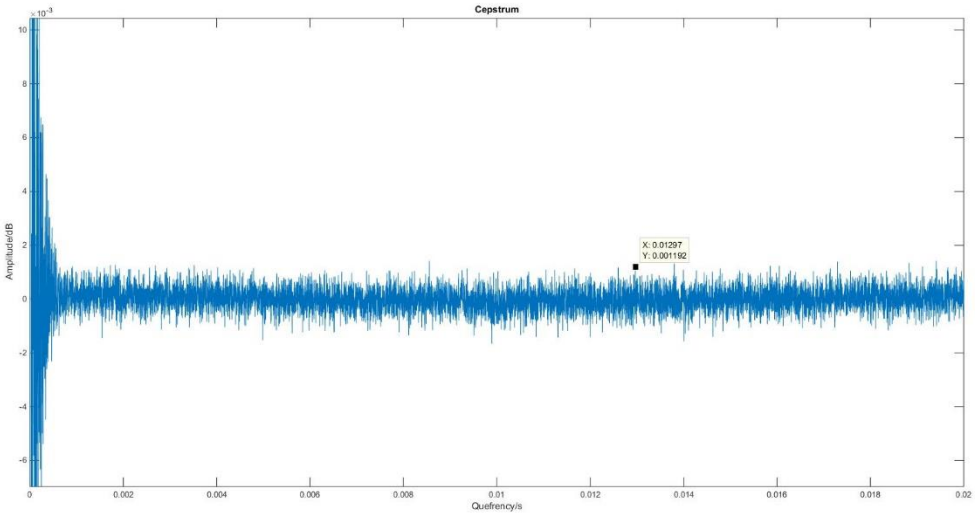

Figure 7-0-34: Cepstrum plot of the acoustic emission signal. No obvious peaks are visible

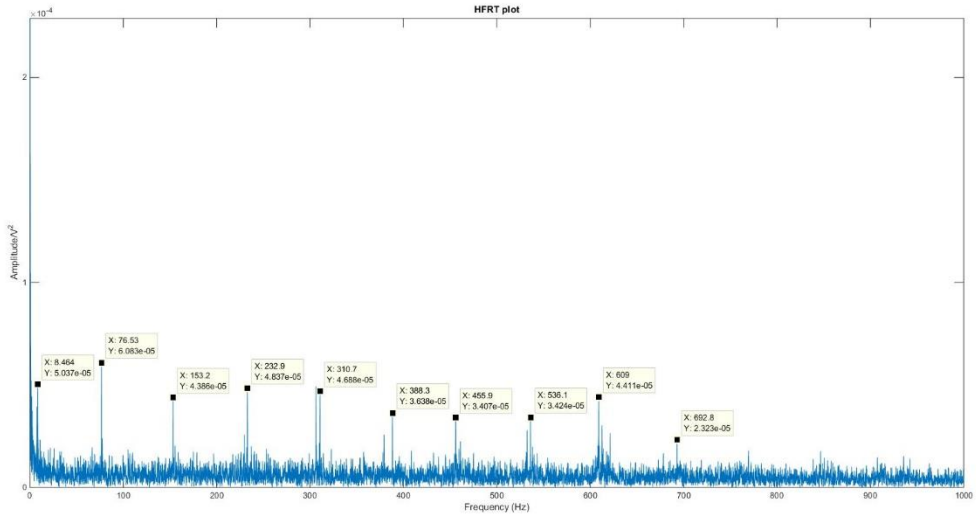

Figure 7-0-35: HFRT plot. The BPFO frequency and its harmonics can be identified. No BPFI frequency is visible at the HFRT results

In order to evaluate the capability of vibration technique to monitor damage in both races on the test bearing, a relevant set of experiments were carried out. The rotational speed was between and 100 and 700 RPM. Figure 7-36 presents a raw vibration signal generated by a defective bearing with damage in both inner and outer races at 500 RPM. Figure 7-37 shows the power spectrum of the vibration signal. High amplitude peaks between 1000 and 2500 Hz are visible. This frequency band can be used as a reference for further processing. Figure 7-

38 shows the zoomed-in plot of the power spectrum. A certain pattern can be recognized due to repeating peaks spaced at 76 Hz. This frequency corresponds to the BPFO frequency at 500 RPM. Therefore, low frequency analysis can confirm the presence of the outer race defect.

HFRT algorithm has been applied on the vibration signal in order to identify the type of the defects. The Figure 7-39 shows the HFRT results. The fundamental frequency of 76.87 Hz followed by its harmonics are clearly visible. This frequency corresponds to the BPFO frequency at 500 RPM. Figure 7-40 presents the zoomed-in plot of the HFRT results. The fundamental frequency of 93.65 Hz can be recognised. This frequency corresponds to the BPFI frequency at 500RPM. There is a slight offset between the theoretical and the observed fundamental frequencies due to the slight variation in the rotational speed during the test.

Furthermore, the application of Cepstrum analysis was investigated to detect the two fundamental frequencies of the bearing. Figure 7-41 shows the Cepstrum results. The peak at 0.013 corresponds to the BPFO frequency at 500 RPM ($\frac{1}{76.92} = 0.013$). The fundamental frequency followed by its harmonics. Figure 7-42 shows the zoomed-in Cepstrum plot. The peak at 0.01084 corresponds to the BPFI frequency at 500 PRM ($\frac{1}{92.25} = 0.01084$). Therefore, vibration Cepstrum analysis is able to detect defective bearings with multiple defects.

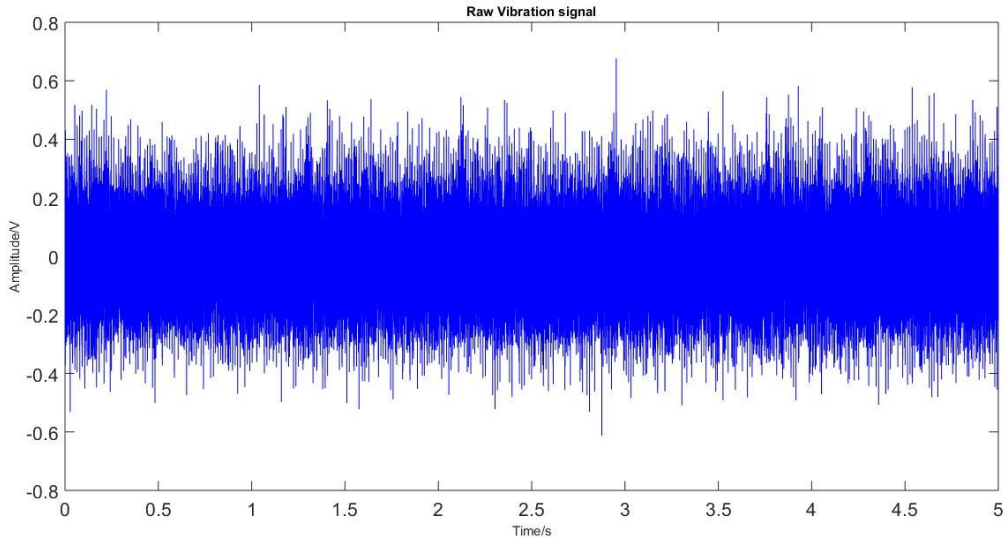

Figure 7-0-36: Raw vibration signal generated by defective bearing with damage in both races at 500RPM

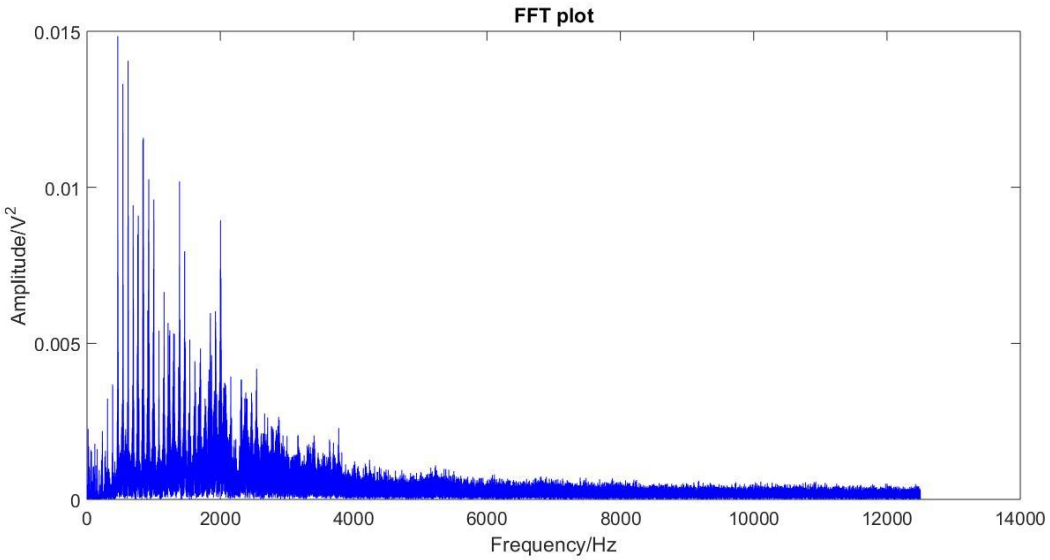

Figure 7-0-37: Power spectrum results of the vibration signal

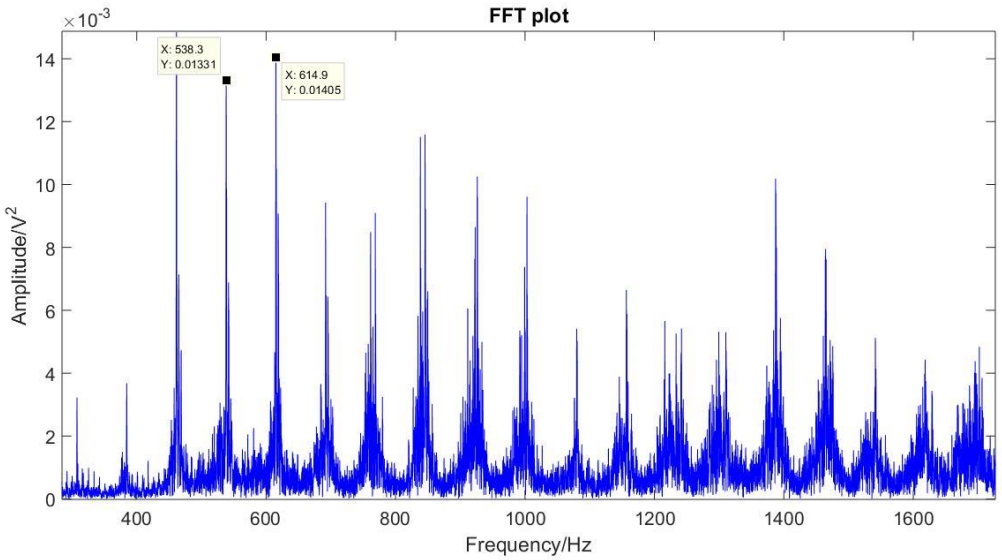

Figure 7-0-38: Zoomed-in power spectrum of the raw vibration signal. Number of peaks spaced at 76Hz indicating the presence of outer race fault

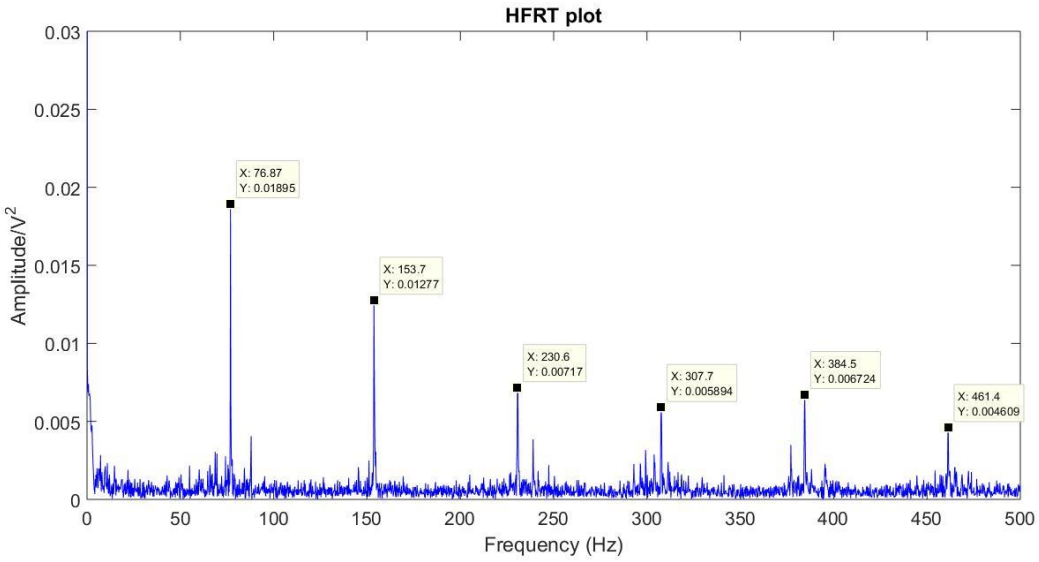

Figure 7-0-39: HFRT plot. The BPFO and its harmonics are clearly visible

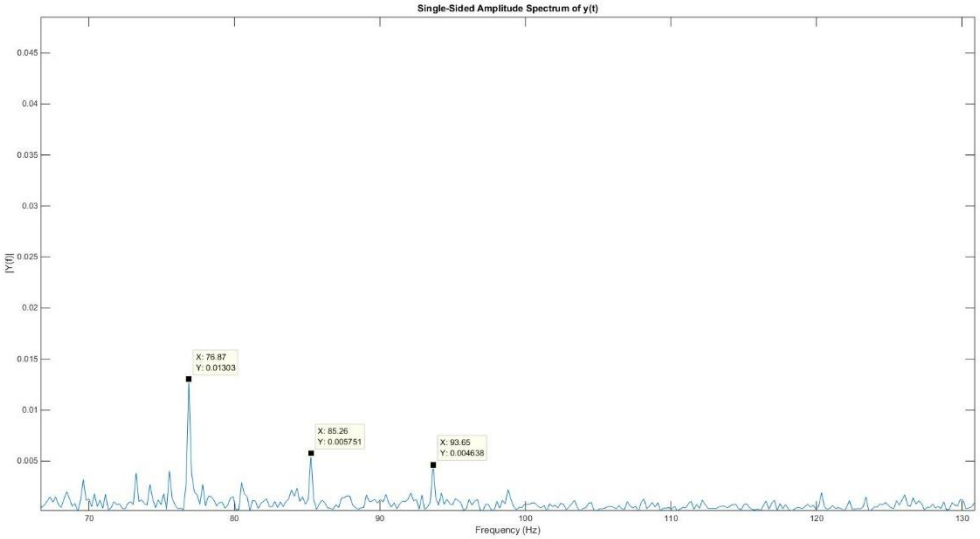

Figure 7-0-40: Zoomed-in HFRT results. The BPFI is also recognized

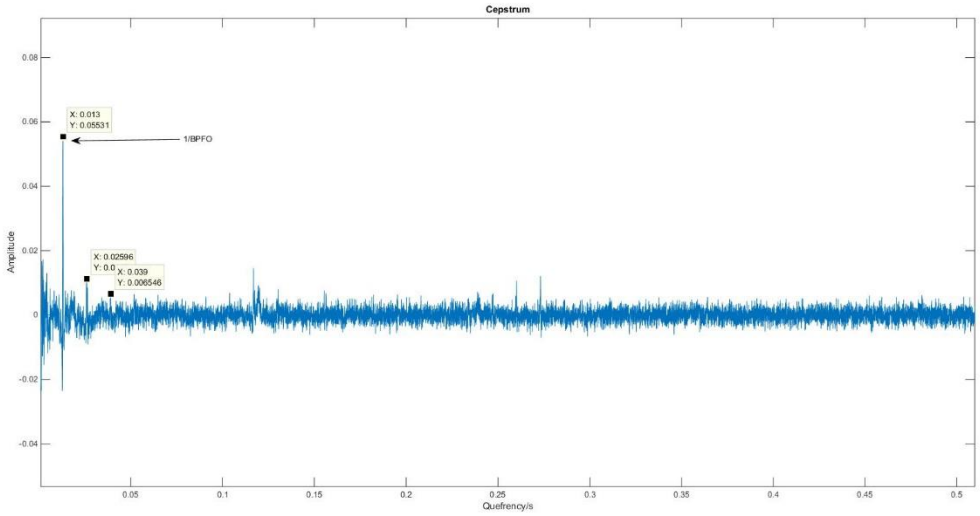

Figure 7-0-41: Cepstrum plot showing the BPFI frequency followed by its harmonics

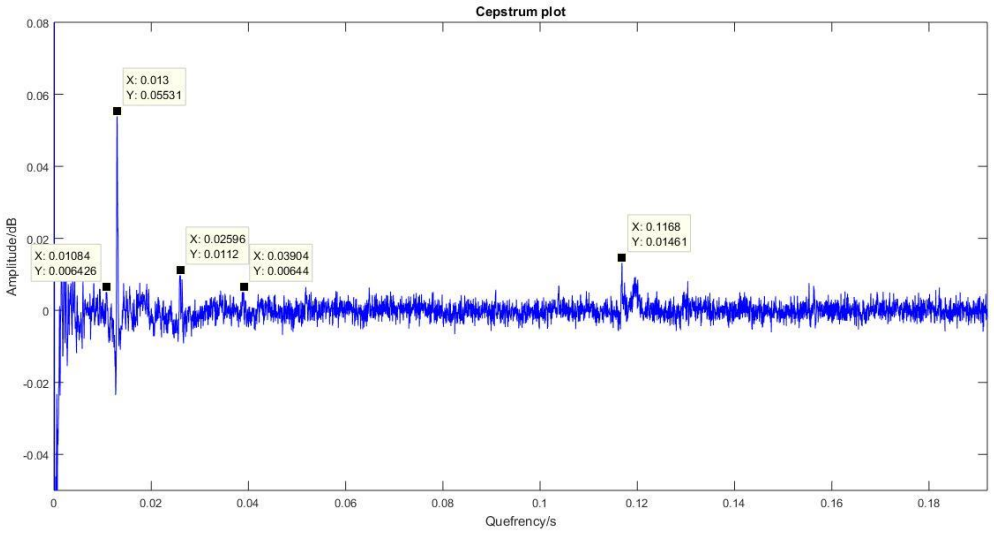

Figure 7-0-42: Zoomed-in Cepstrum plot. The BPFI frequency is also visible

7.1.5. Case study 4 - Effect of load and speed in Amplitude and in Normalized Moving RMS peak value

During laboratory trials, AE measurements on roller defective bearings were conducted in order to evaluate the effect of speed and load on AE signatures. Two sets of experiments with different fault severity were carried out. The speed was between 100 and 700 RPM. Origin V.9.0 Software was used for the line-graphs. Figure 7-43 shows the effect of speed in peak amplitude of the raw signal and in Moving RMS peak values after normalisation. The sample was a roller defective bearing with fault length 10%. It is visible that the AE amplitude raised as the rotational speed increases. More energy released by the impact produced by the roller defect at higher speed resulting in amplitude increase. The Moving RMS peak value after normalisation was maximum between 300 and 500 RPM.

Figure 7-44shows the effect of speed in peak amplitude of the raw signal and Moving RMS peak value after normalisation when the roller defective bearing has fault length 50%. The same pattern in amplitude peak as previous is observed. The peak value after normalisation was maximum between 400 and 700 RPM with exception of 600 RPM rotational.

The effect of load in AE signals was also evaluated. The load was between 5 and 9 bar. Figure 7-45 presents the effect of load in amplitude peak of the raw signal and in Moving RMS peak value after normalisation. The sample was a roller defective bearing with 10% length. The higher value in both parameters was observed at 8 bar.

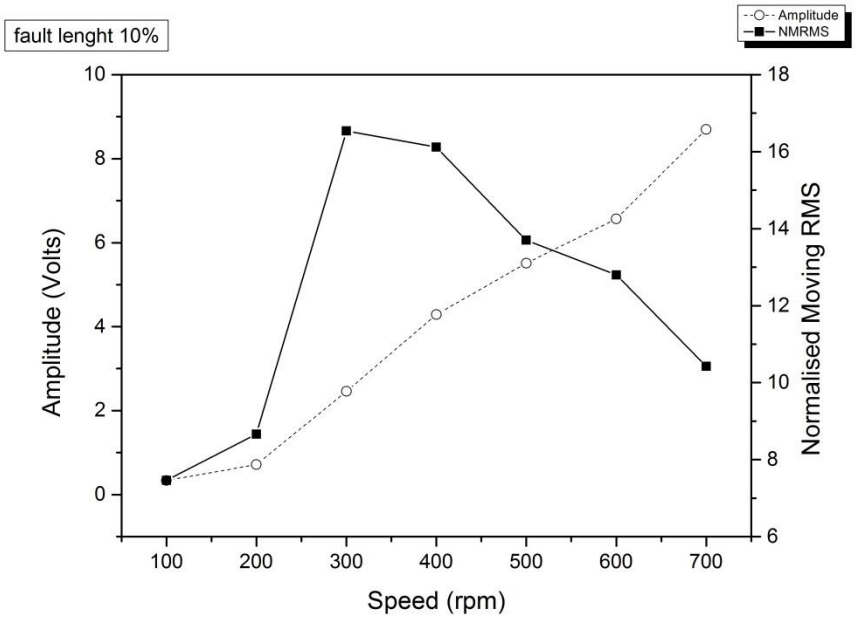

Figure 7-0-43: The effect of speed in amplitude peak and in Normalized Moving RMS peak value. The sample was a roller defective bearing with 10% fault length

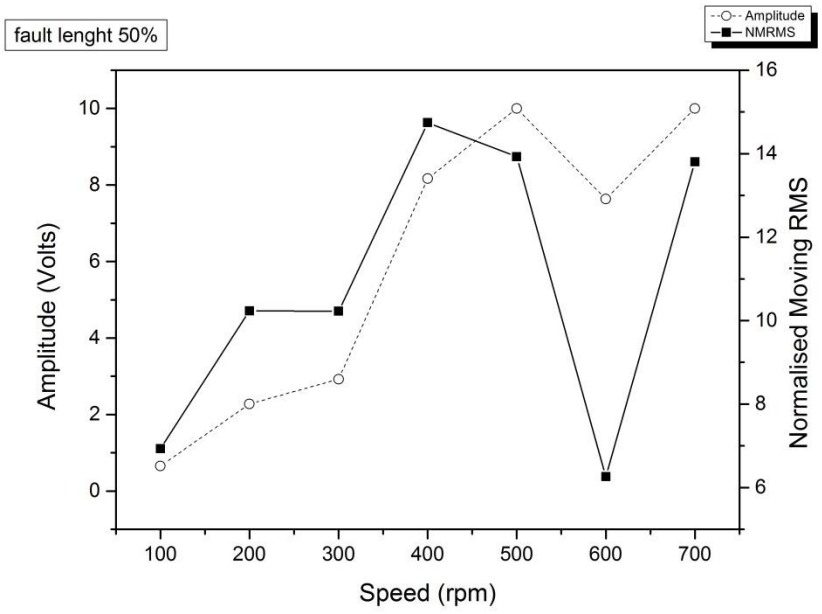

Figure 7-0-44: The effect of speed in amplitude peak and in Normalized Moving RMS peak value. The sample was a roller defective bearing with 50% fault length

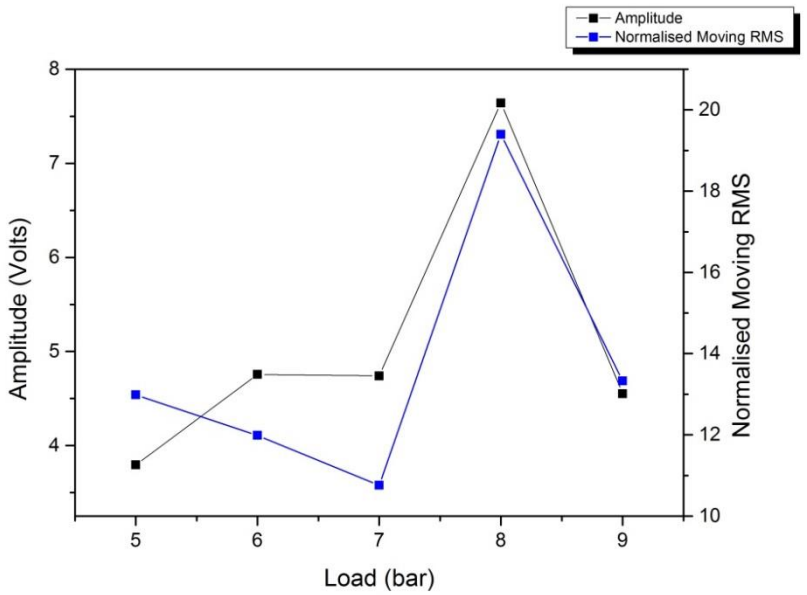

Figure 7-0-45: The effect of load in amplitude peak and in Normalized Moving RMS peak value. The sample was a roller defective bearing with 10% fault length

7.1.6 Case study 5- Trolley tests with a wheel flat defect

Trolley experiments with a wheel flat defect were employed at the University of Birmingham in order to evaluate vibration analysis in detecting and identifying the type of the defect. Despite vibration signatures from in-service wheels are unique, trolley results are more clearly due to less noise. Vibration signatures from a defect-free wheel were also recorded for comparison and validation purposes.

Figure 7-46 shows an example of raw vibration signals generated during these tests. The blue trace signal was acquired from the wheel with the flat defect whereas the red trace signal was recorded by the defect-free wheel. The peaks related to the wheel contained the flat defect are clearly visible.

Vibration power spectra are shown in Figure 7-47. High amplitude between 1.5 and 2.5 kHz can be clearly identified. This frequency range can be used as a reference for further processing. No obvious peaks are observed at the power spectrum generated by the defect-free signal (red signal). A healthy threshold can also be applied in order to compare the datasets automatically.

Figure 7-48 shows the Moving RMS results after they have been normalised. The impacts produced by the wheel flat defect release more energy. Sharp peaks related to the energy released during its impact event are clearly visible indicating the presence of the defect.

The HFRT algorithm has been applied on the recorded signals. Figure 7-49 shows the HFRT results. The peaks are related to the number of wheel revolutions. According to the vibration signature analysis plot, this pattern is observed at wheel flat defects. Therefore, the type of the defect was identified.

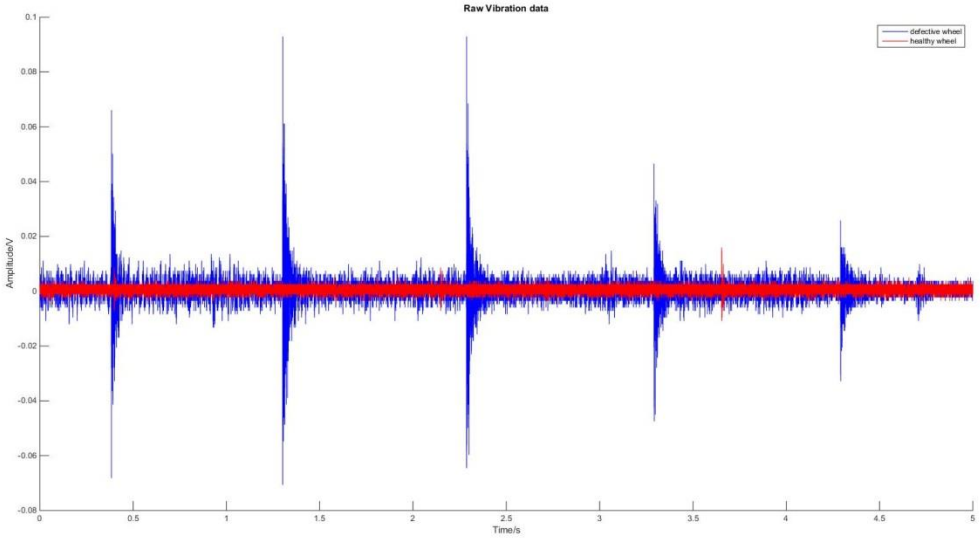

Figure 7-0-46: Raw vibration signals generated by wheel flat defect (blue signal) and defect-free wheel (red signal)

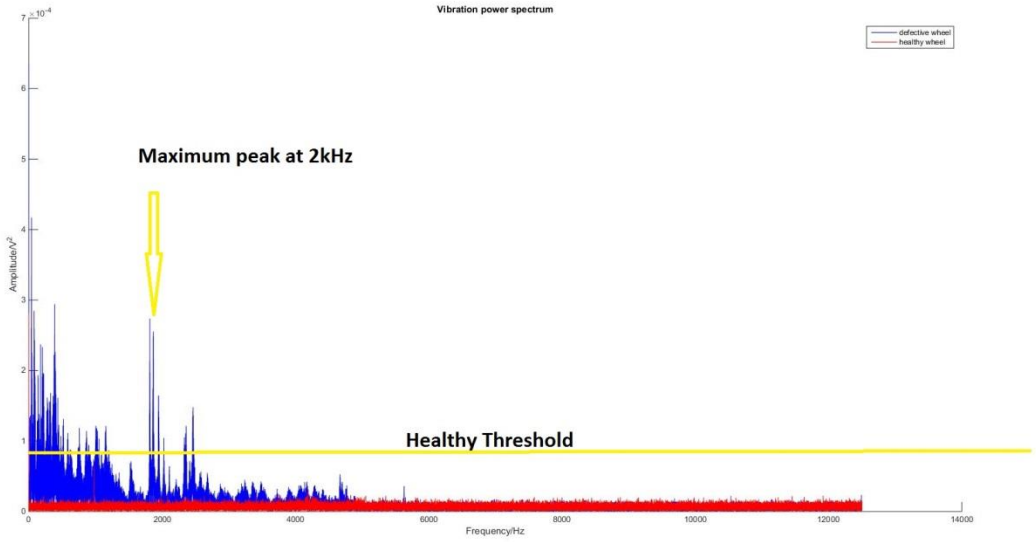

Figure 7-0-47: Vibration power spectrums from previous signals. A peak at 2 kHz can be observed at the spectrum acquired by the defective wheel

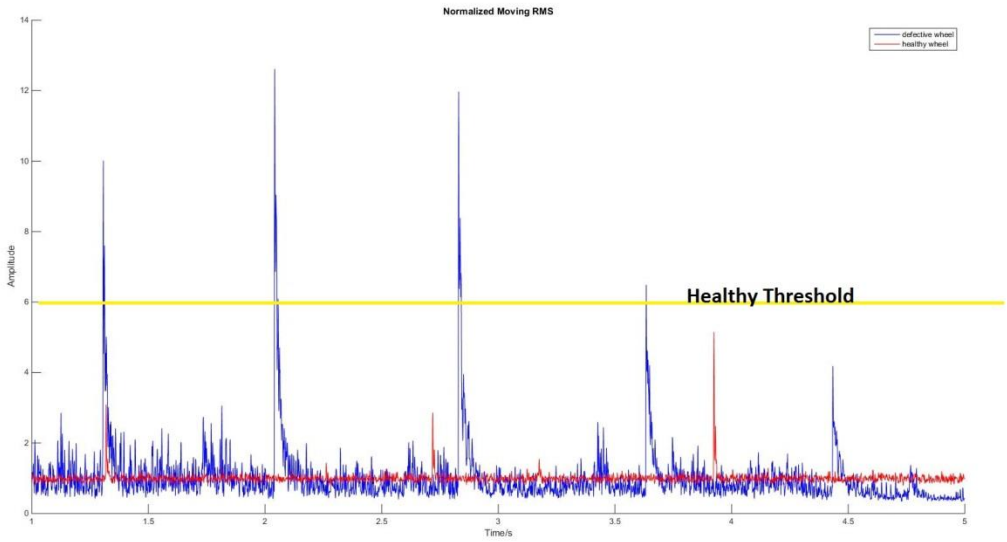

Figure 7-0-48: Normalized Moving RMS from previous signals (blue signal-wheel flat defect and red signal-defect-free wheel)

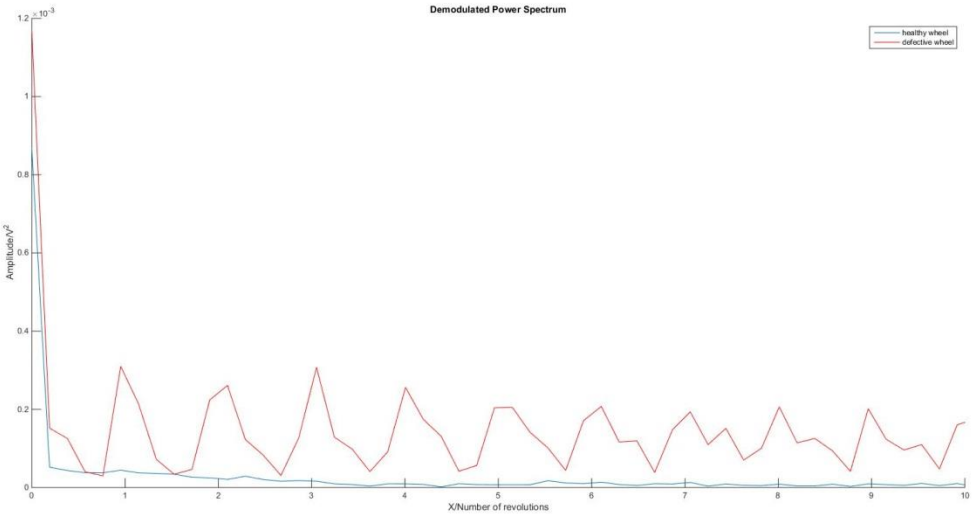

Figure 7-0-49: HFRT results of vibration signals (red signal-wheel flat defect and blue signal-defect-free wheel)

In summary, results and data analysis performed during this work are described briefly below. The ability of Acoustic Emission and vibration monitoring techniques in wheel and axle bearing damage detection has been evaluated and assessed by the novel methodology applied at the acquired signals.

Before the experimental part of this project, pencil lead tip breaks (Hsu-Nielsen) tests were carried out in order to assess the proper installation of AE sensors. Several laboratory cases

studies have been considered in this thesis using customised test rigs. Firstly, detection and evaluation of outer race bearing defects were investigated. The rotating speed was between 100 and 1000 RPM. Representative results of a defective bearing at 500 RPM have been presented. HFRT algorithm has been applied at the raw data in order to identify the type of the defect. From the results obtained, the fundamental faulty frequency and its harmonics have been clearly seen. This frequency corresponds to a known faulty frequency for this model of bearing at 500 RPM. The same pattern of results is observed at vibration signals. Therefore, the accuracy of the proposed analysis method is validated.

In addition, Acoustic emission and vibration signals were acquired using two roller defective bearings with different severity. Signals of defect-free bearing was also recorded for comparison purposes. Bearing defect quantification has been achieved when Normalized Moving RMS applied at the raw signals. Comparison between frequency spectra has been presented and discussed. High amplitude peaks at frequency spectrum of defective bearing can be used as a reference for further processing. HFRT algorithm has been applied in the raw signals. Bearing characteristic frequency and its harmonics can be recognised. Thus, HFRT analysis has been considered as the appropriate signal processing method for identifying the type of the defect.

As part of the experimental plan of this project, the performance of Acoustic emission and vibration technique in detecting bearing with multiple defects was evaluated. Two sets of experiments were carried out using the test rig. The first testing configuration considered, involving a bearing with significant damage in both outer and inner races and in six rollers in each side. The second one involved a bearing with damage in outer and inner races. In raw signals, high amplitude peaks are generated by the impacts of the faults. HFRT analysis has

been applied at the acquired signals. The three faulty frequencies has been identified (BPFO, BPFI, BSF). However, the BPFO harmonics are only observed in the HFRT plot. BPFI and BSF harmonics are not presented in the results. Furthermore, Cepstrum analysis has been applied at the raw signals and it has been proved that Cepstrum analysis is more suitable for detecting multiple defects. The three bearing faulty frequencies and their harmonics have been presented in cepstrum. Therefore, cepstrum analysis provides more consistent results than HFRT algorithm when multiple defects considered. The same pattern in results is also observed for the defective bearing with damage in outer and inner race.

The effect of speed and in load in amplitude of raw signals and in Normalized Moving RMS peak value is also evaluated and discussed in this work. From the results obtained, AE amplitude raised as the rotational speed increases. The sample was a roller defective bearing. The range of speed was between 100 and 700 RPM. The Normalized Moving RMS peak value was maximum between 300 and 500 RPM. The effect of load in AE signal was also presented. The load was between 5 and 9 bar. The higher value in both parameters was observed at 8 bar.

Wayside vibration signals were also acquired from simulated wheel flats using a test trolley. The experiments have been considered in order to evaluate vibration monitoring in wheel flat detection. High amplitude peaks were observed in raw signals. Moving RMS analysis has been applied in the collected data. The impacts produced by the wheel flat release more energy. Sharp peaks related to the energy release during its impact event are clearly visible indicating the presence of the defect. In addition, HFRT algorithm has been applied on the recorded signals. The peaks are related to the number of wheel revolutions. This pattern is

observed at wheel flat defects. Therefore, the type of the defect has been detected successfully.

7.2 Long Marston field trials

7.2.1 On- board measurements

Experiments were carried out under actual conditions in Long Marston rail track in order to evaluate the customised AE and vibration analysis RCM system. On-board and wayside measurements were recorded and processed in order to assess the condition of axle bearings. The test train run forward with consistent speed of 48 km/h and backward with speed of 32 km/h over the instrumented area. The sampling rate used was set at 500 k Samples/s. The acquisition duration was 12s for both scenarios in order to record the entire train waveform.

In the first set of trials on-board measurements were carried out in order to detect simulated inner race defects. The test configuration is shown in Figure 7-50. Figure 7-51 shows an example of a raw AE signal generated by an inner race defective axle bearing. The power spectrum of the defective axle bearing is presented in Figure 7-52. Sharp amplitude peaks are clearly visible indicating the presence of the defect. These frequencies can be used as a reference for the band-pass filtering during the HFRT process.

The HFRT results are provided in Figure 7-53. The fundamental frequency of 49.95 Hz and its harmonics can be recognised. According to manufacturer's datasheet, the BPFI is 11.7 Hz when the bearing rotational frequency is 1Hz. The train speed was 48 km/h which corresponds to a wheel rotational speed of 4.2 Hz (256RPM)

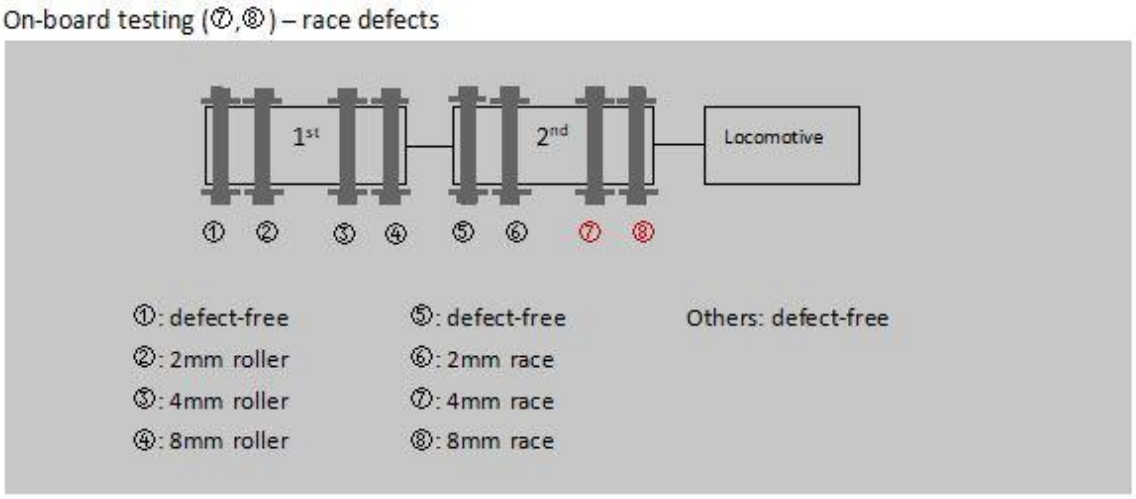

Figure 7-0-50: Test configuration at on-board Long Marston trials

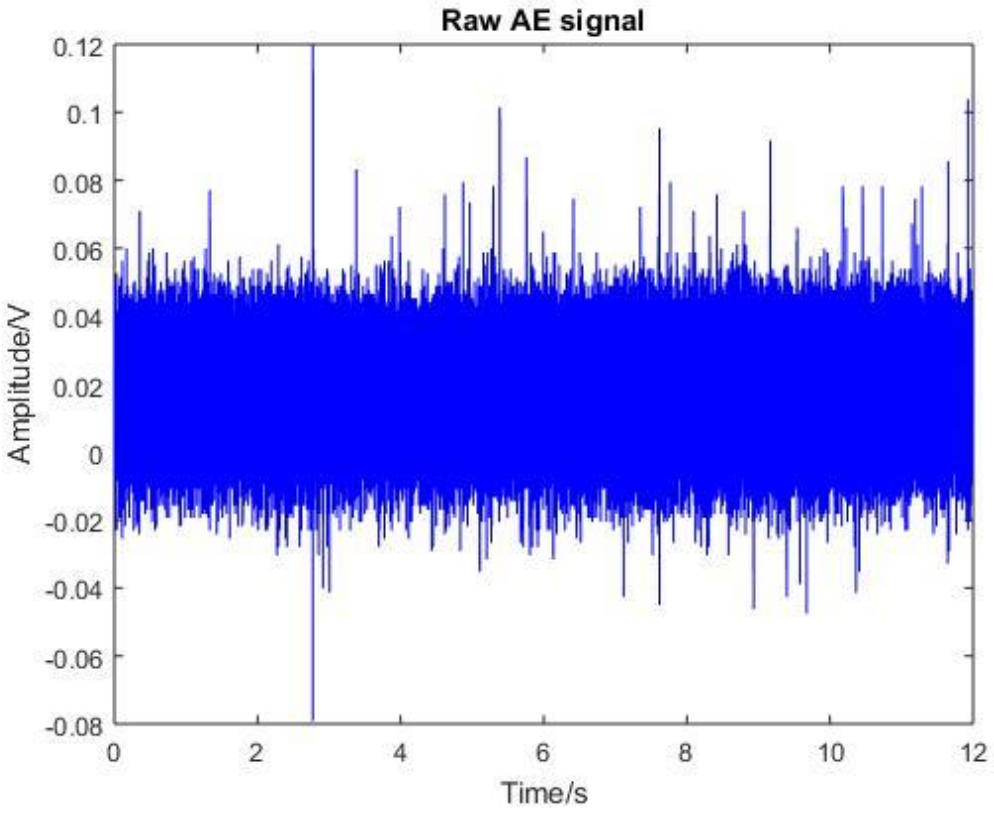

Figure 7-0-51: Raw acoustic emission signal generated by an inner race defective axle bearing

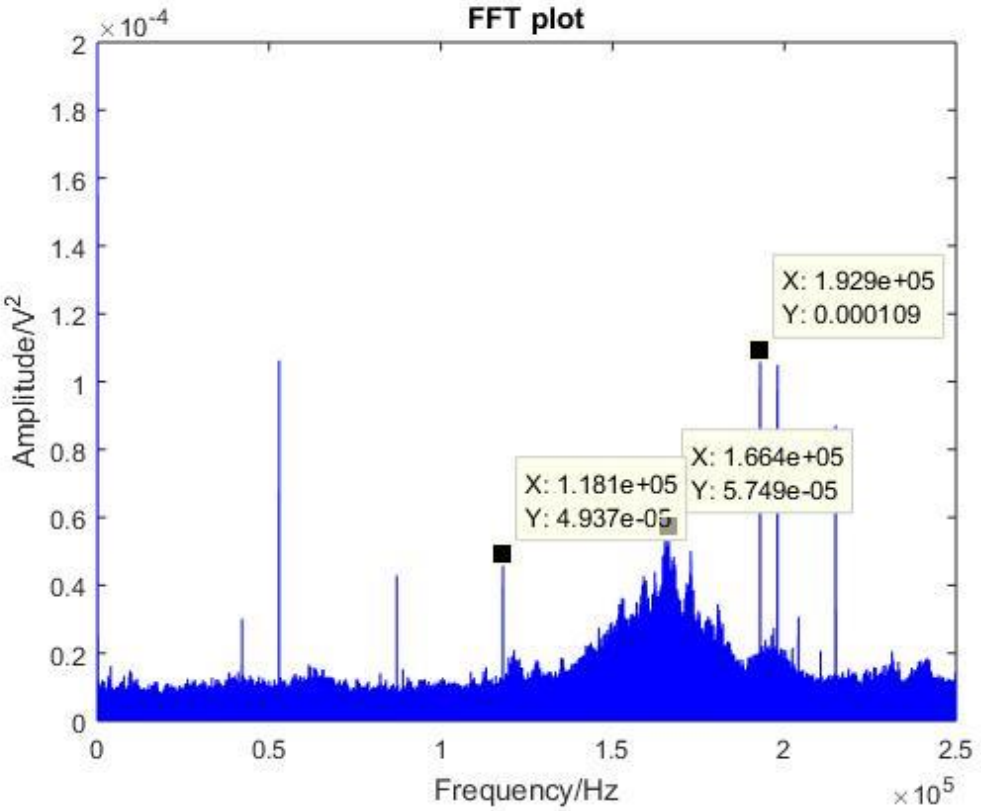

Figure 7-0-52: Power spectrum plot of inner race defective axle bearing

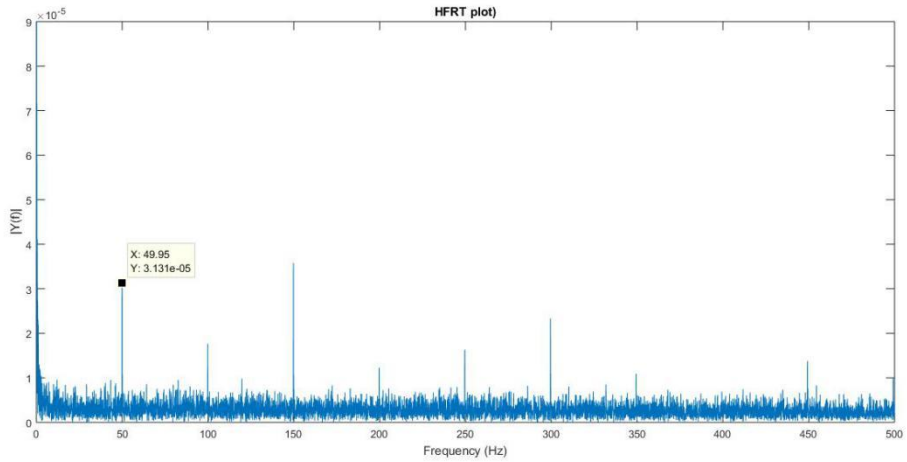

Figure 7-0-53: HFRT results of the inner race defective axle bearing. The fundamental frequency of 49.95 Hz and its harmonics are clearly visible

7.2.2 Wayside measurements

As part of Long Marston test plan, wayside measurements were also carried out in order to evaluate the capability of AE to detect and quantify roller defects. AE testing were carried out on axle bearings with roller defects at different severity (2, 4, 8 mm deep). Defect type

evaluation was achieved by frequency analysis and severity fault quantification was accomplished by Normalized Moving RMS analysis.

The test configuration is shown in Figure 7-54. The speed was 48 km/h and the movement of the train was with engine in the front. The schematic diagram in Figure 7-55 shows the distance between the wheels of the tested train.

Figure 7-56 shows the raw AE signal generated by the train. The distance between the wheels was known. Therefore, the peaks at 5.452s, 6.36s and 6.38s are related to 2mm, 4mm and 8mm roller defects. Peak at 5.452s corresponds to 2mm roller defect. The acoustic emission was truncated from time window 5.45s to 5.46s. This signal was selected as a template. The power spectrum of the template is shown in Figure 7-57. This spectrum was compared with the spectra generated by 4mm and 8mm roller defects. In addition, the template was compared with the spectrum generated by the noise of the braking event towards the end of the acquisition. The results are shown in Figure 7-58, Figure 7-59 and Figure 7-60.

Two signals which are generated by the same fault are expected to have similar frequency distribution. From the results obtain, it obvious that high similarity in frequency distributions is clearly visible in Figure 7-58 and Figure 7-59. No similarity in frequency spectrum is observed in Figure 7-60. Therefore, acoustic emission frequency analysis can identify type of the defect at wayside trials.

The effect of fault severity on Moving RMS peak values after normalisation is shown in Figure 7-61. The Moving RMS amplitude increases as the axle bearing condition deteriorates.

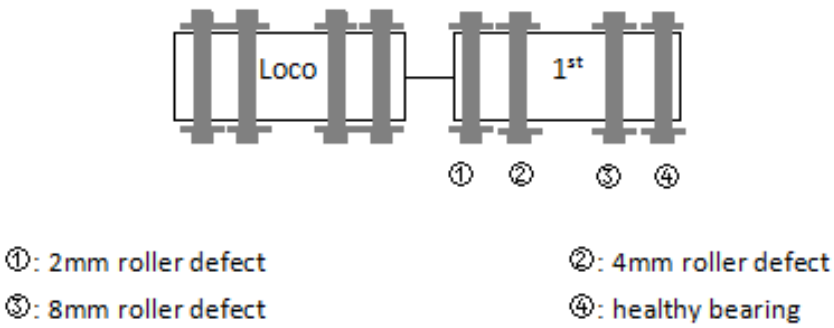

Figure 7-0-54: Test configuration at wayside Long Marston trials

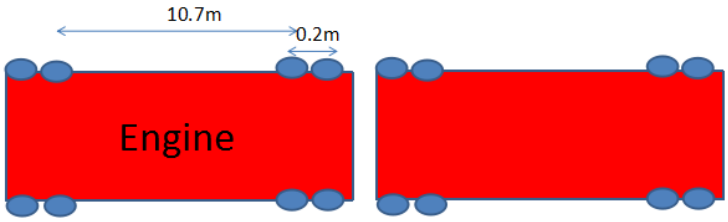

Figure 7-0-55: Schematic showing the distance between the wheels

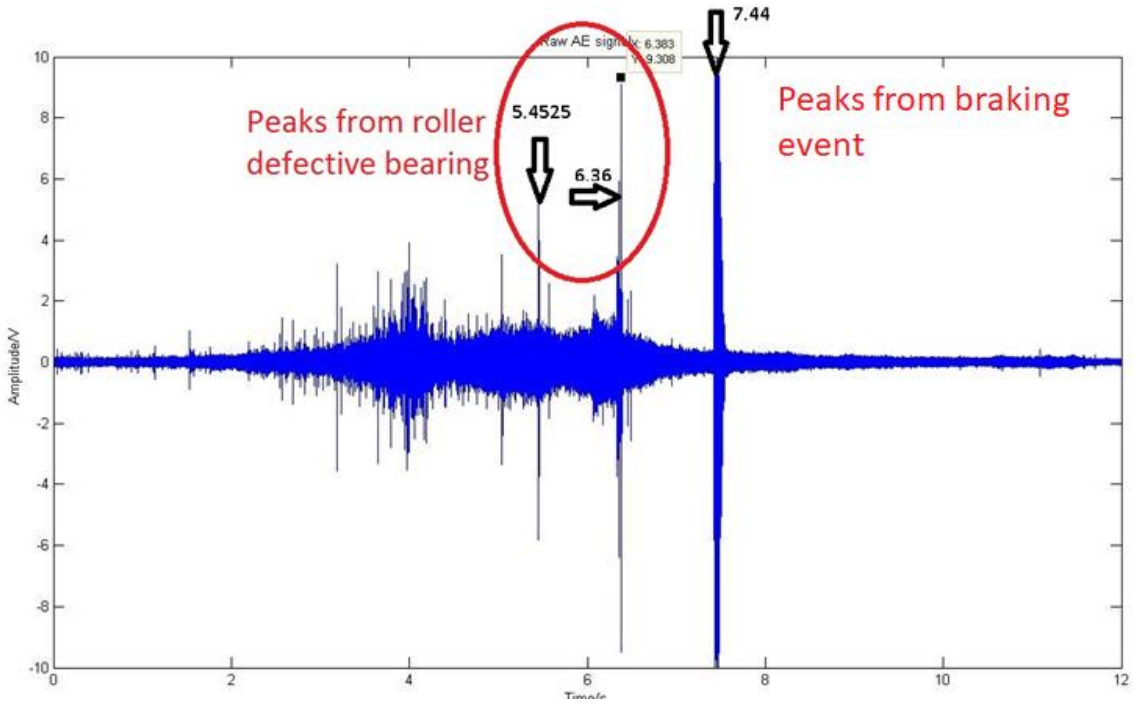

Figure 7-0-56: Raw acoustic emission signal generated by three different roller defective axle bearings

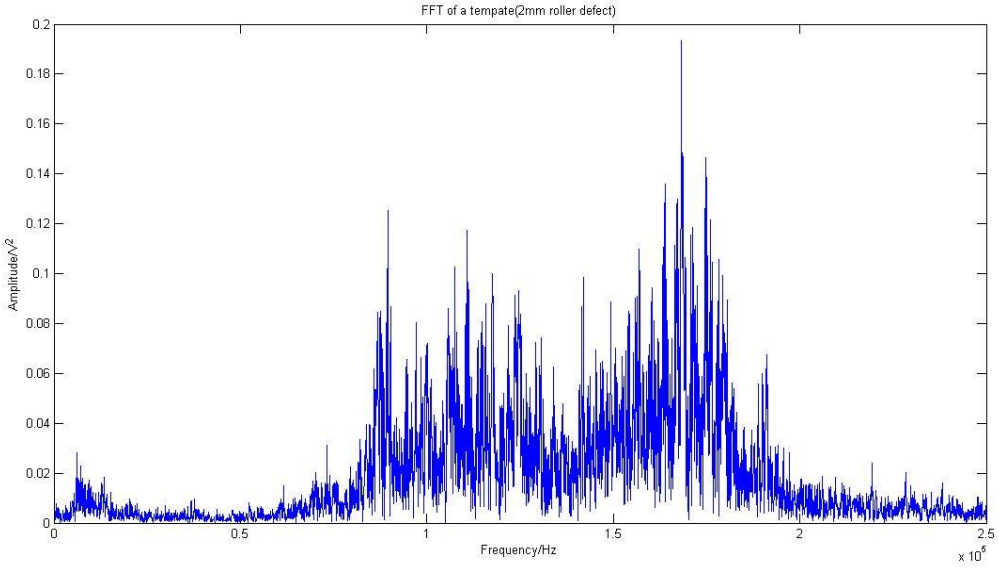

Figure 7-0-57: Power spectrum of acoustic emission signal generated from time window 5.45 to 5.46s. Peak at 5.452s corresponds to 2mm roller defect. This signal is selected as a template

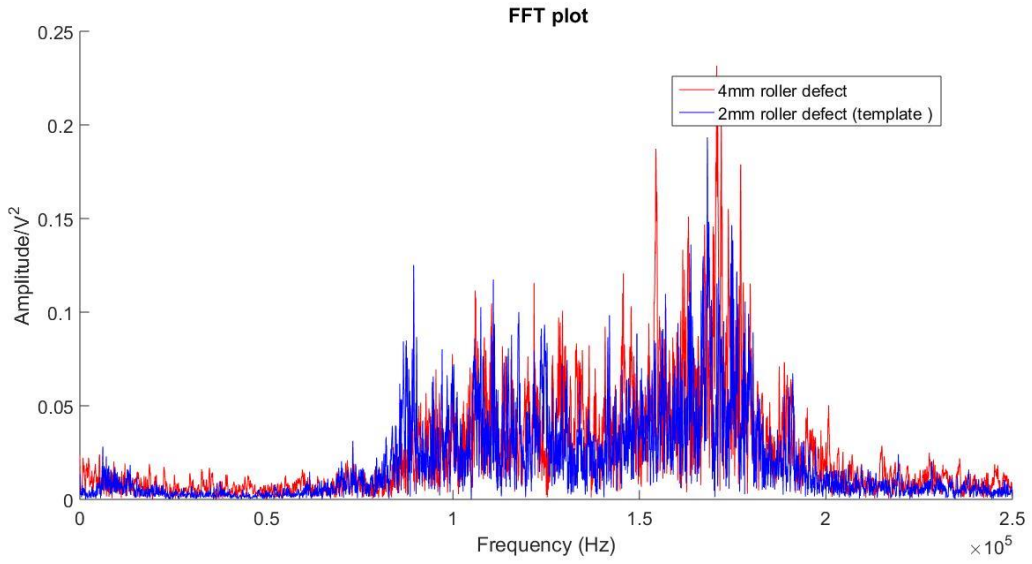

Figure 7-0-58: The red signal is the power spectrum of the acoustic emission signal from time window 6.36 to 6.37. Peak at 6.36 corresponds to 4mm roller defect. Blue signal is the power spectrum generated by 2mm roller defect (template). High Similarity can be clearly seen

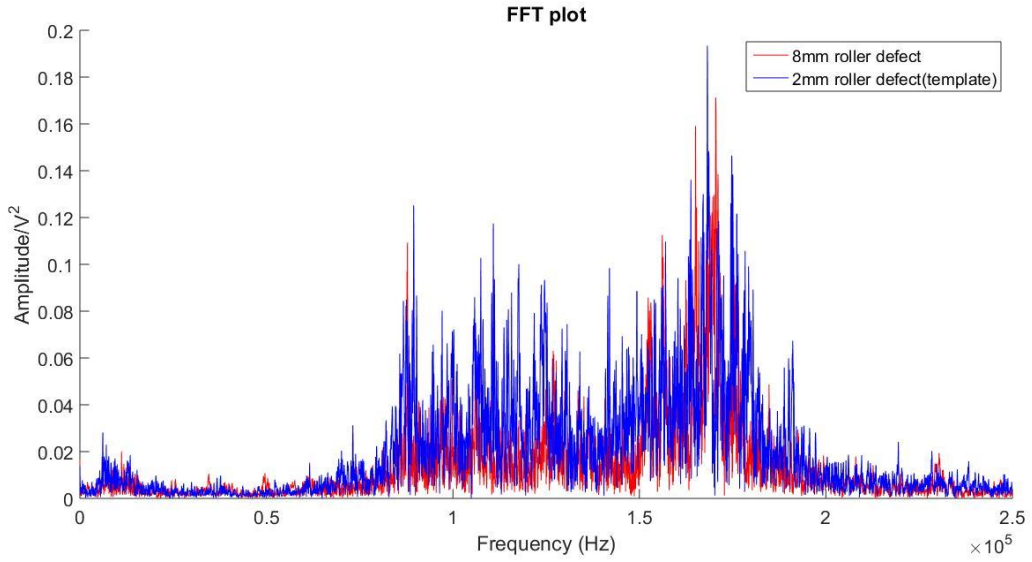

Figure 7-0-59: The red signal is the power spectrum of the acoustic emission signal from time window 6.38 to 6.39. Peak at 6.383 corresponds to 8 mm roller defect. Blue signal is the power spectrum generated by 2mm roller defect (template). High Similarity can also be seen

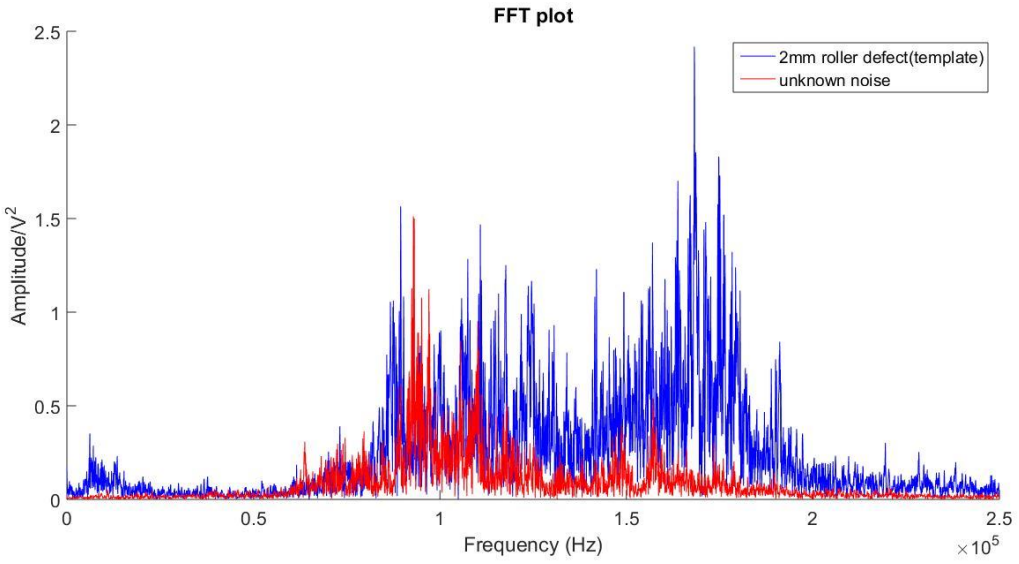

Figure 7-0-60: The red signal is the power spectrum of the acoustic emission signal from time window 7.44 to 7.45s. Peak at 7.44s corresponds unknown noise. Blue signal is the power spectrum generated by 2mm roller defect (template). No similarity can be observed

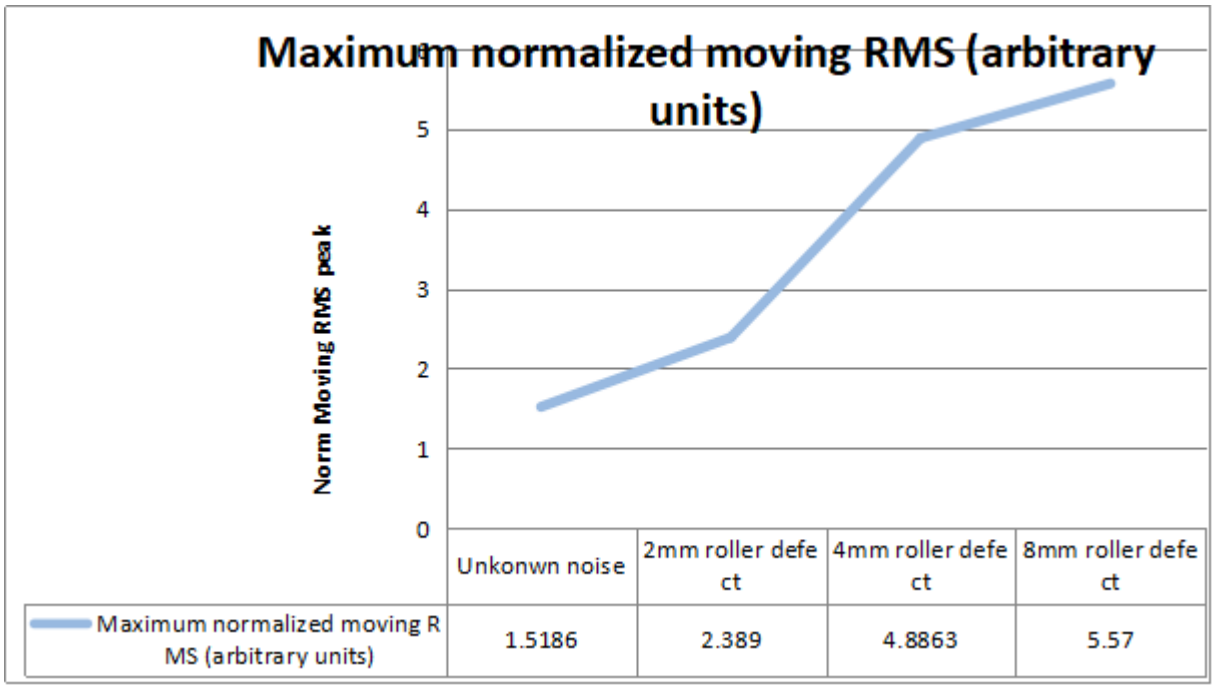

Figure 7-0-61: Line graph presents the effect of fault severity on Normalized Moving RMS peak value. The Normalized Moving RMS amplitude increases as the axle bearing condition deteriorates

Summing up, on-board and wayside experiments were carried out under controlled conditions in Long Marston, UK rail track in order to evaluate and assess the ability of the customised vibroacoustic monitoring system to detect bearing faults at early stage. In the first set of

trials, on-board measurements were carried out in order to detect simulated inner race defects. Sharp amplitude peaks were visible in the power spectrum indicating the presence of the defect. These frequencies can be used as a reference for designing the band pass filter of the HFRT process. Furthermore, HFRT algorithm has been applied at the collected signals. The fundamental faulty frequency and its harmonics have been successfully recognized at the envelope spectrum. Therefore, frequency domain analysis can detect the presence of a defect and identifying the type of the defect.

In the second sets of experiments, wayside measurements were collected in order to evaluate the capability of acoustic emission in detection and quantification of bearing roller defects. From the results obtained, defect type evaluation has been achieved by frequency domain analysis. In addition, severity quantification has been accomplished by Normalized Moving RMS analysis.

A peak related to 2mm roller defect has been selected as a template. The power spectrum of the template has been presented and compared with power spectra generated by 4mm and 8mm roller defects. Furthermore, the power spectrum of the template has been compared with the spectrum generated by the noise of the braking event.

Two signals generated by the same fault are expected to have similar frequency distributions. High similarity in frequency distributions generated by the roller defects were observed. In contrast, no similarity between the template and the noise of the braking event has been presented. Therefore, frequency domain analysis is suitable for type fault detection at wayside trials.

The effect of fault severity on Normalized Moving RMS peak value has also been discussed. From the results obtained, the Normalized Moving RMS amplitude increases as the bearing condition deteriorates. Hence, severity fault quantification can be achieved by Normalized Moving RMS analysis.

7.3 Cropredy in-service trials

7.3.1 Example of freight and passenger trains waveform

A series of wayside measurements were carried under actual operational conditions at the instrumented Cropredy site in-order to evaluate the customised RCM system under rail network conditions. The AE and vibration RCM system has been installed next to a Hot Axle box detector for validation purposes. Freight and passenger trains have been recorded. Each dataset represents the AE signal generated by the train. The acquisition time was 5 sec for passenger trains whereas 18 sec was selected as the optimum time for freight trains.

Figure 7-62 is a representative example of a typical AE waveform generated from a passenger train with rolling stock free of defect. In contrast, Figure 7-63 shows an AE signal acquired from a freight train. The difference between two kinds of waveforms is clearly visible. The amplitude of AE signal generated by the freight train is lower than the passenger one due to the fact that the freight wagons do not have motorised axles which are noisier causing wheel sliding during traction. In addition, the length of the freight train was longer whilst its speed was lower.

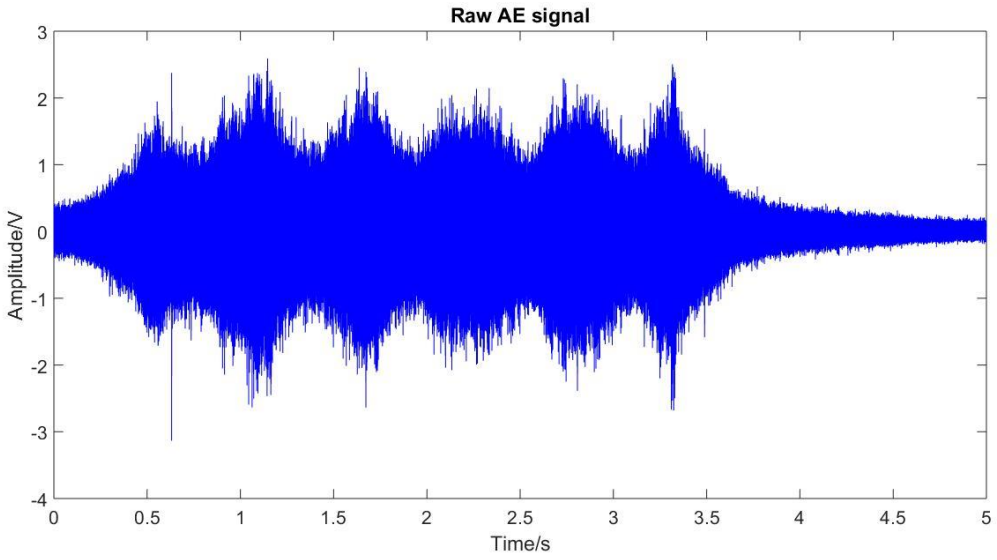

Figure 7-0-62: Raw acoustic emission waveform from passenger train with rolling stock free of defect

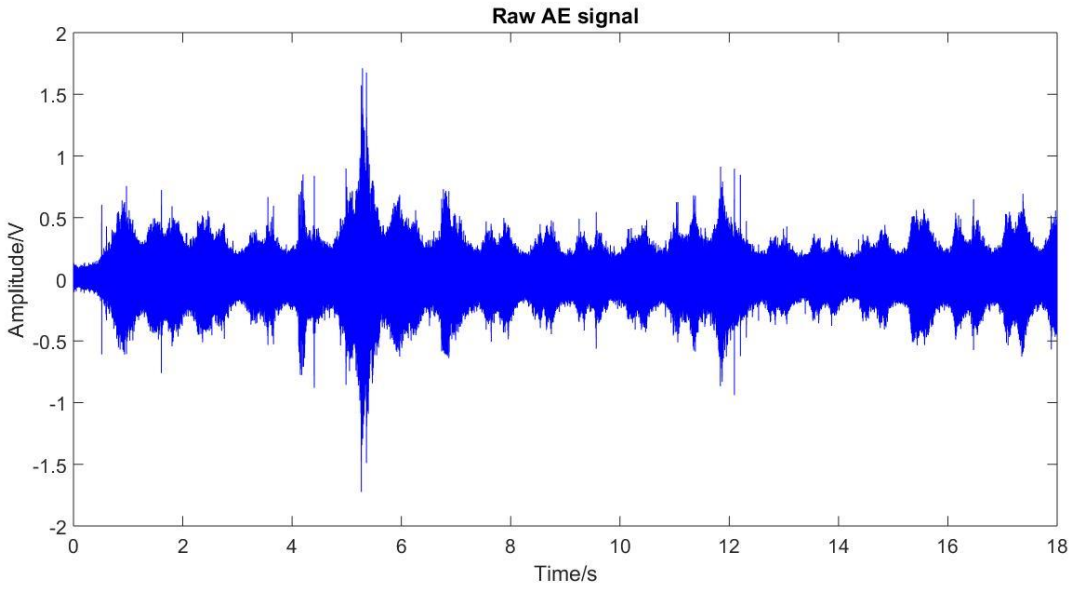

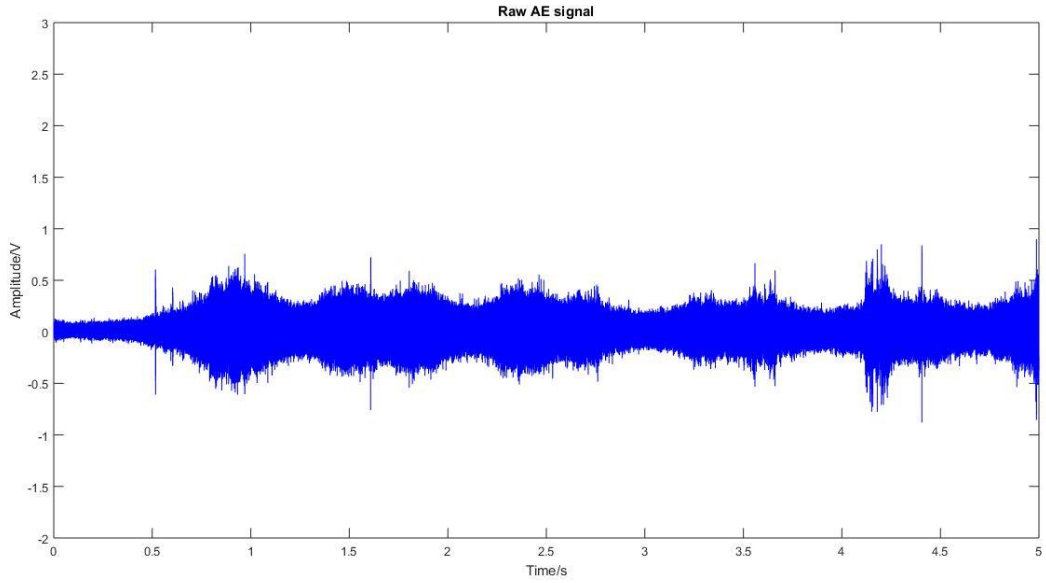

Figure 7-0-63: Raw acoustic emission waveform from freight train with rolling stock free of defect (top) and zoomed-in of the raw acoustic emission waveform (bottom).

7.3.2 Freight and passenger trains waveform with potential faults

During signal processing certain freight and passenger train waveforms were identified to contain evidence of potential bearing faults. The results still require follow up validation from Network Rail. Figure 7-64 shows an AE signal collected from a freight train passing through the instrumented Cropredy site. High amplitude peaks and signal modulation indicates the presence of a defect. The raw signal acquired by the other three sensors is presented in Figure 7-65, 7-66, 7-67. The raw signal has been analysed using different advanced signal processing techniques in order to confirm the presence and identify the type of the defect.

In Figure 7-68 the raw signal compared with a waveform generated by a train with rolling stock free of defects. Figure 7-69 shows the comparison between two power spectra. High amplitude peaks in the blue trace signal indicate the presence of a defect. The HFRT algorithm has been applied in both signals. The results is shown in Figure 7-70 and Figure 7-

71. From the results obtained, a fundamental frequency of 453 Hz and its harmonics are clearly seen. The sidebands indicating the presence of an inner race bearing defect. No obvious peaks are observed in Figure 7-71.

This particular dataset has been analysed using the TSK algorithm. The results are shown in Figure 7-72. High Kurtosis values also confirm the presence of defects. Frequency bands with high Kurtosis values can been used as a reference for further analysis.

The spectrogram of the AE signal is shown in Figure 7-73. The presence of the defects is also confirmed.

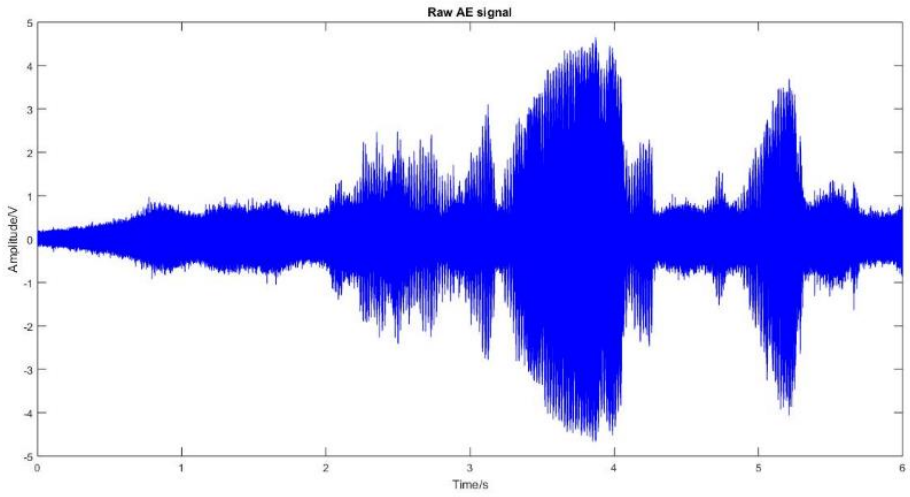

Figure 7-0-64: Raw acoustic emission (CH2) signal generated by freight train. High amplitude peaks and signal modulation can be clearly seen

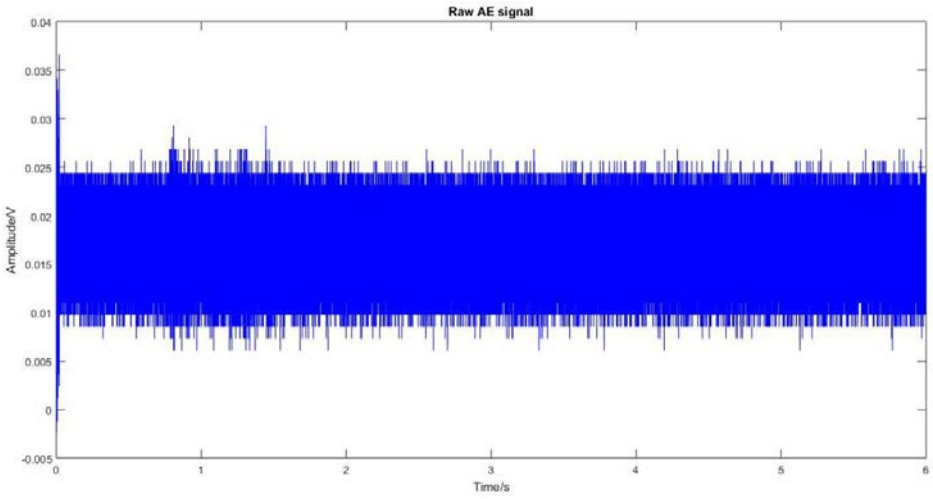

Figure 7-0-65: Raw acoustic emission signal (CH1)

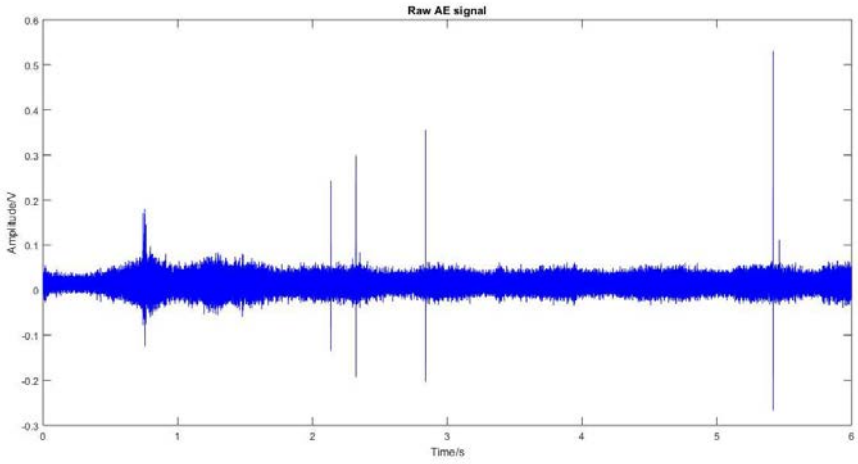

Figure 7-0-66: Raw acoustic emission signal (CH3)

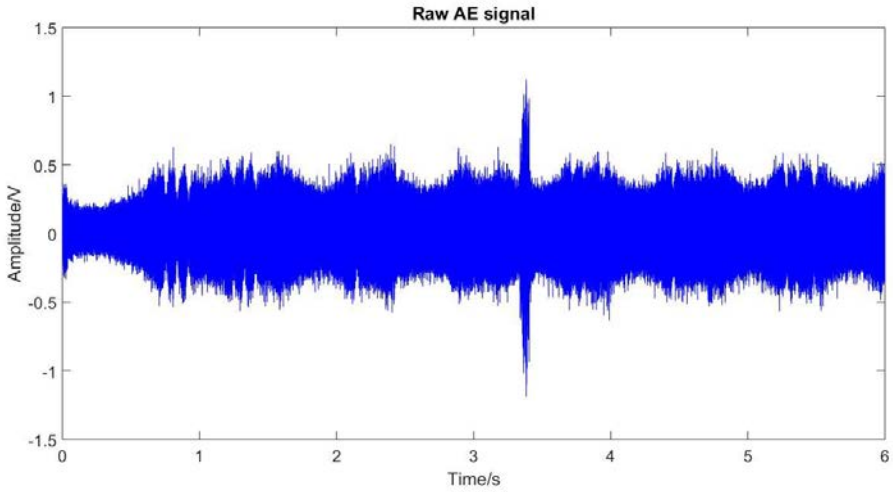

Figure 7-0-67: Raw acoustic emission signal (CH4)

;

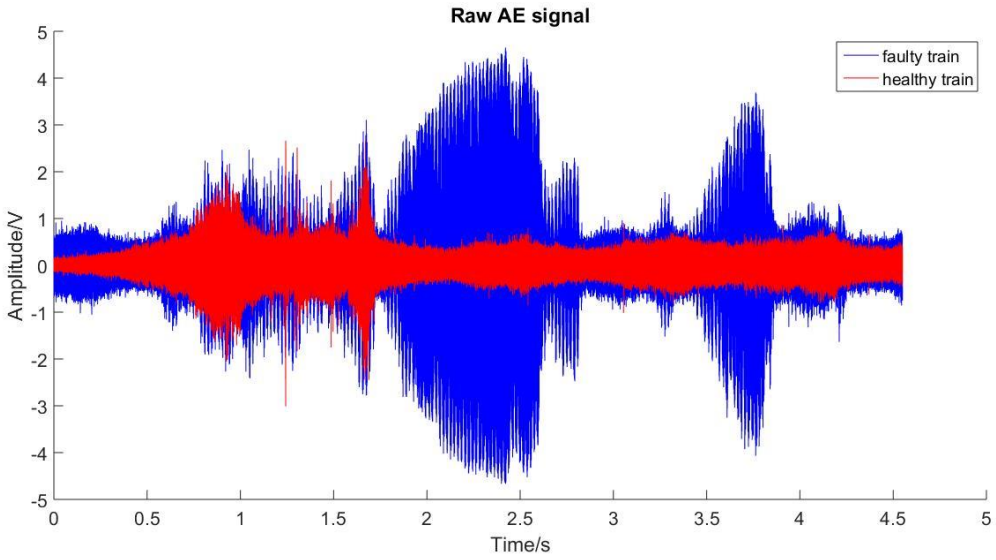

Figure 7-0-68: Raw acoustic emission signals generated by freight trains. Blue signal is acquired by freight train with faulty wheelsets whereas red signal by freight train with healthy wheelset. The different in amplitude can be clearly seen

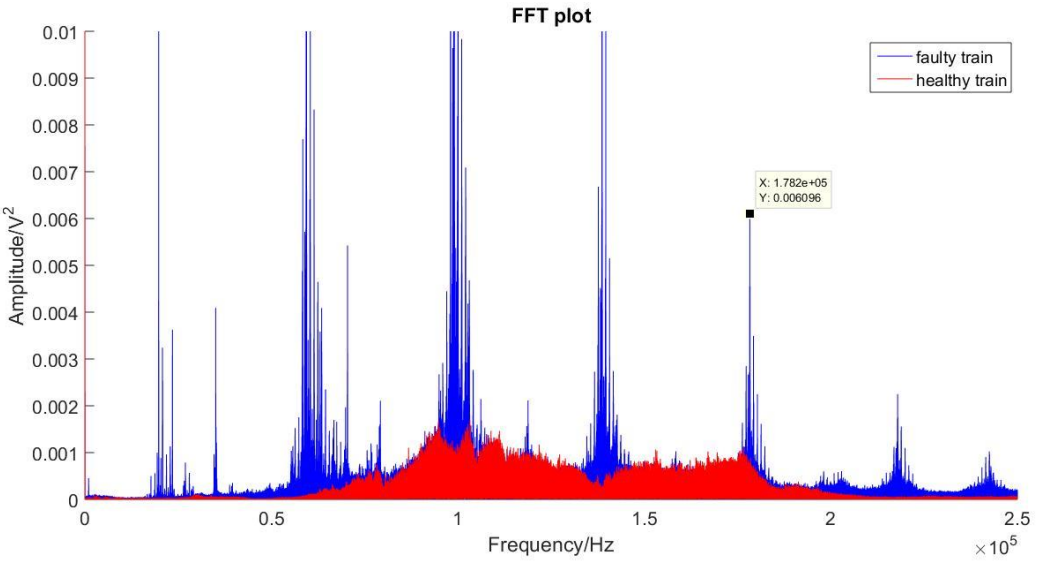

Figure 7-0-69: Comparison between frequency responses of freight trains. Sharp peaks in specific frequencies are clearly visible. These frequencies can be used as a reference for further processing

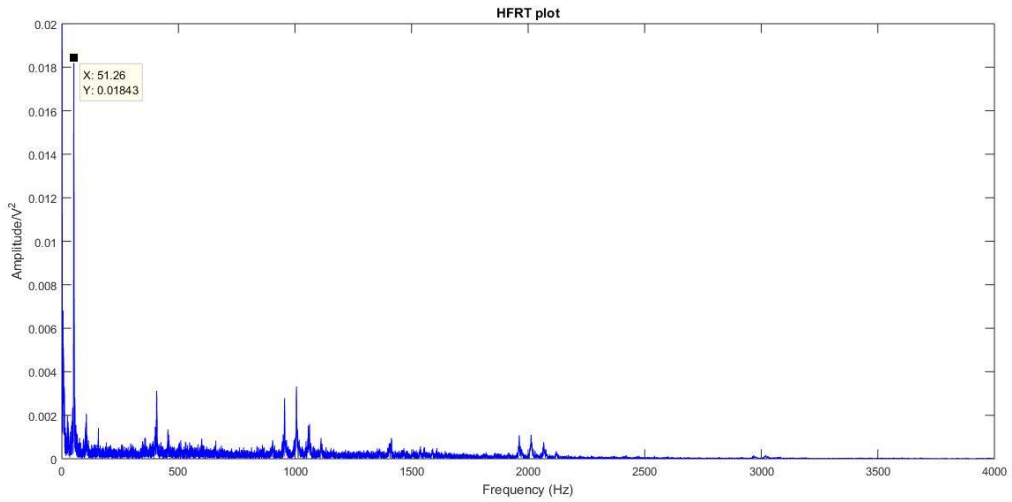

Figure 7-0-70: HFRT results of signal generated by train with potential fault. Fundamental frequency of 453Hz and its harmonics can be clearly seen. Side-bands are also visible. This pattern can indicate an inner race defect

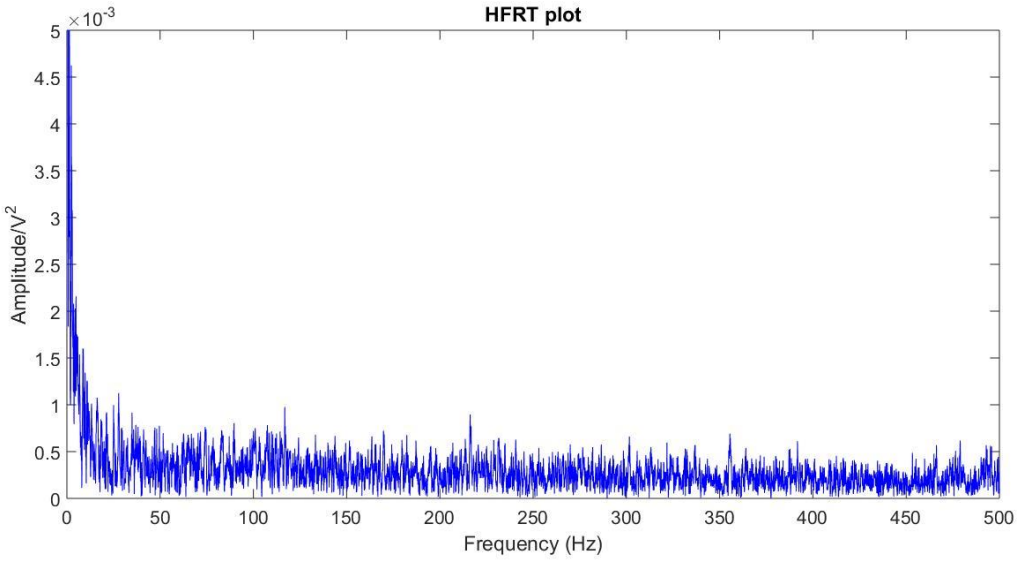

Figure 7-0-71: HFRT plot of acoustic emission generated by freight train with healthy wheelset. No obvious peaks are observed

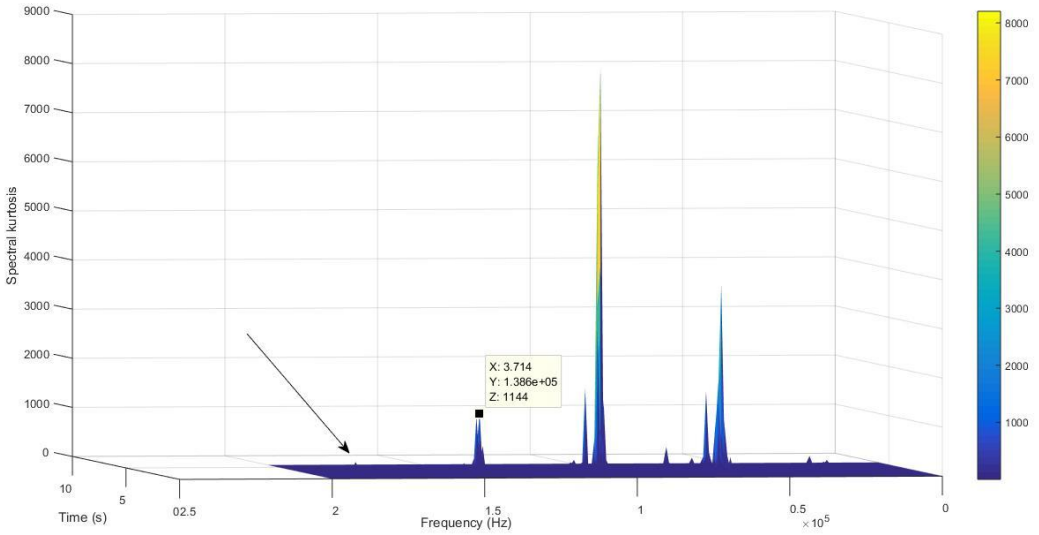

Figure 7-0-72: TSK results. Frequency bands with high Kurtosis value can be used as reference for the band-pass filter of the HFRT algorithm

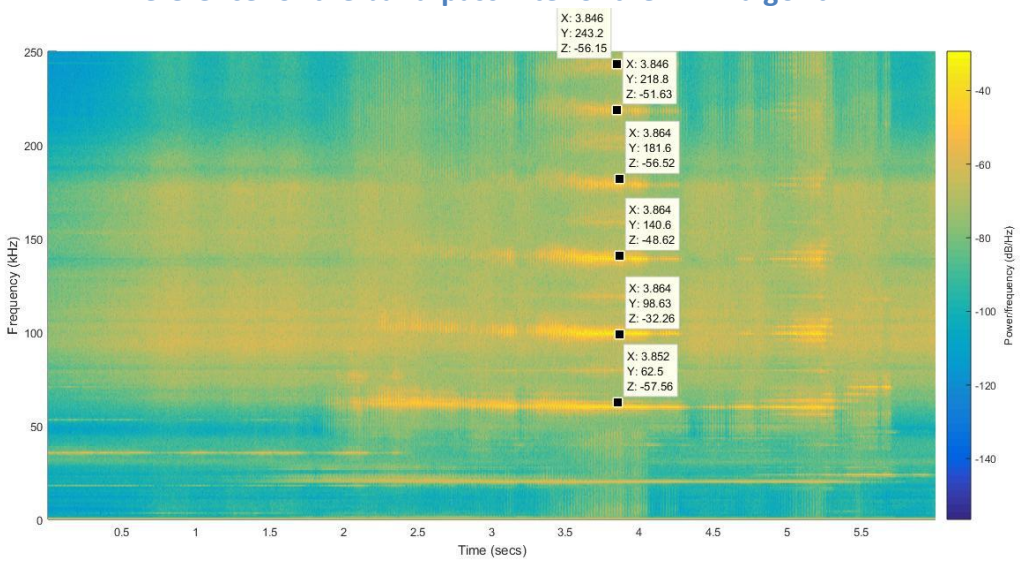

Figure 7-0-73: Spectrogram plot. High frequency peaks also confirm the presence of the defect

Figure 7-74 shows an example of AE signal generated by passenger train. Strong signal modulation between 3.4s and 4.4s indicates the presence of a defect. The power spectrum is shown in Figure 7-75. Harmonics in frequency distribution can be clearly seen. These frequency bands can be used as reference for the band-pass filter at the HFRT process.

Figure 7-76 shows the HFRT results. The fundamental frequency of 771.8 Hz and its harmonics are visible. The sidebands are also observed. Figure 7-77 presents the TSK results. High Kurtosis value at 159 kHz indicating the presence of a fault. Therefore, frequency analysis and TSK algorithm can indicate the presence of a defect.

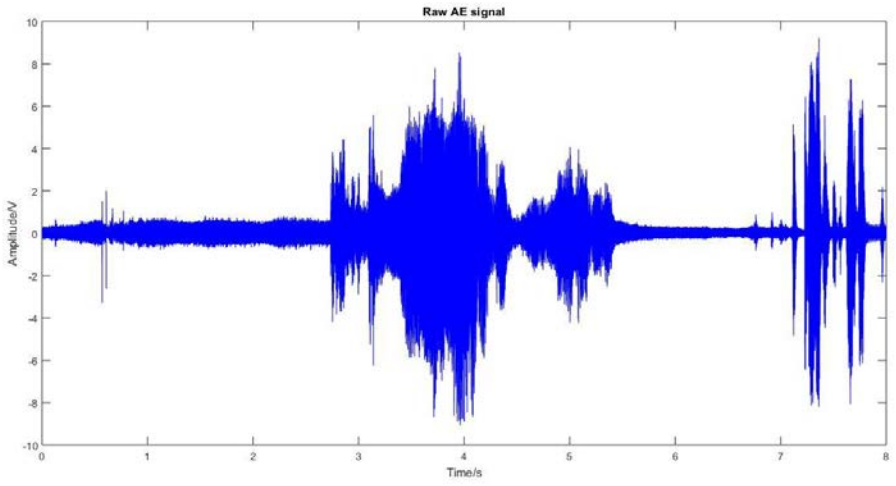

Figure 7-0-74: Raw acoustic emission signal generated by passenger train. High amplitude and strong modulation can indicate the presence of a defect

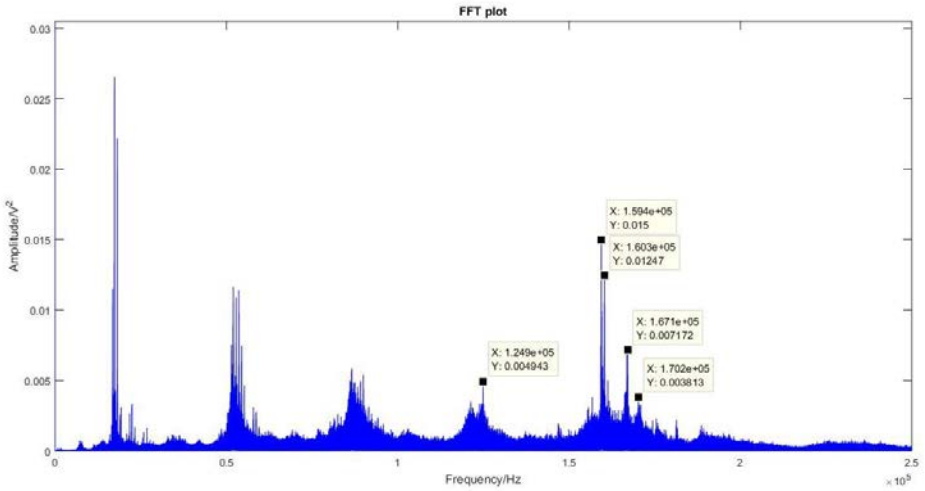

Figure 7-0-75: Power spectrum of previous acoustic emission signal. Harmonics in frequency distribution are clearly visible

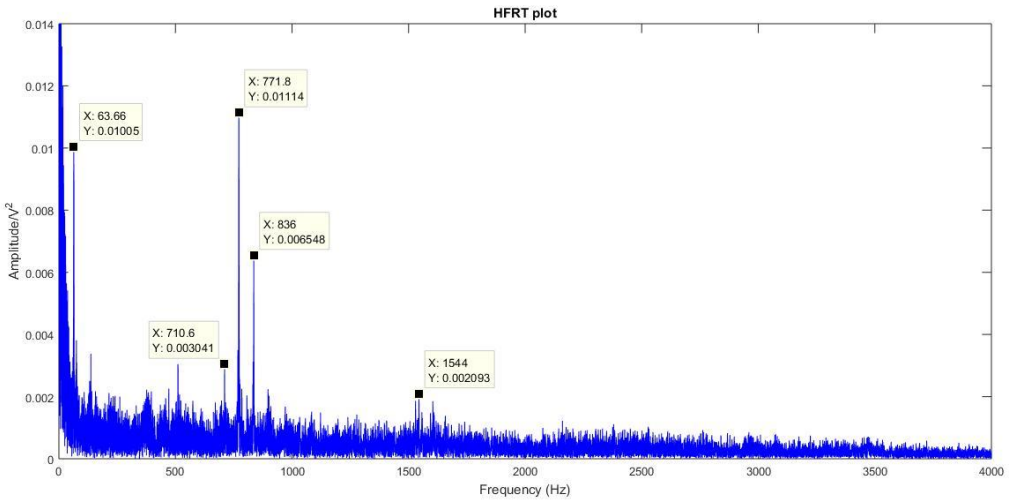

Figure 7-0-76: HFRT results. The fundamental frequency of 771.8 Hz and its harmonics are visible. Sidebands can also be observed

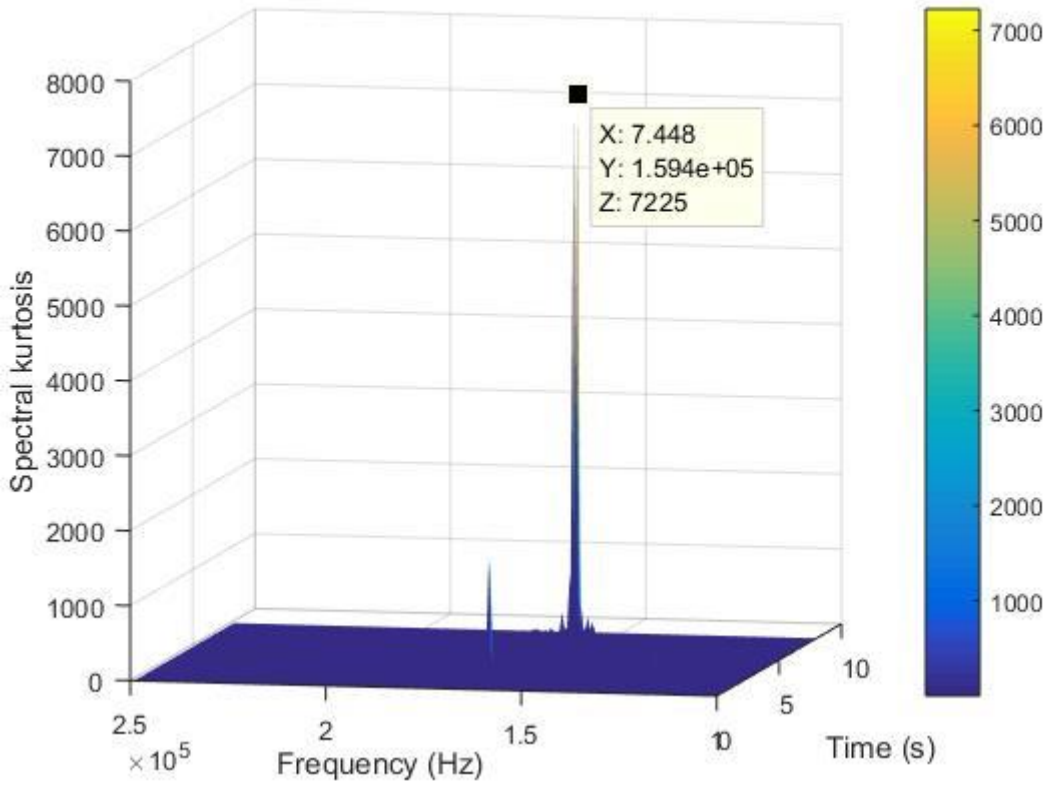

Figure 7-0-77: TSK results. High Kurtosis value at 1.59 kHz indicating the presence of a fault

Figure 7-78 shows a raw AE signal generated by passenger train. Strong signal modulation between 3.8s and 5.2s indicating the presence of a defect. The power spectrum is shown in Figure 7-79. Harmonics in frequency distribution can be clearly seen. These frequency bands can be used as reference for the band-pass filter at the HFRT process.

Figure 7-80 shows the HFRT results. The fundamental frequency of 459 Hz and its harmonics are visible. Figure 7-81 presents the TSK results. High Kurtosis value at 109 kHz indicating the presence of a fault. Therefore, frequency analysis and TSK algorithm can indicate the presence of a defect. In addition, the fundamental frequency can be detected by HFRT process.

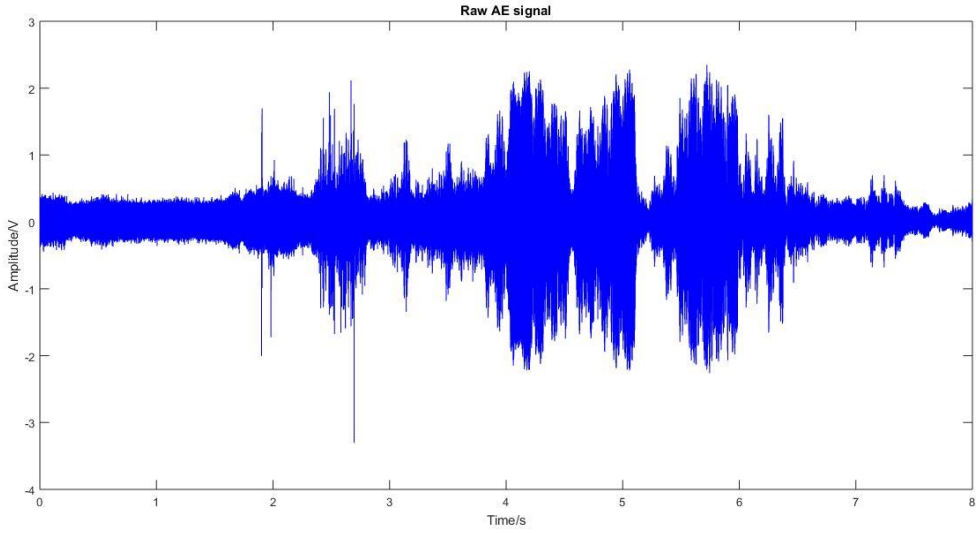

Figure 7-0-78: Raw acoustic emission signal recorded by passenger train. Signal modulation can be observed

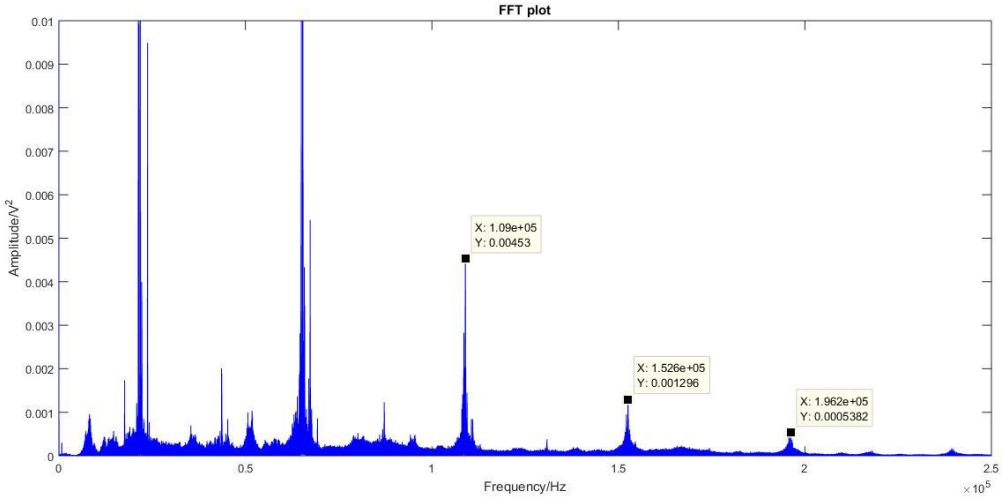

Figure 7-0-79 : Power spectrum of previous signal. Harmonics in frequency distribution can be observed indicating the presence of potential fault

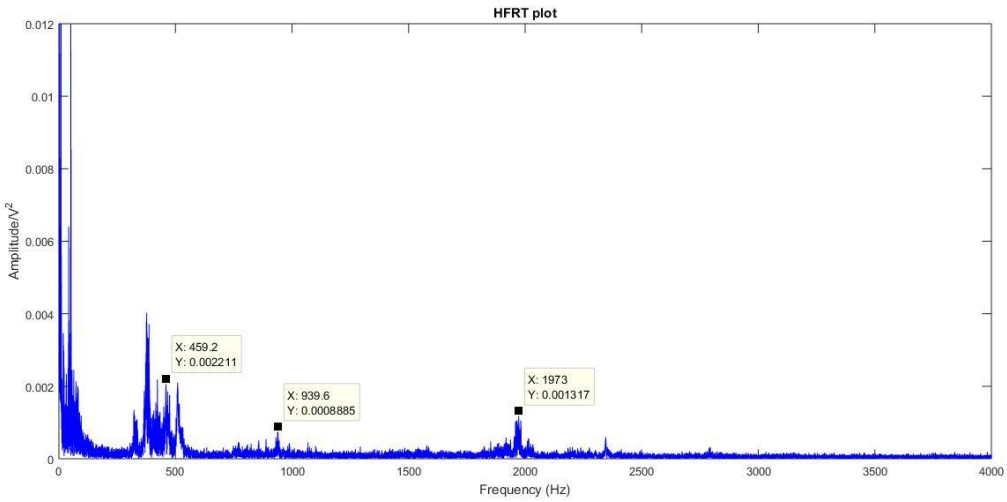

Figure 7-0-80: HFRT results. The fundamental frequency of 459.2 Hz and its harmonics can be clearly seen

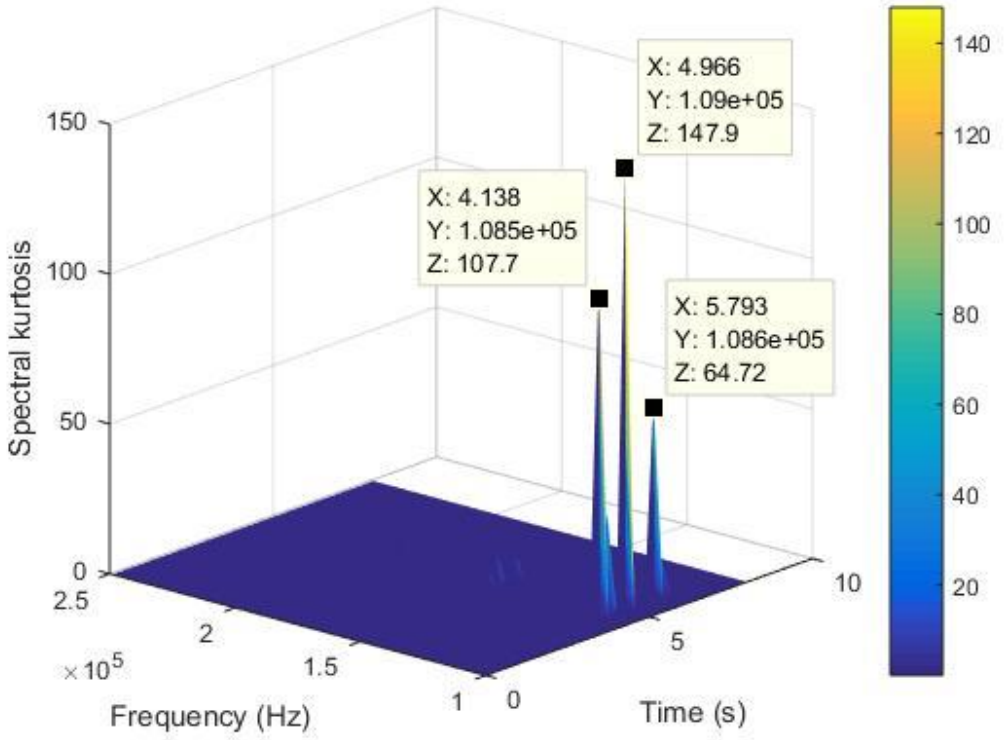

Figure 7-0-81: TSK results. High Kurtosis value at 1.09 kHz is visible indicating the presence of a fault

Figure 7-82 shows an acoustic emission signal acquired by passenger train. Strong signal modulation between 1.6s and 2.5s indicating the presence of a defect. The power spectrum is shown in Figure 7-83. Harmonics in frequency distribution can be clearly seen. These frequency bands can be used as reference for the band-pass filter at the HFRT process.

Figure 7-84 shows the HFRT results. The fundamental frequency of 2450 Hz and its harmonics are visible. Figure 7-85 presents the TSK results. High Kurtosis value at 149 kHz indicating the presence of a fault. Therefore, frequency analysis and TSK algorithm can indicate the presence of a defect.

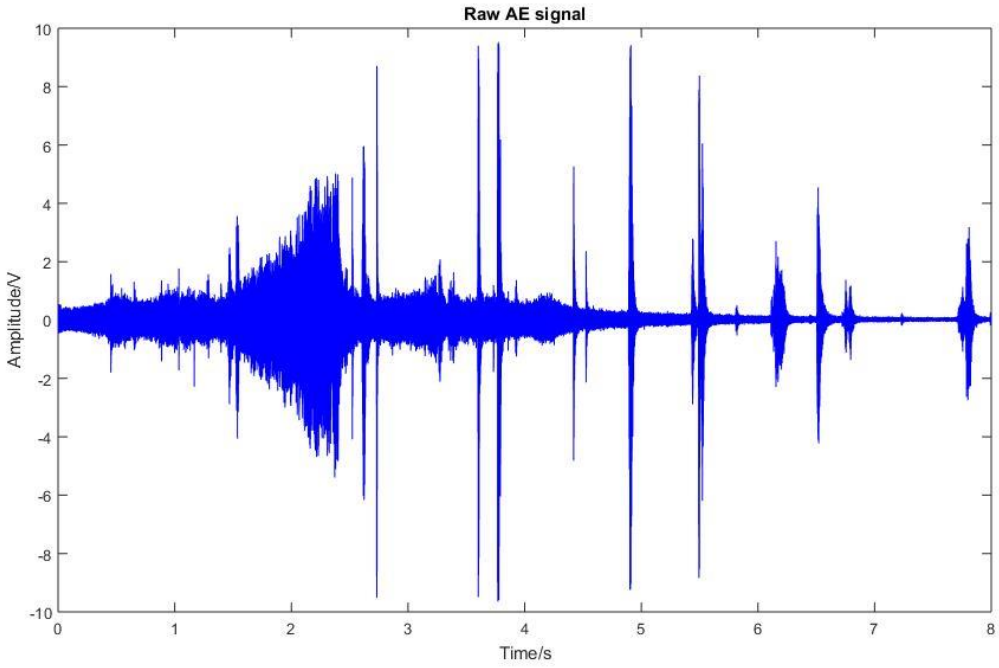

Figure 7-0-82: Raw acoustic emission signal generated by a passenger train. High amplitude and signal modulation can be clearly seen

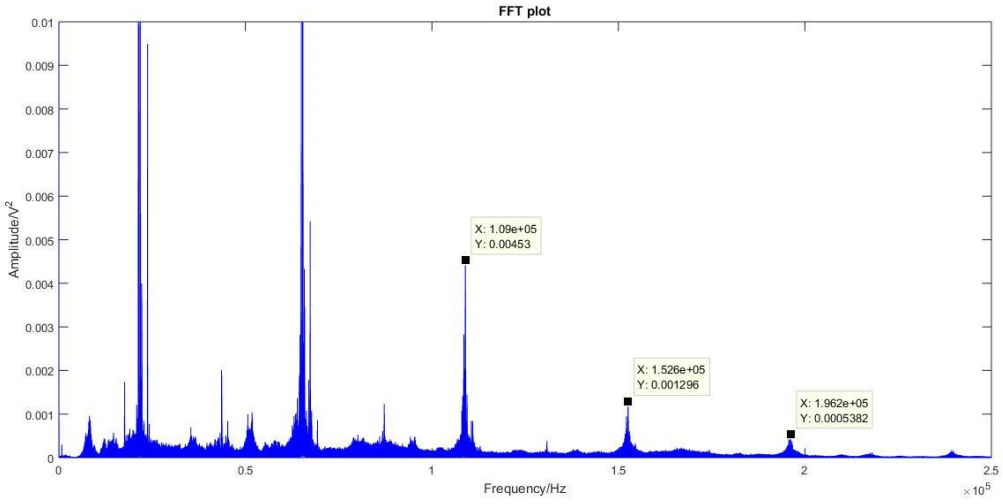

Figure 7-0-83: Power spectrum of previous signal. Harmonics in frequency distribution can be observed indicating the presence of a fault

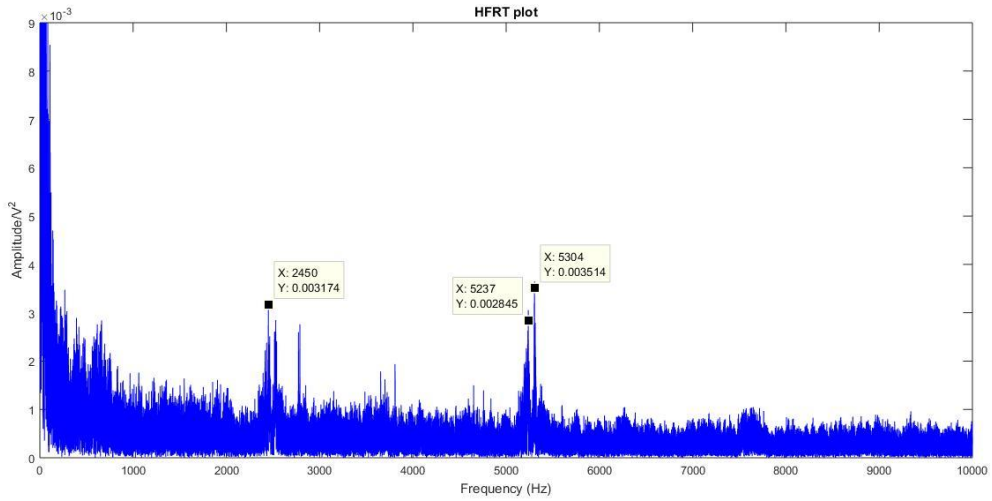

Figure 7-0-84: HFRT plot. The fundamental frequency of 2450 Hz and its harmonics are clearly visible

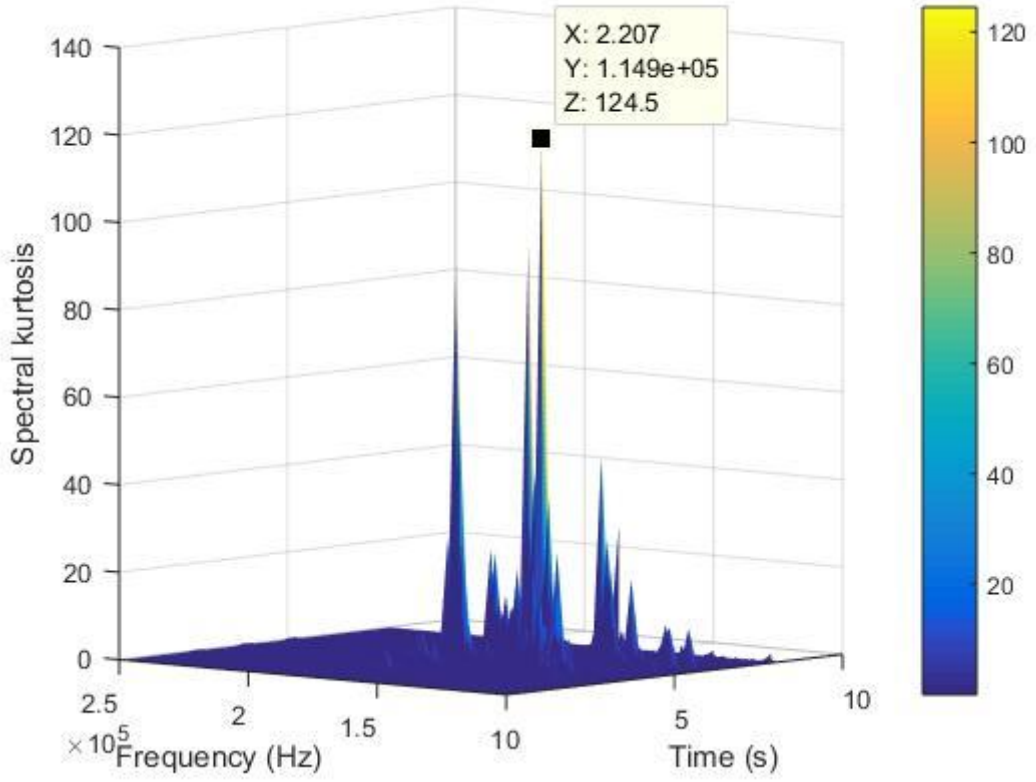

Figure 7-0-85: TSK results. High Kurtosis value at 1.149 kHz indicating a potential fault

To sum up, a series of wayside measurements were carried out under actual operational conditions at the instrumental Cropredy site in order to evaluate the customised RCM system in wheel and axle bearing damage detection. Freight and passenger trains have been recorded.

Representative examples of acoustic emission waveforms generated by passenger and freight trains with rolling stock free of defects have been presented.

During signal processing, several freight and passenger train waveforms has been detected to contain evidence of potential bearing faults. High amplitude peaks at raw signal and signal modulation indicate the presence of a defect. Harmonics in frequency distribution has been observed indicating the presence of a potential fault. In addition, HFRT algorithm has been applied at the collected data. Bearing fundamental frequency and its harmonics are visible in the envelope spectrum. The captured signals have also been analysed using the TSK algorithm. High kurtosis values also confirm the presence of a defect. Frequency bands with high kurtosis value can be used as a reference for designing the band-pass filter of the HFRT process. Furthermore, the presence of the defect is also confirmed by the Spectrogram.

Chapter 8 Conclusions and Recommendations for future work

8.1 Conclusions

This thesis has presented the further advancement of an integrated online vibroacoustic RCM system for rolling stock wheelsets. AE and vibration analysis have been carried out in order to evaluate the condition of wheelsets under different experimental setups including measurements of in-service rolling stock operating on the Chiltern rail line in the UK. Laboratory, field and in-service experiments have been performed. On-board and wayside measurements have been carried out together with the associated signal processing required for the evaluation of the data obtained. Time, frequency and time-frequency analysis have been considered for processing the captured data.

This study has proposed a procedure for undertaking a literature review of railway rolling stock wheelsets and faults. Common wheel, axle bearing and axle defects have been presented. Inspection using various NDT techniques for railway rolling stock wheelsets have been reviewed and discussed in details. Commercial and non-commercial RCM systems for

the evaluation of the structural integrity of railway wheelsets are presented. University of Illinois at Chicago on-board monitoring system has a few similarities with the integrated on-line vibroacoustic RCM of this study. Comparison between the two systems have been presented.

Acoustic Emission (AE) and Vibration signal analysis in evaluation of railway wheelsets health integrity have also been reviewed and discussed. Fundamental of AE testing and AE signal has been presented in details. Time Driven Data have been recorded during the experimental part of this project. Furthermore, the two categories of AE sensor have been described. Resonance sensors have been considered as a suitable option for the developed condition monitoring system due to their frequency response. Advantages and limitations of AE testing have been presented. Advance signal processing of AE signals can overcome the most of limitations and can be effective for monitoring the damage initiation and degradation in railway wheelsets. Thus, AE has been employed as the appropriate structural health monitoring technique for this project.

State-of the art in Acoustic Emission and Vibration signal analysis have been reviewed and discussed. Several researches have used AE and vibration in order to detect wheelset defect. The data analysis and the results of their experiments have been presented together with their conclusions.

Current state of work using AE and vibration signal analysis have been described. The experimental methodology and data analysis employed in the current study have been presented. The effectiveness of acoustic emission and vibration techniques supported by the experiments.

Advanced signal processing algorithms of railway wheelsets fault detection have been reviewed. Time, frequency and time-frequency domain analysis are the three approaches of

signal analysis that are discussed in the current work. Signal processing techniques such as moving RMS, moving Kurtosis, Peak to Peak analysis, Fast Fourier Transform, High Frequency Resonant Technique, Cepstrum analysis and Time- Spectral kurtosis have been presented in details. Comparison between these signal processing techniques have been described.

Integrated Remote Condition Monitoring system's equipment and experimental methodology employed in the current work have been described. Two customised test rigs were used for the experimental part of this project. During laboratory-based testing, on-board experiments have been carried out using healthy and defective bearings in order to evaluate the effectiveness of Acoustic Emission and Vibration signal analysis. In addition, wayside testing on artificial-induced wheel flat have been performed using motorized trials. AE and vibration signals of defect-free and defective wheel have been recorded for comparison purposes.

During field trials in collaboration with VTG Rail Limited, the customised vibroacoustic monitoring system have been installed under controlled conditions at Long Marston, UK. Wayside and on-board data have been acquired and analysed using the advanced signal processing techniques. The artificially induced axle bearing faults have been detected efficiently. An optical infrared triggering system has also been used in order to trigger automated the data acquisition system when the test-vehicle pass the detection zone.

During in-service experiments, the novel remote condition monitoring system has been installed on the UK rail network at Cropredy at Chiltern Railway line (direction from London to Birmingham) adjacent to Hot Box Axle Detectors for comparison purposes. Wayside AE and Vibration signals have been recorded. The results and the main conclusions of the experimental work of this project have been presented below.

From the results obtained to date, it has been effectively demonstrated that fault detection, defect type evaluation and fault quantification can be achieved using appropriate signal analysis methodology.

During Long Marston and Cropredy trials, frequency distribution has been used in order to detect the presence of defects. Comparison between a template signal of defect-free bearing and a defective bearing have been presented. Harmonics in frequency distribution can be an indication of a fault. High amplitude peaks in raw signal and signal modulation can also be appeared due to a potential defect. In addition, TSK analysis enhanced the ability of the system to identify bearing defects. Frequency bands with high kurtosis values can be used as a reference for further analysis in order to confirm the type of the defect. The HFRT algorithm has been effectively applied in the captured data obtained during various measurements in order to identify the characteristic faulty frequency. The bearing defects were known in advance during laboratory and Long Marston experiments. Therefore, the bearing faulty frequencies were known by the manufacturer of the bearings. However, Cropredy tests were blind trials as they were performed on in-service rolling stock. From the analysis carried out on Cropredy measurements from different freight and passenger trains a number of potential faults have been detected. The results indicating the potential presence of defects still need to be confirmed with help of Network Rail. Moving RMS analysis has also been applied at laboratory and fields measurements. Defect quantification has been shown to be possible by establishing appropriate threshold limits which however need to be confirmed more accurately for different rolling stock types.

During laboratory trials using bearings with multiple defects, Cepstrum analysis have been considered as the appropriate signal analysis methodology in order to confirm the presence of all the defects. Three different fundamental faulty frequencies and their harmonics have been

detected. In addition, wheel flat on motorized trials have been confirmed by vibration signal analysis.

High frequency AE and vibration have been shown to be useful techniques for railway wheel and axle bearing fault detection, providing superior capabilities over state-of-the art techniques. This has been supported by laboratory, field and in-service measurements.

To conclude, the research contribution of current work has been achieved by the development of a novel vibroacoustic monitoring system for railway wheelsets. High frequency acoustic emission and vibration testing have been considered in order to detect wheelsets defects at the early stage. During the experimental part of this project, in-service trials were carried out at Cropredy. Potential bearing faults have been detected. Therefore, the signal processing methodology has been evaluated using in-service data. In addition, comparison between advanced signal processing techniques have been carried out using signals acquired by laboratory, in-field and in-service experiments. The properties of each algorithm have been supported by results. During the application of HFRT method, a band-pass filter should be designed. Novel methodology about frequency range selection of the band –pass filter has also been considered. TSK algorithm and frequency distribution of the signal can both enhance the selection of the appropriate frequency band. Harmonics in frequency distribution is evidence that a defect is appeared. Thus, the frequency range that the harmonics presented is the appropriate frequency range for the design of the band pass filter. Furthermore, frequency bands with high kurtosis values can be used as a reference for the band pass filter.

8.2 Recommendations for future work

The work carried out to date has yielded promising results. However, there is still substantial scope for future research and development in the field of wheel and axle bearing fault

detection and quantification. The influence of speed and weight of rolling stock on the AE and vibration signals obtained needs to be evaluated in more depth to confirm the quantification capability of the techniques. This will also require that the suspected defective wheels and bearings will need to be checked manually after detection by the system.

Additional, development should also focus on wireless sensing and energy harvesting to increase the autonomy of the system and simplify operational principles. Further advancements are also possible in the signal processing, particularly towards decreasing computational costs of more complex algorithms such as moving kurtosis and spectral kurtosis. The possibility of using wavelets is an area worth of further investigation.

As the complexity of machinery increases, the possibility of fault detection by single- sensor based methods decreases gradually. Along with the rapid development of computers, a multi-sensor based monitoring system will be expected to yield more independent results.

Data fusion techniques are suggested as the best solution for increasing the effectiveness of the condition based maintenance (Niu et al. 2010). Data fusion methods have recently gained ground within the research communities due to rapid development of signal processing methods and to rapid progress of advanced sensors. Data fusion is defined as a process of combining data and information from different sources in order to maximize the accuracy of identifying a potential defect in a machinery (Hall and Llinas 2001).

Data fusion techniques can be categorised into 3 groups according to their requirements (Hall and Llinas 2001) :

- Signal level fusion
- Feature level fusion

- Decision level fusion

The customised monitoring system consists of four AE sensors and two accelerometers. Signal level fusion can be achieved in order to enhance the important information, improve detectability and reliability of the system. Signals from different sensors can be fused into a new signal using several methods such as Weighed Averaging algorithm,Weighted Averaging based on correlation function and Kalman filter (Hall and Llinas 1997) , (GUANGFU et al. 2011). The new fused signal then can be analyzed using the advanced signal processing techniques that are presented in this thesis.

In addition, comparison between the novel customised monitoring system that is presented in this work and a new multi-sensor monitoring system can be presented. Evaluation of the effectiveness of the multi-sensor system in detecting several wheelsets faults can also be achieved.

According to Liu and Wang, the fusion of multi-sensor data provides an increased accuracy over a single sensor alone (Q. C. Liu and Wang 2001). In addition, data fusion reduces the quantity of data resulting in a faster system's response. Furthermore, signal fusion extends spatial coverage of system and reduce sensor's redundancy. Therefore, data fusion is highly recommended as a future work of this thesis.

References

Acoustics, Physical (2020), 'R50a sensor', <http://www.pacjwest.com/AESensorProduct/PDF/R50-Alpha.pdf>, accessed 27/10/2020.

Acoustics', Physical (2020), 'PREAMPLIFIERS', <https://www.physicalacoustics.com/preamplifiers/>, accessed 27/10/2020.

Al-Dalabeeh, J, Roberts, C, and Papaelias, M (2012), 'Analysis of alternating current field measurement rail inspection signals', *Fifty-first annual conference of the British non-destructive testing, NDT 2012*, 11-13.

Al-Ghamd, Abdullah M. and Mba, David (2006), 'A comparative experimental study on the use of acoustic emission and vibration analysis for bearing defect identification and estimation of defect size', *Mechanical Systems and Signal Processing,* 20 (7), 1537-71.

Amini, Arash (2016a), 'Online condition monitoring of railway wheelsets', Ph.D. (University of Birmingham).

--- (2016b), 'Online condition monitoring of railway wheelsets', (University of Birmingham).

Amini, Arash, Entezami, Mani, and Papaelias, Mayorkinos (2016a), 'Onboard detection of railway axle bearing defects using envelope analysis of high frequency acoustic emission signals', *Case Studies in Nondestructive Testing and Evaluation,* 6, Part A, 8-16.

Amini, Arash, et al. (2017), 'Evaluation of the effect of speed and defect size on high-frequency acoustic emission and vibration condition monitoring of railway axle bearings', *Insight-Non-Destructive Testing and Condition Monitoring,* 59 (4), 184-88.

Amini, Arash, et al. (2016b), 'Wayside detection of faults in railway axle bearings using time spectral kurtosis analysis on high-frequency acoustic emission signals', 8 (11), 1687814016676000.

Amini, Arash, et al. (2016c), 'Wayside detection of faults in railway axle bearings using time spectral kurtosis analysis on high-frequency acoustic emission signals', *Advances in Mechanical Engineering,* 8 (11), 1687814016676000.

Anastasopoulos, Athanasios, et al. (2010), 'Acoustic emission on-line inspection of rail wheels', *Proc. 29th Eur. Conf. Acoust. Emission Testing*, 1-8.

Antoni, Jérôme (2007), 'Fast computation of the kurtogram for the detection of transient faults', *Mechanical Systems and Signal Processing,* 21 (1), 108-24.

Antoni, Jérôme and Randall, R. B. (2006), 'The spectral kurtosis: application to the vibratory surveillance and diagnostics of rotating machines', *Mechanical Systems and Signal Processing,* 20 (2), 308-31.

Antoni, Jérôme %J Mechanical systems and processing, signal (2006), 'The spectral kurtosis: a useful tool for characterising non-stationary signals', 20 (2), 282-307.

Barke, Derek and Chiu, WK (2005), 'Structural health monitoring in the railway industry: a review', *Structural Health Monitoring,* 4 (1), 81-93.

Barszcz, Tomasz and Randall, Robert B. (2009), 'Application of spectral kurtosis for detection of a tooth crack in the planetary gear of a wind turbine', *Mechanical Systems and Signal Processing,* 23 (4), 1352-65.

Bladon, Keith, et al. (2004), 'Predictive Condition Monitoring of Railway Rolling Stock', *Conference On Railway Engineering*.

Bracciali, A and Cascini, G (1997), 'Detection of corrugation and wheelflats of railway wheels using energy and cepstrum analysis of rail acceleration', *Proceedings of the Institution of Mechanical Engineers, Part F: Journal of Rail and Rapid Transit,* 211 (2), 109-16.

C.Vale (2014), 'Advanced Approaches for Axle Bearing Condition Monitoring', in J. Pombo (ed.), *Proceedings of the Second International Conference on Railway Technology: Research, Development and Maintenance* (Stirlingshire, UK,).

Cao, Hongrui, et al. (2016), 'Wheel-bearing fault diagnosis of trains using empirical wavelet transform', *Measurement,* 82, 439-49.

Chen, Bin, Yan, Zhaoli, and Chen, Wei (2014), 'Defect detection for wheel-bearings with time-spectral kurtosis and entropy', *Entropy,* 16 (1), 607-26.

Cline, J. E., Bilodeau, J. R., and Smith, R. L. (1998), 'Acoustic wayside identification of freight car roller bearing defects', *Railroad Conference, 1998. Proceedings of the 1998 ASME/IEEE Joint*, 79-83.

Cockerill, A, et al. (2016), 'Determination of rolling element bearing condition via acoustic emission', *Proceedings of the Institution of Mechanical Engineers, Part J: Journal of Engineering Tribology,* 230 (11), 1377-88.
Corni, Ilaria, et al. (2015), 'Real-time on-board condition monitoring of train axle bearings', *The Stephenson Conference: Research for railway* (Imeche).
Corni, Ilaria, et al. (2017), 'Characterization and mapping of rolling contact fatigue in rail-axle bearings', *Engineering Failure Analysis,* 82, 617-30.
Cummings, Scott and Sammon, Devin (2015), 'Tread Buildup on Railroad Wheels'.
Dornfeld, David A. (1990), 'Neural Network Sensor Fusion for Tool Condition Monitoring', *Annals of the CIRP,* 39, pp 101-05.
Du, Kun, et al. (2020), 'Experimental study on acoustic emission (AE) characteristics and crack classification during rock fracture in several basic lab tests', *International Journal of Rock Mechanics and Mining Sciences,* 133, 104411.
Dykas, Brian, Hood, Adrian, and Becker, Andrew (2017), *Acoustic Emission in Grease-Lubricated Helicopter Drivetrain Bearings*.
Edwards, RS, et al. (2008), 'Ultrasonic detection of surface-breaking railhead defects', 50 (7), 369-73.
Eftekharnejad, B., et al. (2011), 'The application of spectral kurtosis on Acoustic Emission and vibrations from a defective bearing', *Mechanical Systems and Signal Processing,* 25 (1), 266-84.
Ekberg, Anders and Kabo, Elena (2005), 'Fatigue of railway wheels and rails under rolling contact and thermal loading—an overview', *Wear,* 258 (7–8), 1288-300.
Elasha, Faris, et al. (2017), 'A comparative study of the effectiveness of vibration and acoustic emission in diagnosing a defective bearing in a planetry gearbox', *Applied Acoustics,* 115, 181-95.
Elforjani, M. and Mba, D. (2010), 'Accelerated natural fault diagnosis in slow speed bearings with Acoustic Emission', *Engineering Fracture Mechanics,* 77 (1), 112-27.
Elforjani, Mohamed (2018), 'Diagnosis and prognosis of slow speed bearing behavior under grease starvation condition', *Structural Health Monitoring,* 17 (3), 532-48.
Entezami, M, et al. (2014), 'Acoustic analysis techniques for condition monitoring of roller bearings', *Railway Condition Monitoring (RCM 2014), 6th IET Conference on* (IET), 1-8.
EUAR (2020), 'Report on Railway Safety and Interoperability in the EU'.
Ferrando Chacon, Juan Luis, et al. (2016), 'An experimental study on the applicability of acoustic emission for wind turbine gearbox health diagnosis', 35 (1), 64-76.
Gao, Lixin, et al. (2011), 'Study and Application of Acoustic Emission Testing in Fault Diagnosis of Low-Speed Heavy-Duty Gears', 11 (1), 599-611.
Graney, Brian P and Starry, Ken (2012), 'Rolling element bearing analysis', *Materials Evaluation,* 70 (1), 78.
Green, Robert E. (1980), 'Basic Wave Analysis of Acoustic Emission', in W. W. Stinchcomb, et al. (eds.), *Mechanics of Nondestructive Testing* (Boston, MA: Springer US), 55-76.
Grosse, Christian U and Ohtsu, Masayasu (2008), *Acoustic emission testing* (Springer Science & Business Media).
Hall, David L. and Llinas, James (1997), 'An introduction to multisensor data fusion', *Processing of the IEEE,* 85 (1), pp. 6-23.
--- (2001), 'Multisensor Data Fusion', *Intoduction to Multisensor Data Fusion*.
Hawman, M. W. and Galinaitis, W. S. (1988), 'Acoustic emission monitoring of rolling element bearings', *IEEE 1988 Ultrasonics Symposium Proceedings.*, 885-89 vol.2.
He, Miao and He, David (2020), 'A new hybrid deep signal processing approach for bearing fault diagnosis using vibration signals', *Neurocomputing,* 396, 542-55.
Ho, D. and Randall, R. B. (2000), *Randall, R.B.: Optimisation of bearing diagnostic techniques using simulated and actual bearing fault signals. Mechanical Systems and Signal Processing 14, 763-788* (14) 763-88.
Huang, Z., M.Papaelias, and Lang, Z.Q. (2014a), 'Wayside detection of axle bearing faults in rolling stock though correlation signal processing', *International Conference in Condition Monitoring and Machinery Failure Prevention Technologies 2014* (Manchester,UK).
Huang, Z., et al. (2014b), 'On line evaluation of railway axle bearing faults using acoustic emission and vibration analysis', *International Conference in Condition Monitoring and Machinery Failure Prevention Technologies 2014* (Manchester,UK).
Huang, Zheng (2017), 'Integrated railway remote condition monitoring', (University of Birmingham).
Kaphle, Manindra, et al. (2012), 'Effective discrimination of acoustic emission source signals for structural health monitoring', *Advances in Structural Engineering,* 15 (5), 707-16.

Kappes, W, et al. (2000), 'Non-destructive testing of wheel-sets as a contribution to safety of rail traffic', *CORENDE 2000 Proceedings*.
Klausen, Andreas and Robbersmyr, Kjell G. (2019), 'Cross-correlation of whitened vibration signals for low-speed bearing diagnostics', *Mechanical Systems and Signal Processing,* 118, 226-44.
Kschischang, Frank R (2006), 'The hilbert transform', *University of Toronto*.
Lagnebäck, Robert (2007), 'Evaluation of wayside condition monitoring technologies for condition-based maintenance of railway vehicles', Licentiate thesis (Luleå University of Technology).
Lebold, Mitchell, et al. (2000), 'Review of vibration analysis methods for gearbox diagnostics and prognostics', *Proceedings of the 54th meeting of the society for machinery failure prevention technology* (634), 16.
Liu, Chang, et al. (2017), 'Acoustic emission signal processing for rolling bearing running state assessment using compressive sensing', *Mechanical Systems and Signal Processing,* 91, 395-406.
Liu, Dan, et al. (2018), *An Optimized Kurtogram Method for Early Fault Detection of Rolling Element Bearings Using Acoustic Emission* 365-70.
Liu, Qing (Charle) and Wang, Hsu-Pin(Ben) (2001), 'A case study on multisensor data fusion for imbalance diagnosis of rotating machinery', *AI EDAM,* 15 (03), pp 203-10.
Liu, Yongfeng, et al. (2020), 'Effects of axle load transfer on wheel rolling contact fatigue of high-power AC locomotives with oblique traction rods', *International Journal of Fatigue*, 105748.
Luke, Michael, et al. (2011), 'Fatigue crack growth in railway axles: assessment concept and validation tests', *Engineering Fracture Mechanics,* 78 (5), 714-30.
M. Entezami, E. Stewart, C. Roberts, et al (2016), 'Wayside acoustic monitoring techniques for railway axlebox bearings on high-speed lines', *11th world congress on railway research (WCRR)* (Milan,Italy).
M., Papaelias (2012), 'Interoperable monitoring, diagnosis and maintenance strategies for axle bearings-MAXBE'.
Mauricio, Alexandre, et al. (2020), 'Bearing diagnostics under strong electromagnetic interference based on Integrated Spectral Coherence', *Mechanical Systems and Signal Processing,* 140, 106673.
Mba, D. (2003), 'Acoustic Emissions and Monitoring Bearing Health', *Tribology Transactions,* 46 (3), 447-51.
McFadden, P. D. and Smith, J. D. (1984), 'Vibration monitoring of rolling element bearings by the high-frequency resonance technique — a review', *Tribology International,* 17 (1), 3-10.
Miettinen, Juha and Pataniitty, Pentti (1999), 'Acoustic emission in monitoring extremely slowly rotating rolling bearing', *Proceedings of COMADEM* (99), 289-97.
Miettinen, Juha and Andersson, Peter (2000), 'Acoustic emission of rolling bearings lubricated with contaminated grease', *Tribology International,* 33 (11), 777-87.
Mjit, Mustapha, Beaujean, PJ, and Vendittis, David J (2011), 'Comparison of fault detection techniques for an ocean turbine', *Annual Conference of the Prognostics and Health Management Society*, 25-29.
Morhain, A and Mba, D (2003), 'Bearing defect diagnosis and acoustic emission', 217 (4), 257-72.
Munoz, JM Chacón, et al. (2013), 'Railroad inspection based on ACFM employing a non-uniform B-spline approach', 40 (2), 605-17.
NDT, Resource center 'NDT Method Summary', <https://www.nde-ed.org/GeneralResources/MethodSummary/MethodSummary.htm>, accessed 19/01/2020.
Nicholson, G, et al. (2011), 'Sizing and tomography of rolling contact fatigue cracks in rails using NDT technology-potential for high speed application', *Proceedings of the 9th World Conference on Railway Research*.
Nielsen, Jens CO and Johansson, Anders (2000), 'Out-of-round railway wheels-a literature survey', *Proceedings of the Institution of Mechanical Engineers, Part F: Journal of Rail and Rapid Transit,* 214 (2), 79-91.
Niknam, Seyed Ali, Songmene, Victor, and Au, Y. H. Joe %J The International Journal of Advanced Manufacturing Technology (2013), 'The use of acoustic emission information to distinguish between dry and lubricated rolling element bearings in low-speed rotating machines', 69 (9), 2679-89.
Niu, Gang, Yang, Bo-Suk, and Pecht, Michael (2010), 'Development of an optimized condition based maintenance system by data fusion and reliability – centered maintenance', *Reliabilty Engineering and System Safety,* 95, pp 786-96.
Papaelias, Fausto Pedro Garcia Marquez and Mayorkinos (2013), *Fault Detection : Classification, Techniques & Role in Industrial Systems, Chapter 2: An integrated strategy for efficient non-destructive evaluation of rails* (New York, United States: Nova Science Publishers).
Papaelias, M (2012), 'Interoperable monitoring, diagnosis and maintenance strategies for axle bearings', *Maxbe report*.

Papaelias, M, et al. (2012), 'The future of rail inspection technology and the INTERAIL FP7 project', *51st Annual Conference of the British Institute of Non-Destructive Testing (BINDT), Northamptonshire, UK, Sept*, 11-13.
Papaelias, M Ph, et al. (2009a), 'High-speed inspection of rails using ACFM techniques', 42 (4), 328-35.
Papaelias, M Ph, et al. (2009b), 'High-speed inspection of rolling contact fatigue in rails using ACFM sensors', 51 (7), 366-69.
--- (2010), 'Further developments in high-speed detection of rail rolling contact fatigue using ACFM techniques', 52 (7), 358-60.
Papaelias, Mayorkinos, et al. (2016), 'Online condition monitoring of rolling stock wheels and axle bearings', 230 (3), 709-23.
Papaelias, Mayorkinos, et al. (2014a), 'Advanced wayside condition monitoring of rolling stock wheelsets', *the Proceedings of the 11 th ECNDT, Prague, Czech Republic*, 6-10.
Papaelias, Mayorkinos, et al. (2014b), 'Advanced wayside condition monitoring of rolling stock wheelsets'.
Patidar, Shyam and Soni, Pradeep Kumar (2013), 'An overview on Vibration analysis techniques for the diagnosis of rolling element bearing faults', *International Journal of Engineering Trends and Technology (IJETT),* 4 (5), 1804-09.
Peng, Jianping, et al. (2014), 'Rolling contact fatigue detection using eddy current pulsed thermography', *2014 IEEE Far East Forum on Nondestructive Evaluation/Testing* (IEEE), 176-80.
Peng, Jianping, et al. (2015), 'Investigation into eddy current pulsed thermography for rolling contact fatigue detection and characterization', 74, 72-80.
Ph Papaelias, M, Roberts, C, and Davis, CL (2008), 'A review on non-destructive evaluation of rails: state-of-the-art and future development', *Proceedings of the Institution of Mechanical Engineers, Part F: Journal of Rail and rapid transit,* 222 (4), 367-84.
Phillips, Charles L, Parr, John M, and Riskin, Eve A (1995), *Signals, systems, and transforms* (Prentice Hall).
physicalacoustics <https://www.physicalacoustics.com/by-product/sensors/R50a-500-kHz-General-Purpose-AE-Sensor>, accessed 28/03/2019.
Pohl, Rainer, et al. (2004), 'NDT techniques for railroad wheel and gauge corner inspection', *NDT & e International,* 37 (2), 89-94.
Qiao Sun, et al. (2004), 'Pattern Recognition for Automatic Machinery Fault Diagnosis', *Journal of Vibration and Acoustics,* 126 (2), pp 307-16
Railway Accident Investigation Unit, RAIU (2009), 'Report into the derailment of a Tara Mines freight train at Skerries on the 10th of January 2008'.
Randall, RB (1982), 'Cepstrum analysis and gearbox fault-diagnosis', *Maintenance Management International,* 3 (3), 183-208.
Randall, Robert B 'A history of cepstrum analysis and its application to mechanical problems', *International Conference*, 29-30.
Randall, Robert B. and Antoni, Jérôme (2011), 'Rolling element bearing diagnostics—A tutorial', *Mechanical Systems and Signal Processing,* 25 (2), 485-520.
Rolek, Paweł, Bruni, Stefano, and Carboni, Michele (2016), 'Condition monitoring of railway axles based on low frequency vibrations', *International Journal of Fatigue,* 86, 88-97.
Rowshandel, H, et al. (2011), 'Development of autonomous ACFM rail inspection techniques', 53 (2), 85-89.
RSSB (2010), 'Railway Group Standard GM/RT2466 Issue 3: Railway Wheelsets'.
Rudlin, John, Muhammed, Amin, and Schneider, Charles (2006), 'Inspection reliability and periodicity for rail axle inspection', *Insight-Non-Destructive Testing and Condition Monitoring,* 48 (6), 348-51.
Rudlin, John, et al. (2014), 'Assessment of Corrosion on Rail Axles', *11th European Conference on Non-Destructive Testing (ECNDT 2014)* (Prague, Czech Republic).
Rudlin, JR and Shipp, R (2003), 'Review of rail axle inspection methods', *Proceedings of the International Seminar on Railway axles, London, UK*.
Saferail (2015), 'The Problem', <http://www.saferail.net/project/problem.jsp>, accessed 05/06/2015.
Sause, Markus (2011), *Investigation of Pencil-Lead Breaks as Acoustic Emission Sources* (29) 184-96.
Segla, M., Shaoping, Wang, and Fang, Wang (2012), 'Bearing fault diagnosis with an improved high frequency resonance technique', *Industrial Informatics (INDIN), 2012 10th IEEE International Conference on*, 580-85.
Shiroishi, J., et al. (1997), 'BEARING CONDITION DIAGNOSTICS VIA VIBRATION AND ACOUSTIC EMISSION MEASUREMENTS', *Mechanical Systems and Signal Processing,* 11 (5), 693-705.
Singh, Ramesh (2020), *Applied welding engineering: processes, codes, and standards* (Butterworth-Heinemann).

SKF *Railway technical handbook* (SKF Axletronic sensors, 1).
--- (2017), 'Bearing damage and failure analysis'.
Snell, OD and Nairne, I (2008), 'Acoustic bearing monitoring-the future RCM 2008'.
Spectra Quest, Inc. (2006), ' Rotating Machinery Fault Diagnosis Techniques Envelope and Cepstrum Analyses', (2015).
Štarman, Stanislav and Matz, Vaclav (2010), 'Automated System for Magnetic Particle Inspection of Railway Wheels'.
Symonds, N., et al. (2015), 'Observing early stage rail axle bearing damage', *Engineering Failure Analysis,* 56, 216-32.
Tandon, N. and Choudhury, A. (1999), 'A review of vibration and acoustic measurement methods for the detection of defects in rolling element bearings', *Tribology International,* 32 (8), 469-80.
Technologies, Keysight (2020), 'U2531A 2MSa/s USB Modular Simultaneous Data Acquisition', <https://www.keysight.com/en/pd-1250130-pn-U2531A/2msa-s-usb-modular-simultaneous-data-acquisition?cc=GB&lc=eng>, accessed 27/10/2020.
Technologies, Wilcoxon Sensing (2020), 'FOR QUANTITIES GREATER THAN 50, PLEASE CONTACT US.

High frequency sensor with integral cable

Model 712F', <https://buy.wilcoxon.com/712f.html>, accessed 25/10/2020.
Teti, R., et al. (2010), 'Advanced monitoring of machining operations', *CIRP Annals - Manufacturing Technology,* 59 (2), 717-39.
Timken (2015), 'AP™ Bearings,Size and Dimensional Data.'.
Topp, D and Smith, M (2005), 'Application of the ACFM inspection method to rail and rail vehicles', *Insight-Non-Destructive Testing and Condition Monitoring,* 47 (6), 354-57.
Transform, Fast Fourier (On line source: http://uk.mathworks.com/help/matlab/ref/fft.html).
Tyagi, Sunil (2003), 'Wavelet Analysis And Envelope Detection For Rolling Element Bearing Fault Diagnosis, A Comparative Study', *Proceedings of the 11th National Conference on Machines and Mechanisms*.
Ulianov, Cristian, et al. (2014), 'Overview of freight train derailments in the EU.

Causes, impacts, prevention and mitigation measures',

TRA2014 Transport Research Arena 2014 (Paris, France).
Usgame Sandoval, H. M, Pedraza Ramirez, C. A, and Quiroga Méndez, J. E (2013), 'Acoustic emission-based early fault detection in tapered roller bearings %J Ingeniería e Investigación', 33, 5-10.
Vallely, Patric (2015), 'A Holistic Approach to Remote Condition Monitoring for the Accurate Evaluation of Railway Infrastructure and Rolling Stock'.
Van Hecke, Brandon Edward (2015), 'Development of Novel Acoustic Emission Based Methodology and Tools for Bearing Fault Diagnostics', (University of Illinois at Chicago).
Vermeulen, F, T Vanhonacker, and Laeremans, M (2010), 'Condition Monitoring of Railway Wheelsets Using High-Frequency Vibration Technology ', (Ettington Chase, Stratford-upon-Avon, England, UK).
Vyas, NS and Gupta, AK (2006), 'Modeling rail wheel-flat dynamics', *Engineering Asset Management* (Springer), 1222-31.
Xu, Jiang, et al. (2012), 'A magnetic flux leakage and magnetostrictive guided wave hybrid transducer for detecting bridge cables', *Sensors,* 12 (1), 518-33.
Yang, Chunsheng and Létourneau, Sylvain (2005), 'Learning to predict train wheel failures', *Proceedings of the eleventh ACM SIGKDD international conference on Knowledge discovery in data mining* (ACM), 516-25.
Yang, Ruizhen, et al. (2015), 'Lateral heat conduction based eddy current thermography for detection of parallel cracks and rail tread oblique cracks', 66, 54-61.
Yasuda, Takeshi, et al. (2014), 'Evaluation of the Surface Roughness using AE method with Air Blowing', *Journal of Physics: Conference Series* (520: IOP Publishing), 012012.
Yilmazer, Pinar, Amini, Arash, and M., Papaelias (2012), 'The Structural health condition monitoring of rail steel using acoustic

emission techniques ', *In the Processing of NDT 2012*.
Zhang, Dingcheng, et al. (2020), 'Wayside acoustic detection of train bearings based on an enhanced spline-kernelled chirplet transform', *Journal of Sound and Vibration*, 115401.
Zhang, Yu-Jiang (2011), 'Rail Vehicle Bearing Defects Detection'.

Zhang, Z, et al. (2017), 'Enhanced fault diagnosis of roller bearing elements using a combination of empirical mode decomposition and minimum entropy deconvolution', 231 (4), 655-71.

Appendix A: Case study 1- Outer race defective bearings

Raw acoustic emission signal obtained from an outer race defective beating at 1000RPM

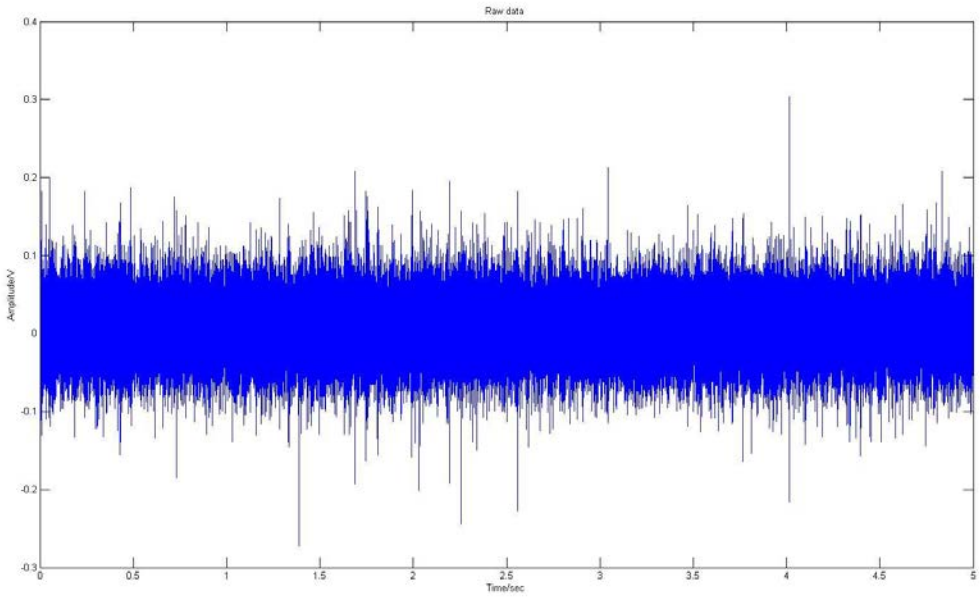

HFRT plot of previous raw acoustic emission signal. The BPFO frequency and its harmonics are clearly seen

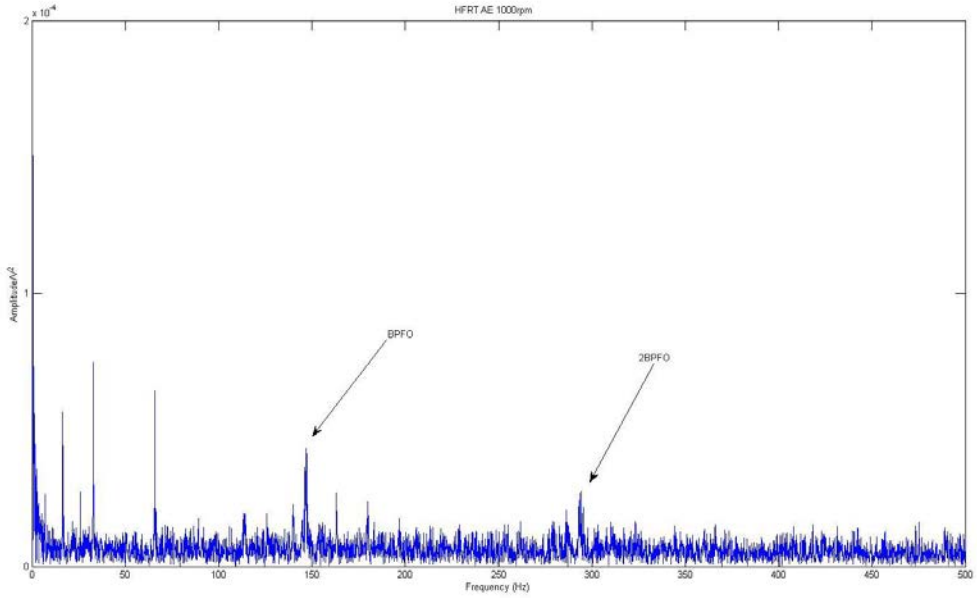

Raw vibration signal acquired by an outer race defective bearing at 100 RPM

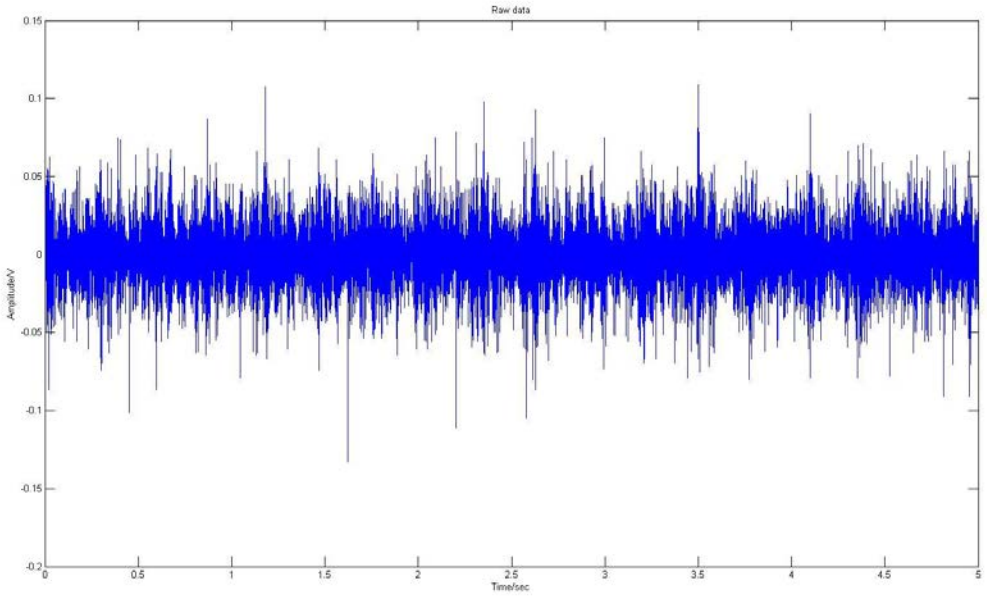

HFRT plot of previous raw vibration signal. The BPFO frequency and its harmonics are clearly observed

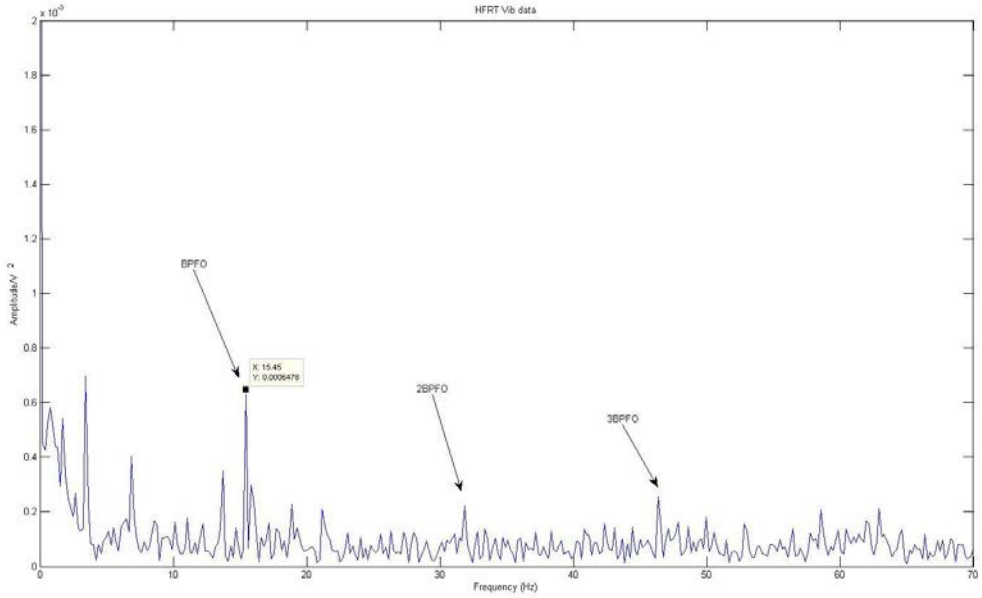

Raw vibration signal acquired by an outer race defective bearing at 1000 RPM

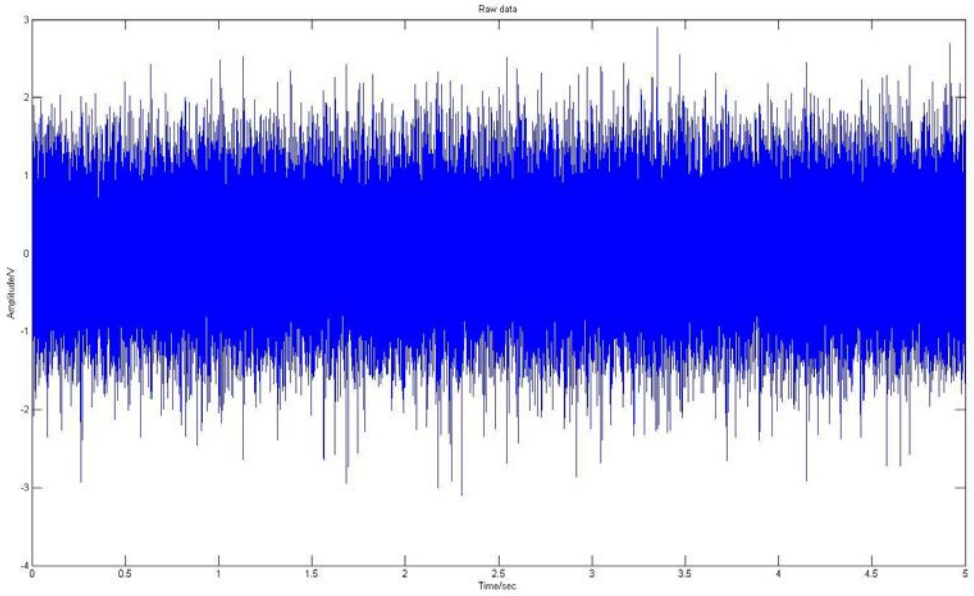

HFRT plot of previous raw vibration signal. The BPFO frequency and its harmonics are clearly illustrated

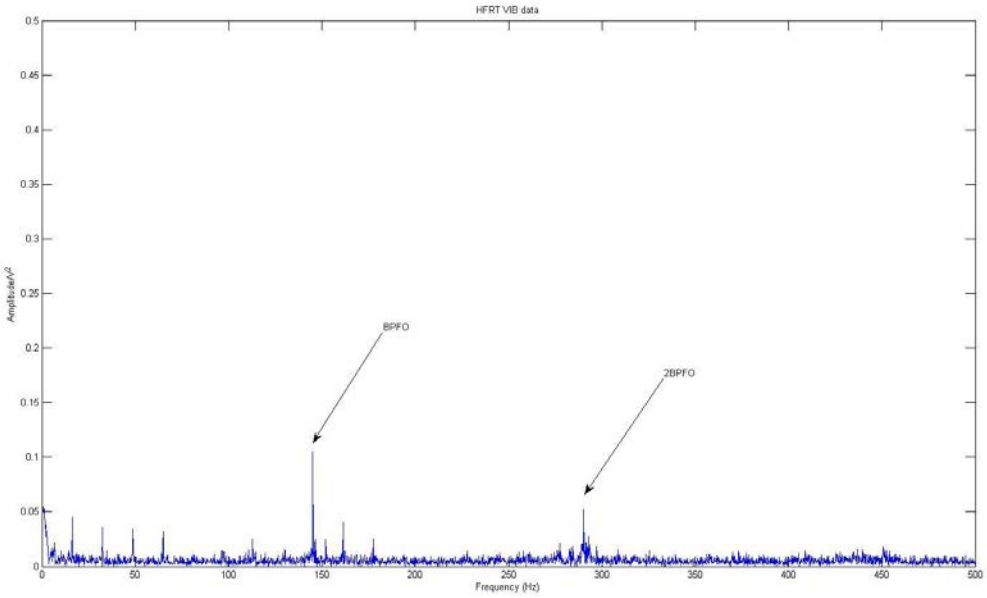
HFRT VIB data
Amplitude/V
Frequency (Hz)
BPFO
2BPFO
0.5
0.45
0.4
0.35
0.3
0.25
0.2
0.15
0.1
0.05
0
0
50
100
150
200
250
300
350
400
450
500

Appendix B: Case study 2- Roller defective bearings

Raw acoustic emission signal obtained from a roller defective beating at 200RPM

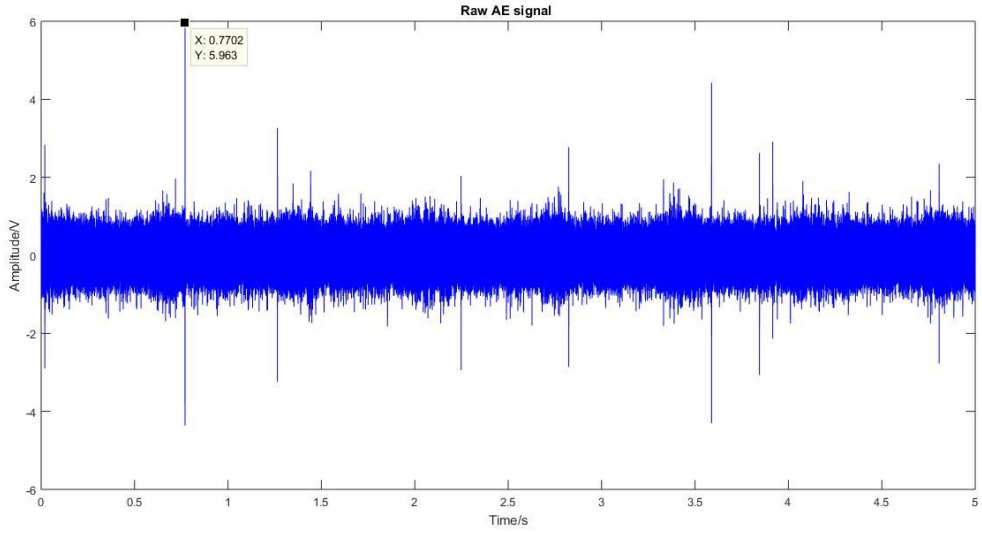

HFRT plot of previous raw acoustic emission signal. The BSF frequency and its harmonics are clearly seen

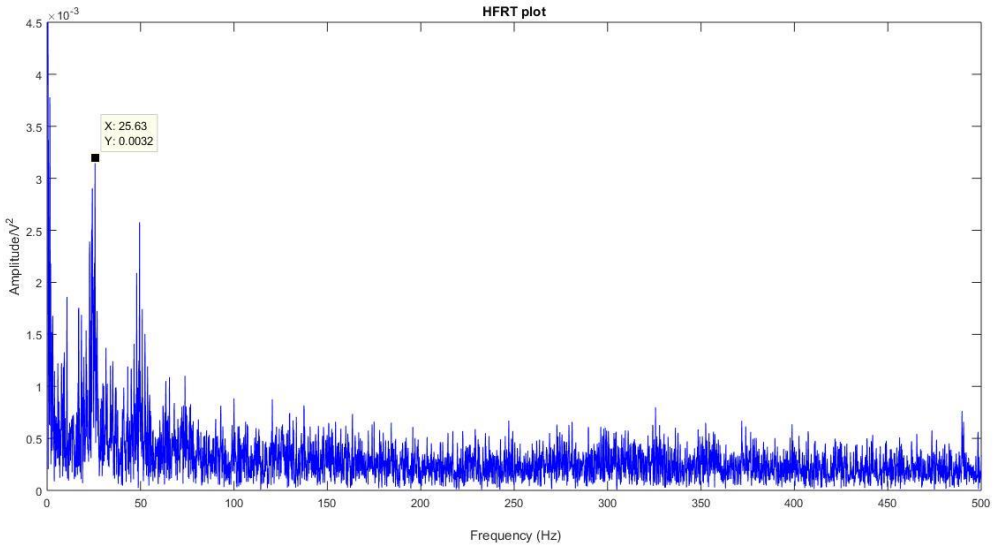
HFRT plot
×10^-3
X: 25.63
Y: 0.0032
Amplitude/V^2
Frequency (Hz)
0
0.5
1
1.5
2
2.5
3
3.5
4
4.5
0
50
100
150
200
250
300
350
400
450
500

Appendix C: Case study 3 - Cropredy in-service trials

Raw AE signal generated by passenger train. High amplitude and strong modulation can indicate the presence of a defect

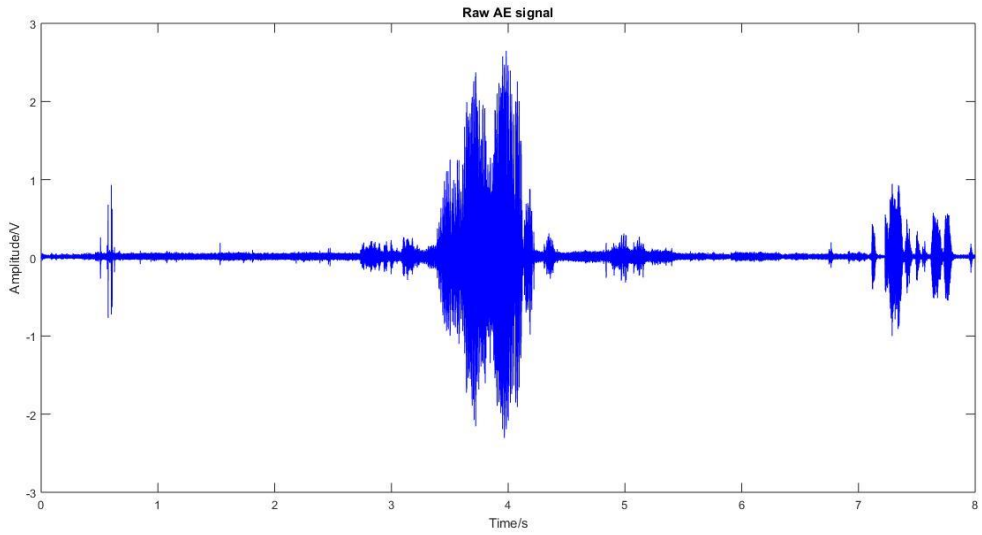

Power spectrum of previous AE signal. Harmonics in frequency distribution are clearly visible

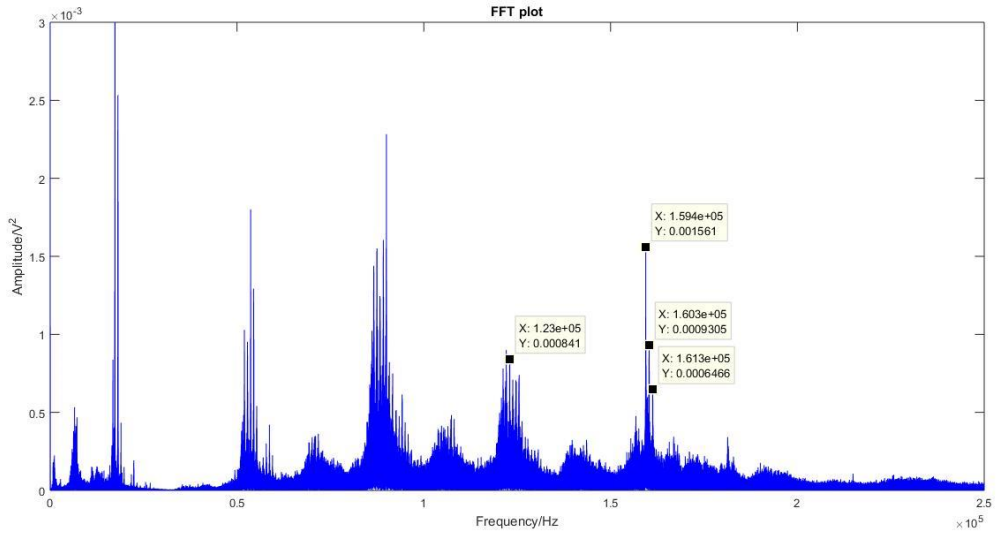

HFRT results. The fundamental frequency of 836.5 Hz and its harmonics are visible. Sidebands can also be observed

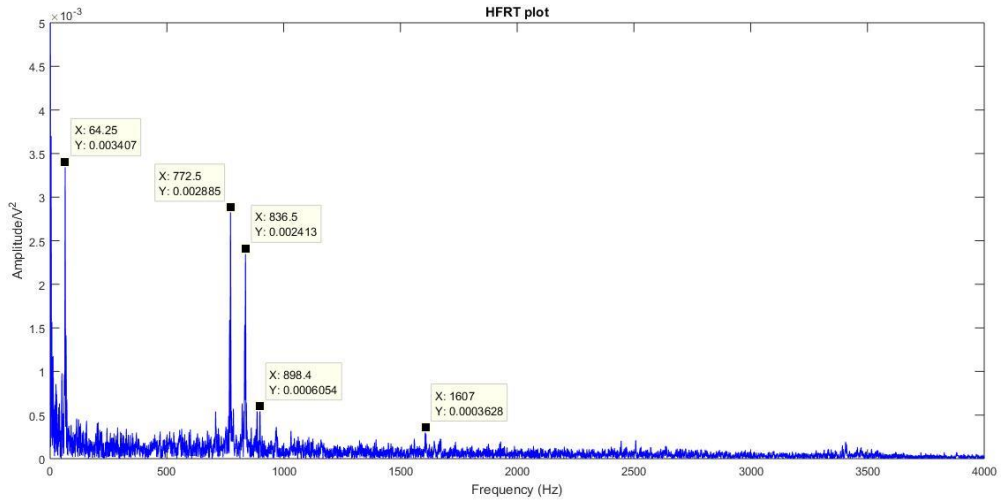

Spectrogram plot. High frequency peaks also confirm the presence of the defect

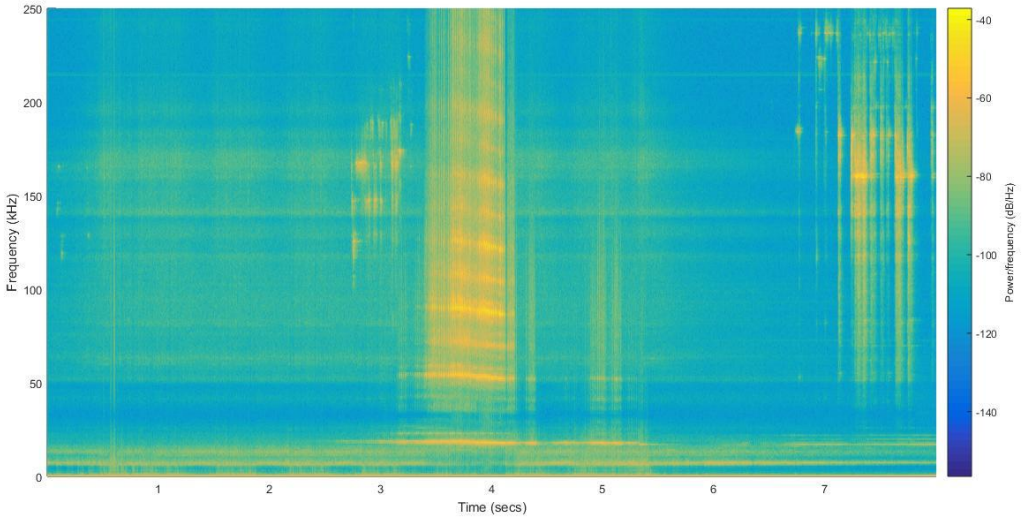

TSK results. High kurtosis value at 159 kHz indicating the presence of a fault

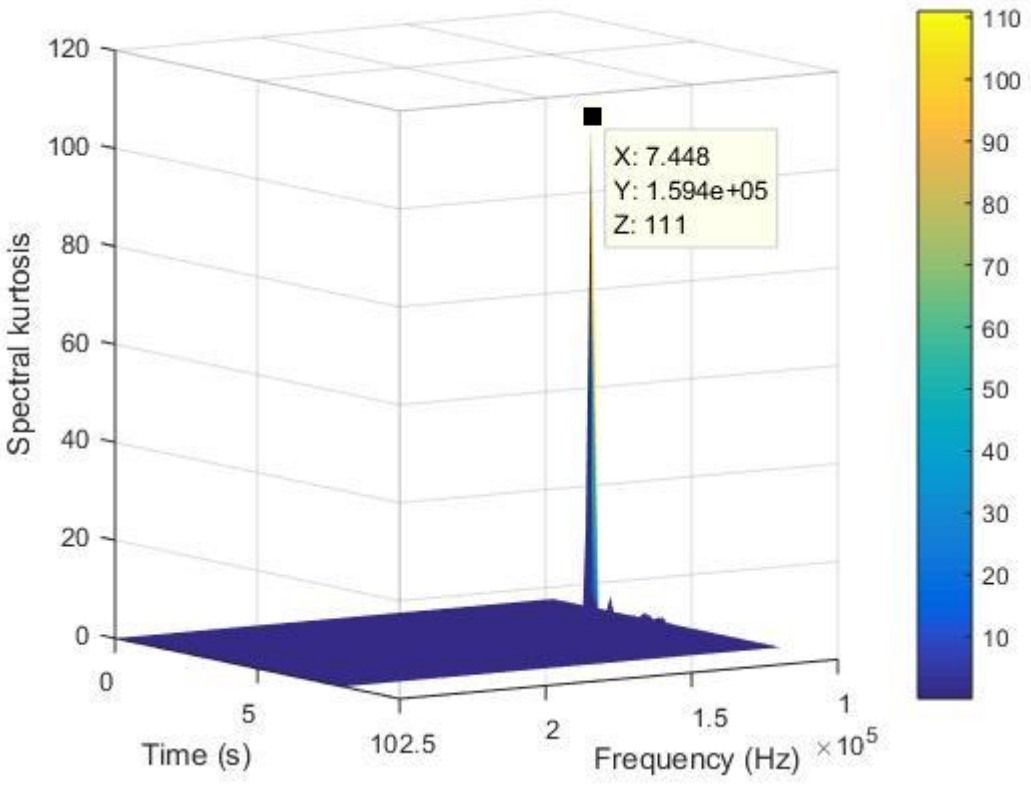

Raw AE signal generated by passenger train. High amplitude and strong modulation can indicate the presence of a defect

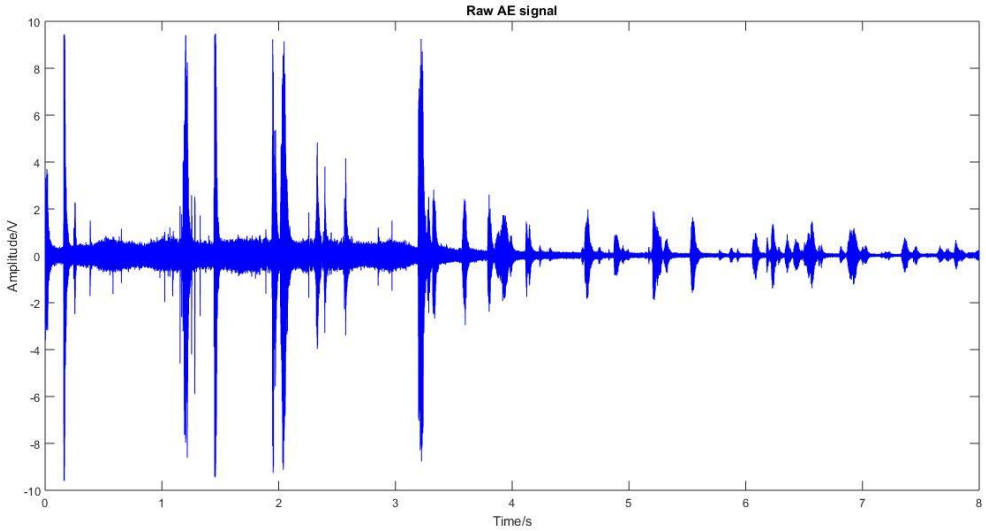

Power Spectrum of previous signal

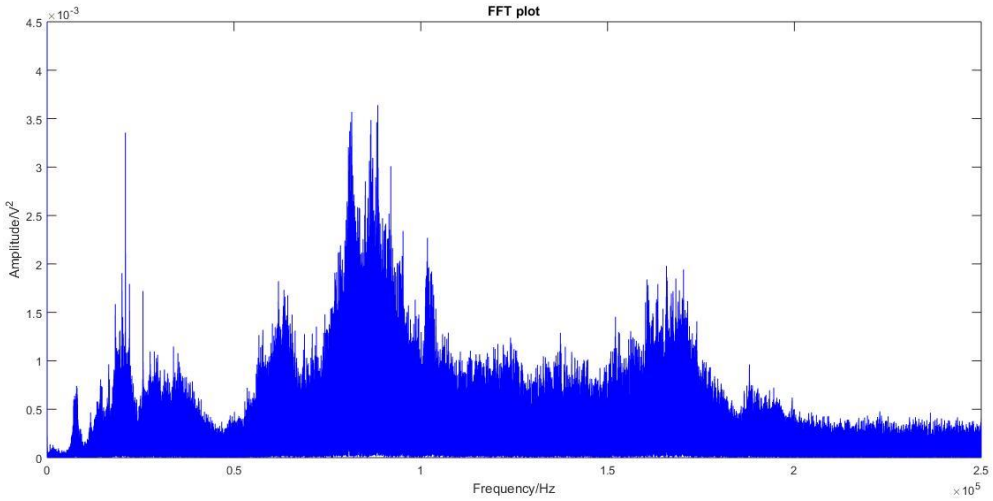

TSK results. High Kurtosis value at 165.8 kHz indicating the presence of a fault

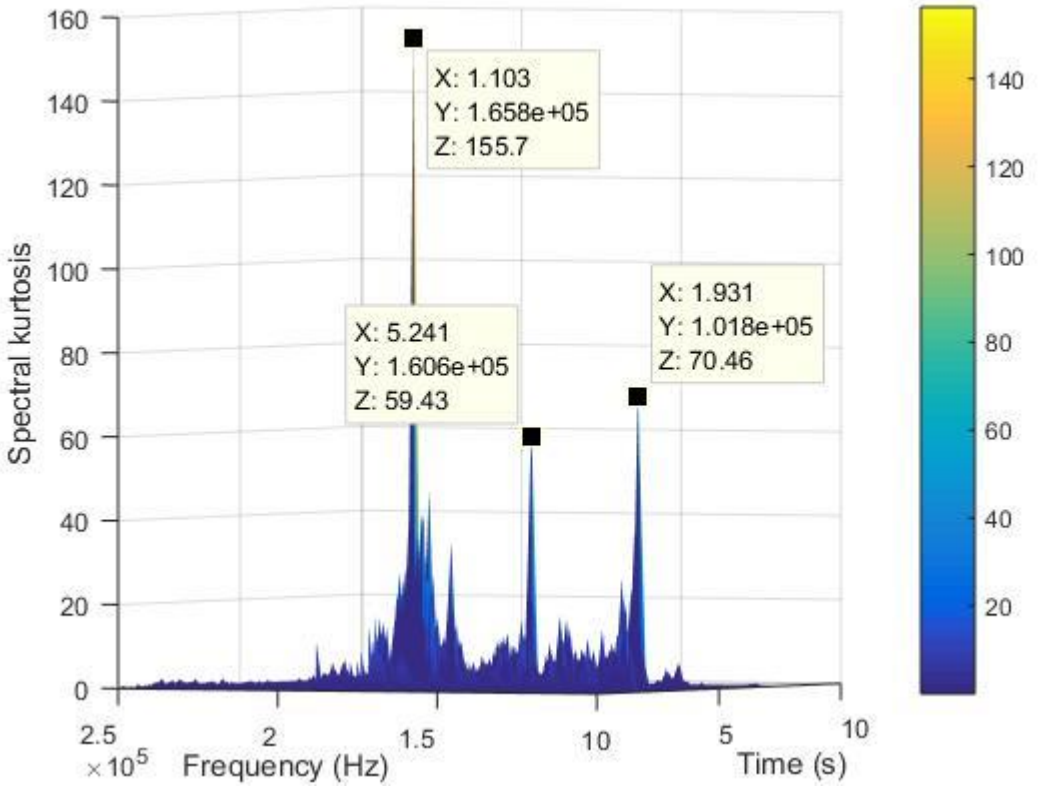

Raw AE signal generated by passenger train. High amplitude can be observed

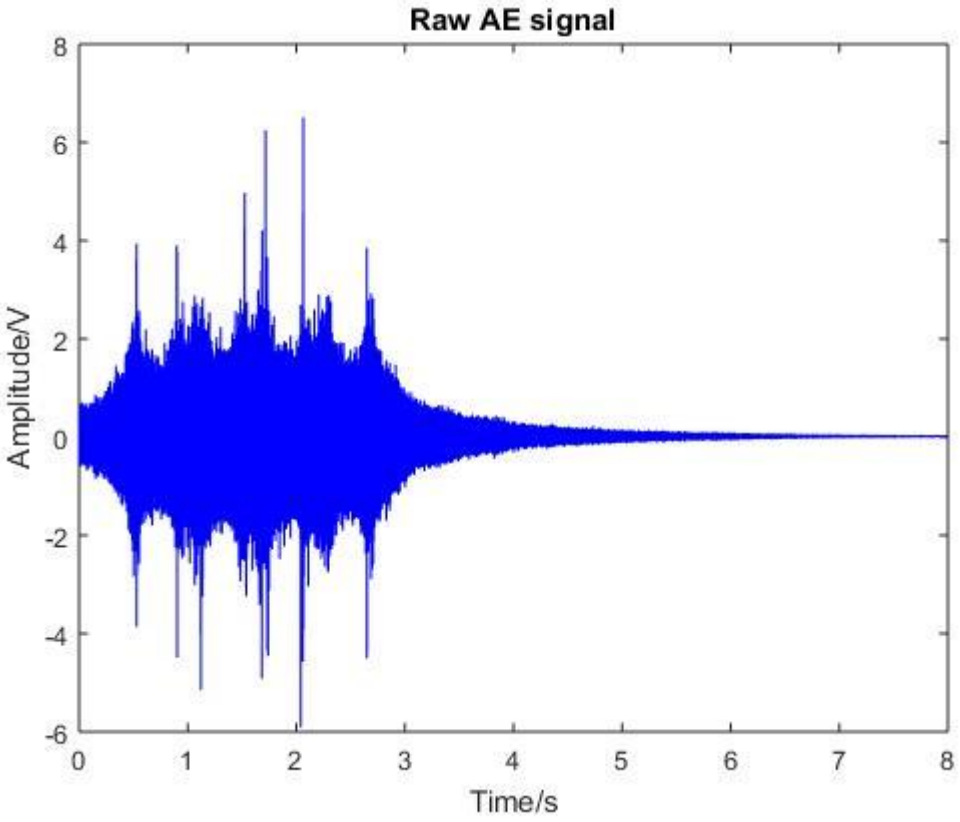

Power Spectrum of previous AE signal

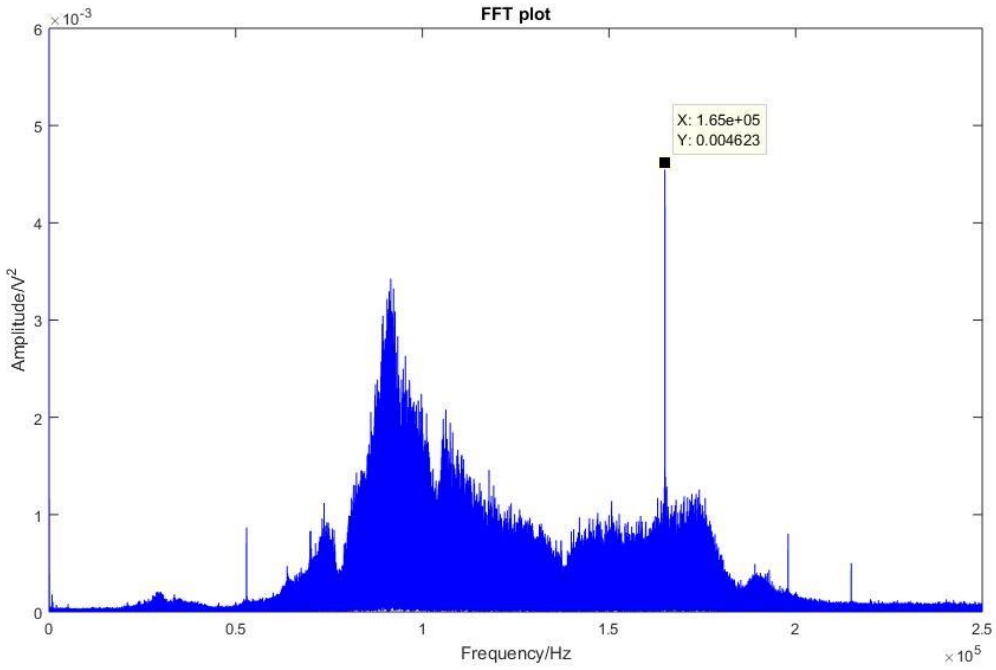

TSK results. High Kurtosis value at 165 kHz indicating the presence of a fault